BIOGEOCHEMISTRY OF ARSENIC CYCLING IN A TIDALLY INFLUENCED RIVER-BANK AQUIFER IN BANGLADESH

A Thesis

by

KATRINA LEE JEWELL

Submitted to the Office of Graduate and Professional Studies of
Texas A&M University
in partial fulfillment of the requirements for the degree of

MASTER OF SCIENCE

Chair of Committee, Peter Knappett

Committee Members, Terry Gentry
Jacqueline Aitkenhead-Peterson

Head of Department, Ronald Kaiser

August 2017

Major Subject: Water Management and Hydrological Science

ABSTRACT

Arsenic (As) groundwater contamination is a common problem in southeast Asia and many people continue to drink water with toxic concentrations of As. More in-depth understanding of the underlying geochemistry, hydrology, and microbiology related to As cycling in groundwater is needed to aid in the development of more comprehensive mitigation options in the future. In geochemically reducing environments, Iron (Fe) oxides (FeOOH) and Fe sulfides (S) have been identified as important sources of As detected in groundwater.

Previous studies have determined that seasonal fluctuations in river water and groundwater table levels sometimes lead to the oxidization of sediments adjacent to the riverbank within the Hyporheic Zone (HZ). This layer has been named a natural reactive barrier (NRB) since it traps As and other trace elements derived from discharging groundwater. Some bacterial strains (e.g. *Shewanella* sp.), are capable of catalyzing the reductive dissolution of As attached to FeOOH, resulting in As mobilization. Bacteria likely play an important role in redox-sensitive geochemical reactions involving As and Fe. Previous studies revealed important processes involved in the biogeochemical cycling of arsenic within groundwater in southeast Asia, however few studies have analyzed these with respect to the fate of As in groundwater discharging to rivers.

This project investigated the fate of As within riverbanks of the Meghna River in Bangladesh by studying the aqueous geochemistry, solid-phase geochemistry, and microbiology; geochemical data was collected from permanent monitoring wells and temporary drive-point piezometers at two different riverbank aquifer study sites. The data were analyzed and geochemical modeling was performed to predict geochemical changes as a function of several processes identified to occur in the riverbank aquifer, specifically dilution, precipitation, and sorption. Solid-phase geochemical data and mineralogy confirmed the presence of phyllosilicate minerals, which may be associated with As cycling. Bacterial diversity analysis performed on filtered groundwater from one of the study sites determined that numerous bacterial genera known to mediate Fe and As redox transformations, were present at locations corresponding to observed changes in pore-water chemistry along the flow path. These bacteria likely play an important role in As cycling. There is a long way to go in terms of finding a solution for the villagers but this project will aid in understanding biogeochemistry behind As cycling at the riverbanks in Bangladesh.

`

CONTRIBUTORS AND FUNDING SOURCES

Contributors

This work was supervised by a thesis committee consisting of Professor Knappett (advisor) of the Department of Geosciences and Professors Gentry, Aitkenhead-Peterson, and Deng of the Department of Soil and Crop Sciences.

The DOC data was provided by Jacqueline Aitkenhead-Peterson from her lab and the DNA extractions took place in Terry Gentry's lab. The X-ray diffraction (XRD) analyses took place in Youjun Deng's lab who also helped with the scanning electron microscope (SEM) work.

Funding Sources

Graduate study was partially supported by the Water Management/Hydrological Sciences scholarship and by the Valeen Silvy scholarship awarded by the college of Geosciences. Research was funded by Dr. Peter Knappett.

`

NOMENCLATURE

ANOSIM	ANalysis Of SImilarities
As	Arsenic
DOC	Dissolved Organic Carbon
DP	Drive-Point
GBMD	Ganges-Brahmaputra-Meghna Delta
HZ	Hyporheic Zone
Fe	Iron
IC	Ion Chromatography
ICP-MS	Inductive Coupled Plasma Mass Spectrometer
Mn	Manganese
NRB	Natural Reactive Barrier
ORP	Oxidative Reductive Potential
PAST	PAleontological STatistics
PCA	Principal Component Analysis
PHREEQC	PH Redox EQuilibrium
SC	Specific Conductance
SEM	Scanning Electron Microscope

`

SI	Saturation Index
TAMU	Texas A&M University
XRD	X-Ray Diffraction
XRF	X-Ray Fluorescence

`

TABLE OF CONTENTS

`

LIST OF FIGURES

`

LIST OF TABLES

1. INTRODUCTION

Clean drinking water is limited and difficult to access in developing countries typically due to water contamination. In southeast Asia, governments and aid agencies have provided people with pathogen-free drinking water by installing tube wells that pump groundwater from shallow aquifers (Nickson et al., 1998, 2000; Zheng et al., 2004). Increasing demands for clean drinking water can often not be met by surface water alone due to limited supplies or limited treatment infrastructure. This has led to greater dependence on groundwater, especially in water-scarce or impoverished regions of the world (Nordstrom, 2002).

South and southeast Asian countries including Bangladesh, India, China, and Vietnam (Fig. 1) experience monsoonal climates and have among the highest naturally occurring arsenic (As) concentrations in groundwater in the world. Over 100 million people in this region consume contaminated water with As over the 10 µg/L maximum recommended concentration in drinking water set by the World Health Organization (Fendorf et al., 2010). Long-term As consumption leads to severe skin disease, increases mortality from cardiovascular diseases and cancers of the liver and bladder and can even inhibit mental development in children (Fendorf et al., 2010). Arsenic poisoning over time from ingestion of drinking water can, over time, even cause more damage to the lungs than heavy smoking (Stuckey et al., 2015).

Most of the people in rural areas throughout much of south and southeast Asia have installed inexpensive wells made out of polyvinyl chloride (PVC) pipe that contain a cast iron hand pump attached to the top to avoid drinking the surface water contaminated with microbial pathogens (Fendorf et al., 2010; Knappett et al., 2011). Unfortunately, little water quality testing and treatment is performed in these regions by the government or local people including testing for As (Fendorf et al., 2010). Thus, people are exposed to unknown and often-high levels of As which is why it is important to understand the geochemical mechanisms behind As contamination (Nickson et al., 1998, 2000).

Arsenic contaminated areas in south and southeast Asia are located in low elevation river deltas, which contain high discharge rivers that flow from the Himalaya Mountains, and share common hydrological characteristics including a near neutral pH and a shallow water table. One region of interest is Bangladesh (Fig. 2), in which the Brahmaputra and Ganges Rivers flow into a common delta basin: the Ganges-Brahmaputra-Meghna Delta (GBMD). The Meghna River joins the Ganges and Brahmaputra Rivers approximately 200 km north of the Bay of Bengal. The sediments from all three rivers have contributed to building the same delta.

`

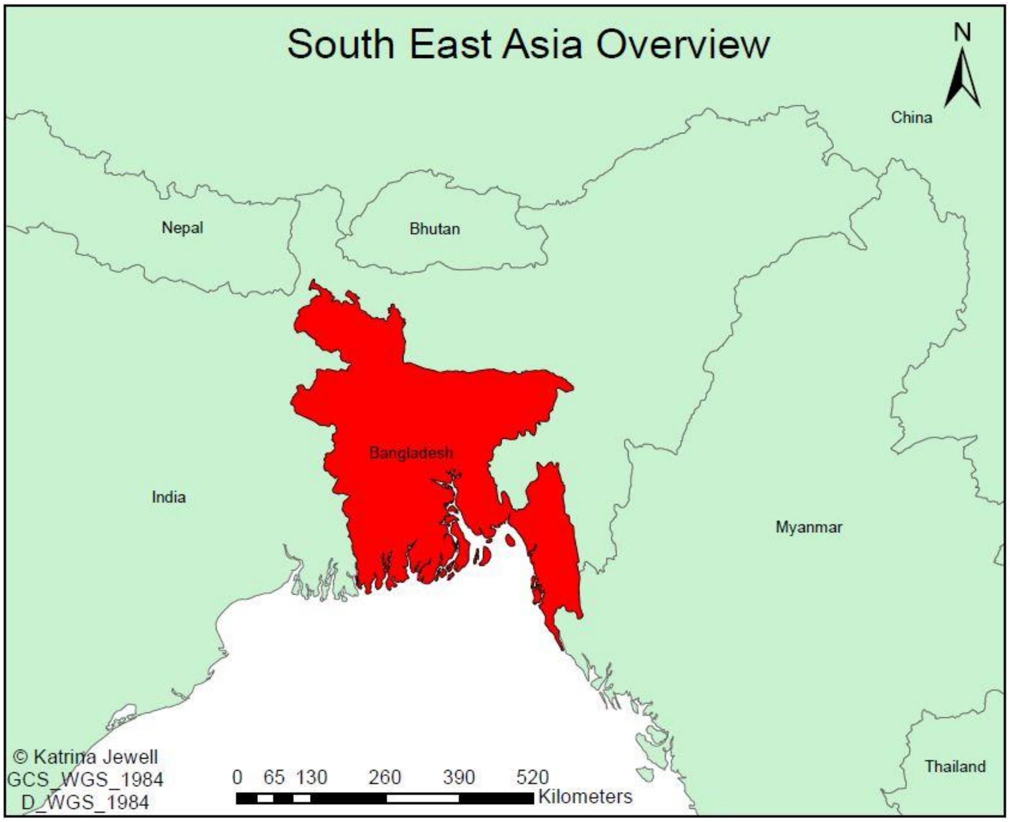

Figure 1: An overview of southeast Asia. This study is focused on Bangladesh but other neighboring countries such as China, India, and Vietnam have As contamination issues as well.

This study takes place in shallow aquifers contaminated with toxic concentrations of dissolved As located near the banks of the Meghna River in Bangladesh (Figs. 1, 2). The As contaminated areas in Bangladesh are mostly located in the lower delta and flood plains of the combined River system. Arsenic contamination also extends to the Sylhet basin and delta and flood plains of the Meghna River in southeast Bangladesh (Acharyya et al., 2000).

2. BACKGROUND

2.1 Context

Arsenic contaminating groundwater in southeast Asia originates from recently exposed, weathered sediments from the Himalayan Mountains that are transported by braided and meandering rivers (Fendorf et al., 2010; Goodbred et al., 2014). In Bangladesh, the As contaminated areas are mostly restricted to the low lying delta flood plains of the Ganges River and extends into the Sylhet Basin and the delta flood plains of the Meghna River (Acharyya et al., 2000). Older oxidized clay and other sediments uplifted in northern Bangladesh are mostly free of As contamination however, the Sylhet basin and the Meghna River delta are highly affected (Acharyya et al., 2000).

Sulfidic minerals and coal seams in the Himalayan Mountains are primary sources of As, which tends to have a strong affinity for pyrite (Nordstrom, 2002). Coal mining is widespread throughout the Meghalaya Hills along the southern edge of the Shillong Plateau, an area that lies within the Meghna River basin (Swer and Singh, 2004). Sulfidic minerals are oxidized when sediment is exposed to the surface and As is released and mobilized in the delta flood plains along with transported sediments (Zheng et al., 2004). The eroded sediment that is deposited along riverbeds and floodplains becomes a source of As to groundwater.

In Bangladesh, As concentrations are typically most concentrated in shallow aquifers (Fendorf et al., 2010). Groundwater pumping can form a cone of depression in the water table redistributing As from the water table to greater depths or even between aquifers. Pumping can also redistribute DOC, which causes microbial reduction and As release (Mailloux et al., 2013). Sediment near the riverbanks frequently accumulate high solid-phase As concentrations (Datta et al., 2009; Postma et al., 2010) and can become a source of As to a shallow aquifer when that aquifer is pumped at a high rate (van Geen et al., 2013; Stahl et al., 2016).

2.2 Hyporheic Zone Riverbank Influences & Natural Reactive Barriers

The HZ is a transition zone between groundwater and surface water (Xie et al., 2014). This zone includes shallow surface water, porewater sediments below the sediment-water column interface, and shallow groundwater (MacKay et al., 2014). Intermediate mixing between the groundwater and surface water may promote chemical and biological reactions among species present only within the HZ (MacKay et al., 2014). Within the HZ, exchanged chemicals that enter the sediments along with water can be oxidized or reduced by biogeochemical reactions (Xie et al., 2014). The HZ can act as either a source or sink for As, however the specific reactions behind As cycling is still being investigated so the effects of the HZ on As are still unknown (Xie et al., 2014).

The two valence states of As that exist in aqueous environments are As(III) and As(V). Arsenic(V) tends to bind to solids and soils, whereas As(III) has a weaker affinity to minerals and tends to be more specific, thus binding to Fe(III) oxides (Tufano et al., 2008, Xiu et al., 2015). Redox sensitive elements, including As that react to precipitated Fe(III) oxides in the HZ can selectively get trapped and removed as groundwater discharges to the river. These permeable reactive barriers have been referred to as “iron curtains” or a natural reactive barrier (NRB). These NRBs trap redox sensitive elements at shallow depths (approximately 1 m) into the riverbed sediment (Jung et al., 2015) which may be enhanced by redox transformations caused by a transition between the reducing groundwater and the relatively oxidized water within the HZ close to the river.

`

Iron and S redox cycling in the HZ favors the mobilization and enrichment of As (Xie et al., 2014). Some FeOOH and Fe S possibly aided by microbial activity sorb and release As (Gorney et al., 2015). When oxygen and fresh dissolved organic carbon (DOC) enter the groundwater, redox sensitive elements such as Fe, Mn, and As in sediments can be oxidized or reduced by biogeochemical reactions often catalyzed by microorganisms residing within the HZ (Xie et al., 2014). Labile, reactive DOC is a common source of both carbon and electrons; DOC donates electrons which are accepted by oxygen, nitrate, Fe(III), and lastly sulfate (Xie et al., 2014). The order that various electron acceptors are utilized depends on the relative bioavailable concentrations in solution, and the potential energy per electron they supply. The redox reactions coupling the cycling of iron and sulfides in the HZ usually favors the mobilization of As (Xie et al., 2014).

2.3 Thermodynamics

Thermodynamic equilibrium calculations based on standard state conditions are used as a reference point to calculate the properties of a solution under varying environmental conditions. Thermodynamics play an important role in determining whether geochemical reactions are favorable under certain environmental conditions. Gibbs free energy (Eq. 1), the energy that can be used to do work, is often used to determine whether a chemical reaction could occur spontaneously. The following equations from Kocar and Fendorf (2009) are frequently used in thermodynamics:

$$\Delta G = \Delta G^{\circ} + RT(ln10)\log(Q) \qquad \text{(Eq. 1)}$$

The reaction quotient, Q is defined for a reaction as:

$$a(A) + b(B) = c(C) + d(D) \qquad \text{(Eq. 2)}$$

`

$$Q = \frac{(C)^c (D)^d}{(A)^a (B)^b} \qquad \text{(Eq. 3)}$$

Kocar and Fendorf, (2009) found that protonating arsenate (As(V)) with hydrogen results in arsenite (As(III)) under standard state conditions. The driving force of these reactions depends on the reaction favorability and concentration gradients of the reactants and products. Based on thermodynamics alone, As(V) reduction is expected to occur regardless of the presence of Fe(III) or sulfate, but could be inhibited in the presence of high oxygen or nitrate (Kocar and Fendorf, 2009).

Iron reduction is typically an exergonic process (a chemical reaction accompanied by the release of energy) when DOC is involved, however the microbial processes are not well understood (Kocar and Fendorf, 2009). Under anaerobic conditions, microorganisms may couple the oxidation of organic and inorganic compounds into reducing As(V)/Fe(III). Both As(III) and As(V) can extensively adsorb onto sediments and minerals including Fe(III) oxides, but As(V) tends to have a stronger affinity to minerals and will bond more strongly than As(III) (Ghorbanzadeh et al., 2015; Xiu et al., 2015).

2.4 Microbial Arsenic Transformations in the Environment

The biogeochemical reactions of multiple trace elements such as As are driven by redox reactions and bioavailability (Borch, 2010). Iron and Mn minerals can provide chemical pathways for As reduction however, bacteria can act as enzyme catalysts towards As reduction through bacterially mediated respiratory pathways under appropriate environmental conditions (Kocar and Fendorf, 2009, Borch, 2010, Xiu et al., 2015). In a river that experiences daily and seasonal tidal fluctuations, intermediate mixing between two

`

endmember mixing waters may promote biological reactions that characterize that mixing zone (MacKay et al., 2014).

Bacteria gain energy by coupling the reduction of Fe(III), Mn(III), and Mn(IV) to the oxidation of organic matter or reduced inorganic compounds. After As(III) is oxidized by Mn oxides, it adsorbs as As(V) onto Fe(III) oxyhydroxide surfaces (Ehlert et al., 2014). For microorganisms, Mn oxides are thermodynamically more favorable electron acceptors than FeOOH. Under reducing environments, As(III) that was produced by the bacterium *Shewanella* in ferrihydrite ($(Fe^{3+})_2O_3 \cdot 0.5H_2O$) and birnessite ($(Na_{0.3}Ca_{0.1}K_{0.1}Mn^{4+}Mn^{3+}O_4 \cdot 1.5(H_2O))$) sands was not oxidized by birnessite which suggests that oxygen aids As(III) oxidation in the presence of Mn reducing bacteria (Ehlert et al., 2014).

Some bacterial species thrive in reducing environments. Bacteria that belong to the *Shewanella* genus are one example and can reduce redox sensitive elements such as As(V) to As(III) and Fe(III) to Fe(II). Cummings et al., (1999) and Ehlert et al., (2014) studied *Shewanella alga* strains and found that they promote As(III) mobilization. Ghorbanzadeh et al., 2015 suggested that *Shewanella putrefaciens* reduced >98% of As(V) to As(III) in batch experiments. *Sulfurospirillum barnesii* is another bacterium that has been found in reducing environments and has been found to reduce As(V) to As(III) (Zobrist, 2000).

Some bacteria species thrive in oxic environments. *Thiobacillus ferrooxidans* and *Acidithiobacillus ferrooxidans* are bacterial species that have been studied and have the capability to re-oxidize Fe(II) in arsenopyrite to Fe(III) (Gorny et al., 2015). Other bacteria that have been found to oxidize and precipitate Fe include *Pseudomonas, Dechlorospirillum*,

`

Gallionella ferruginea, *Leptothrix ochracea*, and *Acidovorax*. *Gallionella ferruginea*, *Leptothrix ochraea*, and *Acidovorax* are Fe(II) oxidizing bacteria that mobilize As(III) by precipitation or sorption during Fe(II) oxidation (Xiu, 2015). *Pseudomonas* sp. strains have been found to oxidize and precipitate ferrihydrite ($(Fe^{3+})_2O_3 \bullet 0.5H_2O$), and *Dechlorospirillum* are involved in Fe redox cycling at the oxic-anoxic transition zones in fresh water environments (Xiu, 2015). Some bacteria have the capability to synthesize arsenite oxidase enzymes which oxidizes As(III) to As (V) (Gorney et al., 2015). Some of these bacteria include *Alcaligenes faecali*, *Agrobacterium tumefaciens*, and *Rhizobium*.

Table 1: Summary of bacteria identified in previous As and Fe cycling experiments in southeast Asia. Most of the listed bacteria were detected within batch experiments in the laboratory. The presence or relative abundance of these bacteria within a tidally influenced riverbank aquifer were determined from a community DNA analysis.

Bacterium Genus	Function	Environment	Strains Studied	Studies done by:
Shewanella	Reduces As(V) & Fe(III)	Anoxic	CN-32, ATCC 12099, BrY	Cummings (1999), Ehlert (2014), Ghorbanzadeh (2015)
Sulfurospirillum barnesii	Reduces As(V)	Anoxic	SES-3	Zobrist (2000)
Acidithiobacillus ferrooxidans	Oxidizes Fe(II)	Oxic	Not Specified	Gorney (2015)
Acidovorax	Oxidizes Fe(II)	Oxic	BoFeN1	Xiu (2015), Muehe (2016)
Alcaligenes	Oxidizes As(III)	Oxic	Not Specified	Gorney (2015)
Agrobacterium	Oxidizes As(III)	Oxic	Not Specified	Gorney (2015)
Dechlorospirillum	Fe redox cycling	Oxic	Not Specified	Xiu (2015)
Gallionella ferruginea	Oxidizes Fe(II)	Oxic	Not Specified	Xiu (2015)
Leptothrix ochracea	Oxidizes Fe(II)	Oxic	Not Specified	Xiu (2015)
Pseudomonas	Oxidizes & precipitates Fe	Oxic	GE-1	Xiu (2015)
Rhizobium	Oxidizes As(III)	Oxic	Not Specified	Gorney (2015)
Thiobacillus ferrooxidans	Oxidizes Fe(II)	Oxic	Not Specified	Gorney (2015)

`

2.5 Processes Leading to Arsenic Mobilization

Arsenic may initially adsorb to Fe oxides as As(V), and may be subsequently released during reductive dissolution of the iron oxides. Mobile As(V) can be reduced to As(III) and either form can re-adsorb to available sites on nearby FeOOH surfaces; however, as the FeOOH surface sites disappear during Fr reduction both As(V) and As(III) are released into the water (Postma et al., 2010). However, reduction of Fe(III) isn't the only way that As can be mobilized and the details of the As release remain unclear. Carbonates and silicates may absorb As, further complicating the As release mechanism.

Weathering of silicate minerals under oxidized conditions has also been found to mobilize As (Masuda et al., 2012). Sequential extraction on sediment cores from shallow aquifers with high As concentrations in central Bangladesh revealed that most As is fixed in silicates in sandy aquifer sediments (Seddique et al., 2008). The sequential extraction procedure used (Masuda et al., 2005) cannot determine the exact As concentration but can give a rough estimation of As partitioned in a series of labile and recalcitrant chemical forms (Masuda et al., 2005). One study found that >90% of total As was concentrated in biotite or organic matter in the GBMD (Seddique et al., 2008). Another study suggested that dissolution of chlorite by oxic weathering in the shallow aquifer may, in some settings, be the primary mechanism for As release in groundwater (Masuda et al., 2012). It is also possible that As is released under both reducing and oxidizing conditions, however, this is not typically considered in most conceptual and numerical models of As mobilization and transport.

The most widely accepted mechanism behind As mobilization occurs in oxygen deprived environments where bacteria couple oxidation of DOC to the reductive dissolution

`

of As-bearing Fe oxides (Stuckey et al., 2015; Nickson et al., 2000). Furthermore, Fe(III) oxides are usually recognized as the primary hosts of mobilizable As in the sediments (Stuckey et al., 2015; Postma et al., 2010). Most research groups focus on the mobilization of As from Fe oxides, which is expected to take place in reduced environments farther from the major rivers.

The research conducted in the current study focuses on the fate of As in groundwater discharging to rivers through riverbank aquifers across a <1 km transiently fluctuating redox gradient. This focus on the fate of As, Fe, and Mn at the end of the groundwater flow path takes place in a different environmental setting from the majority of As research which focuses on the origins of As across broad swaths up to 50 km^2 of shallow aquifers (Tufano and Fendorf, 2008; Stuckey et al., 2015). Arsenic research groups working in southeast Asia have not performed many studies on the riverbank biogeochemistry related to As cycling which makes the current study unique.

`

3. STUDY AREA AND OBJECTIVES

3.1 Study Area

Arsenic occurrence and transport has been extensively studied for over 10 years at the Ganges Brahmaputra Meghna Delta (GBMD), which experiences a dry season and a wet season. The wet season typically starts in late April and a rise of ~3 m in river water levels is typically observed which drives a rapid rise in the water table (Knappett et al., 2016). At the end of the wet season, typically around late October, the river water levels rapidly decrease while the groundwater levels decrease more slowly (Knappett et al., 2016). The Meghna River is made up of alluvial sediments containing multiple layers of sand, silt, and clay. Most of the time the upper shallow aquifer is made up of very-fine to fine sand and is found below a few meters of thick surface clay (Jung et al., 2015).

Areas along the Meghna River that are 0-8 m above sea level are subjected to seasonal flooding. The river stage is controlled by semi-diurnal and neap-spring tidal fluctuations, each approximately 0.5 m in magnitude (Jung et al., 2015; Shuai et al., 2016). The study sites in this thesis are located in the middle of the country, approximately 35 km east of Dhaka, Bangladesh. The study sites for this project were chosen for the elevated As and Fe concentrations within the riverbank aquifers. Furthermore, previous studies such as Datta et al. (2009) found sediment enriched in As along the Meghna River banks (Jung et al., 2012; 2015).

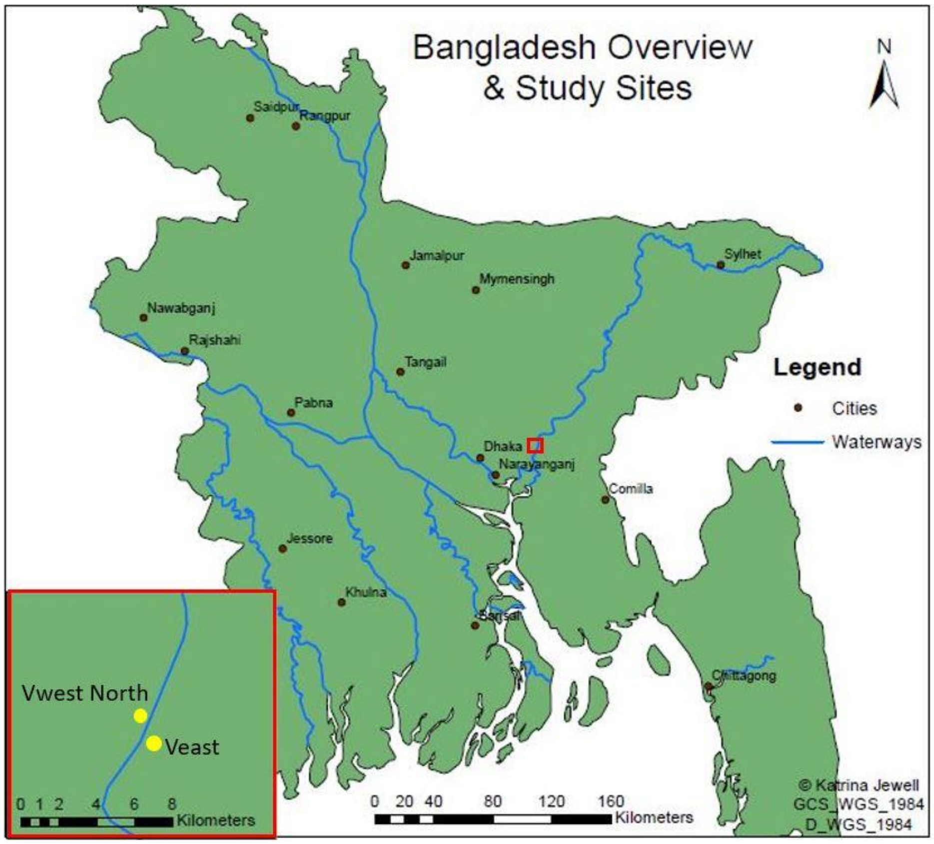

Figure 2: Bangladesh with major cities, rivers, and locations of the study sites. Veast (23.744241^{O}N and 90.729584^{O}E) and Vwest North (23.797625^{O}N, 90.734153^{O}E) in Bangladesh.

The study sites are located along a 10 km reach of the Meghna River in central Bangladesh about 35 km east of the capital city Dhaka. The specific location of both study sites is shown in the red box in figure 2. The first well transect, Veast (Figs. 2, 3) is located on the east side of the river and the second well transect, Vwest North (Figs. 2, 4) is located on the west side of the river, north of the Veast transect. Figures 3 and 4 show geological cross sections of the Veast and Vwest North well transects. The permanently installed

`

monitoring wells are 15 m deep and the temporary, drive-point piezometers, were 1-3 m deep.

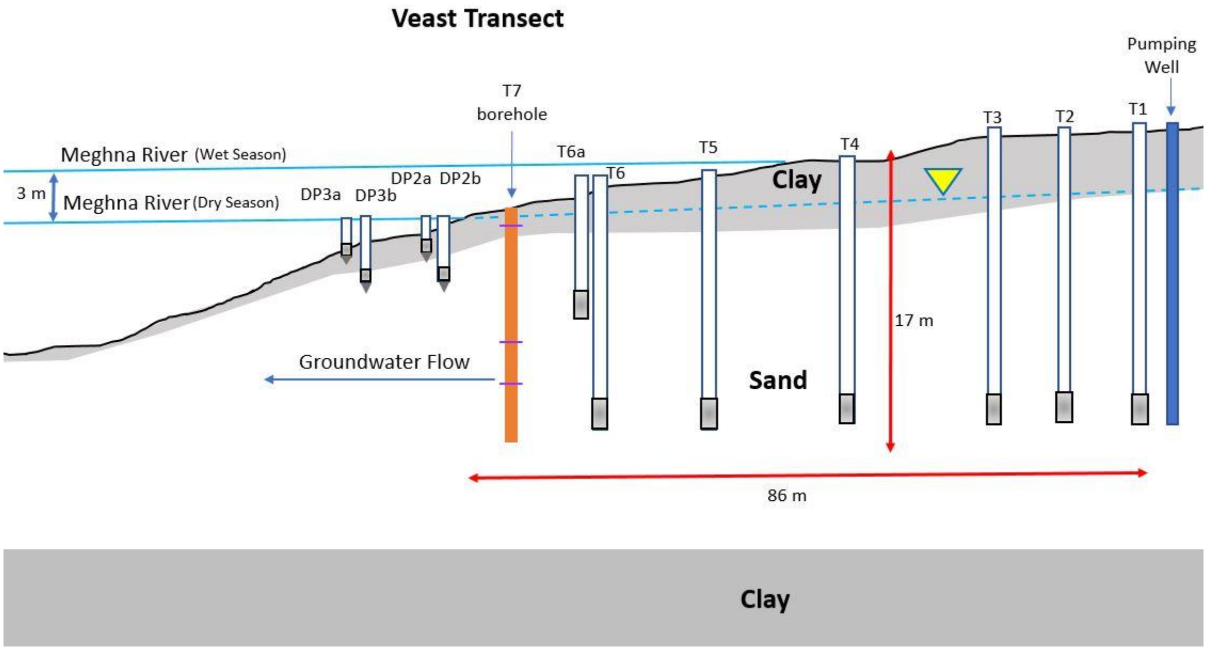

Figure 3: Veast study area monitoring wells (T1-6/6a), drive-point piezometers (DP), sediment borehole T7, irrigation pumping well, and the 3 m river water level fluctuation during the dry and wet seasons. Each well has a 1.5 m screen at the bottom of the well. The horizontal purple lines in borehole T7 represent the depths at which sediments underwent XRD.

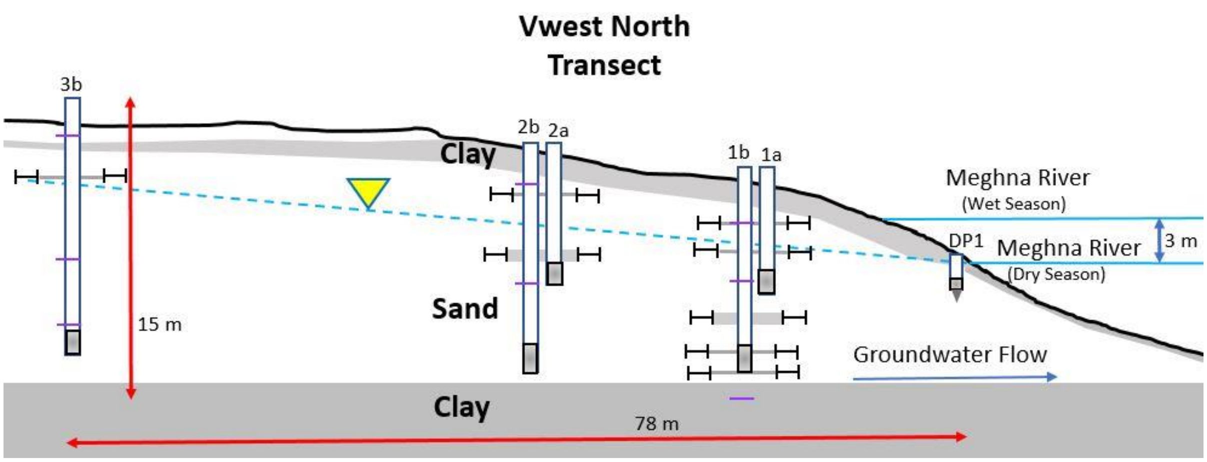

Figure 4: Vwest North study area monitoring wells (3b-1a), drive-point piezometer (DP) and the 3 m river water level fluctuation during the dry and wet seasons. Each well has a 1.5 m screen at the bottom of the well. The horizontal purple lines in wells 1b, 2b, and 3b represent the depths at which sediments underwent XRD.

`

3.2 Objectives

The purpose of this study was to determine the fate of As in groundwater discharging to the seasonally and tidally fluctuating Meghna River in Bangladesh through two shallow riverbank aquifers on the east and west banks of the river (Fig. 2). In this study, combined aqueous geochemical, solid-phase mineralogical, and microbiological observations were analyzed. Groundwater was sampled from wells at <1 km distances from the river and at 1-15 m vertical depths. Spatial distributions in aqueous geochemistry across the sandy riverbank aquifers were compared to locations of poorly conductive silt and clay layers which may separate pore-waters. Geochemical modeling was performed to identify the predominant dissolved ion species of As and Fe and thermodynamically favorable reactions likely to be occurring at each study site. Solid-phase chemistry was studied to identify minerals present in aquifer solids that are known to relate to As cycling in other localities, such as pyrite and Fe oxides (Stuckey et al., 2015, Nickson et al., 2000). Finally, groundwater samples were analyzed from the Veast study site (Figs. 2, 3) for community DNA to identify the presence of bacterial strains known to be involved in the cycling of As and Fe.

Question 1: What geochemical processes with respect to proximity to the river and vertical depth explain observed trends in aqueous cations and anions along the groundwater flow path discharging through the riverbank aquifer? The hypotheses to be tested under this objective include:

> H_0: No geochemical processes are identifiable; cations and anions remain conservative along each well transect.

`

H_1: Dilution of conservative elements such as chloride (Cl^-) are occurring at an equal rate for all conservatively reactive ions.

H_2: Adsorption of redox sensitive reactive elements such as Fe and As to Fe oxide minerals increases with proximity to the river.

Question 2: Which stable minerals and compounds active in As cycling within riverbank aquifers are present within the sediment at our study sites? Is a natural reactive barrier present? The hypotheses to be tested under this objective include:

H_0: No minerals active in As river-bank cycling will be present and no natural reactive barrier will be present.

H_1: The segment of the aquifer analyzed for minerals was Fe reducing so minerals and compounds that are stable in reducing environments such as pyrite and siderite will be present.

H_2: If a natural reactive barrier is present, then Fe oxides will be present, trapping and releasing redox sensitive elements such as As.

Question 3: Which bacterial genera capable of As and/or Fe oxidation or reduction were present, and therefore may be participating in As and Fe transformations? Does the bacterial genera diversity significantly change with proximity to the river and vertical depth? The hypotheses to be tested under this objective include:

H_0: There is no significant difference between the bacterial communities between the deeper, Fe-reducing aquifer and the shallow, relatively oxidized part of the aquifer near the discharge zone.

`

H_1: Bacteria capable of mediating As and Fe reduction will likely dominate the more reducing deeper aquifer zone. Bacteria capable of As and Fe oxidation will likely dominate the shallow, relatively oxidized part of the aquifer near the discharge zone.

3.3 Significance

Since everyone does not have easy access to clean drinking groundwater, water contamination is an important area of study. It is important to study and understand the hydrological, geochemical, and bacteria mediated reactions behind naturally contaminated sites so a solution to the problem can be found.

Arsenic contamination in groundwater is not unique to South East Asia, it is also a problem in the United States. For example, in places where the groundwater exceeds 10 µg/L in the U.S., As release from Fe oxides appear to frequently be the cause of the toxic As concentrations (Welch et al., 2000). Arsenic contamination in groundwater from former landfill sites in the New England region in the U.S. has been linked to dissolution of As-containing Fe oxides (Stollenwerk, 2003).

Even in places like Bangladesh where toxic concentrations of As are widespread, however, the spatial distribution of As within shallow aquifers is highly patchy (van Geen et al., 2003). Since rivers impacted by tidal ad seasonal fluctuations deposited the sediments forming these aquifers, they were subjected to redox fluctuations, which may have impacted the accumulation of solid-phase As that may partially explain the complex spatial distribution of dissolved As in shallow aquifers in Bangladesh today (Weinman et al., 2008; van Geen et al., 2014).

`

4. METHODS

4.1 Data Collection and Sampling in the Field

Monitoring wells were installed in Shuai et al., (2016) using the traditional hand flapper method, a reverse circulation percussion drilling method described in Horneman et al., (2004). Six 15-m deep and one 7-m deep monitoring wells were drilled and installed at the Veast study site (Fig. 3). Three 15-m deep and two 7-m deep monitoring wells were drilled and installed at the Vwest North study site (Fig. 4). Each monitoring well has a 1.5 m screen at the bottom of the well (Shuai et al., 2016).

Several labile, geochemical parameters known to change during sample preservation were measured in the field. At the Veast (Fig. 3) and Vwest North (Fig. 4) field sites, each monitoring well and drive-point piezometer was purged using submersible pumps (Typhoon DTW 50ft, Groundwater Essentials, Bradenton, FL) for approximately 20 minutes at a flow rate of 4-6 L/min. While purging each well the water temperature (℃), specific conductance (SC), pH, and oxidation-reduction potential (ORP) were monitored using a multimeter (YSI Professional Plus, Xylem). After physical-chemical parameters stabilized, samples were collected for subsequent analyses and water was filtered using a sterile filtration apparatus to collect particulates and cells for DNA extraction and next-generation sequencing.

Some of the chemical parameters from each monitoring well and drive-point piezometer were measured in the field using field-testing kits and a photometer (V-2000 Multi-Analytes, CHEMetrics, Inc., Midland, VA). The photometer was used to measure elements and compounds including ammonia (NH_3), sulfides (S^{2-}), iron (Fe(II/III)), manganese (Mn), phosphate (PO_4^{3-}), dissolved oxygen (DO), and nitrate (NO_3^-) (Table 2). Alkalinity was measured in the field by titration with 1M H_2SO_4 (Model AL-DT, HACH

Company, Loveland, CO) and As was measured using a colorimetric ITS Econo-Quick II test kit (Industrial Test Systems, Inc., Rock Hill, SC).

Table 2. Field Test Kit Information including range, method, and method ID

Analyte	Range (ppm)	Method	CHEMetrics, Inc. Method ID
Dissolved Oxygen (DO)	0-1.000	Rhodazine D	K-7553
Dissolved Oxygen (DO)	0-15.0	Indigo Carmine	K-7513
Dissolved Oxygen (DO)	0-1.0	Rhodazine D	K-7501
Nitrate (NO_3^-)	0-50.0	Cadmium Reduction	K-6933
Ammonia (NH_3)	0-30.0	Salicylate	K-1403
Ortho-phosphate (PO_4^{3-})	0-8.00	Stannous Chloride	K-8513
Sulfate (SO_4^{2-})	0-100.0	Turbidimetric	K-9203
Soluble manganese (Mn)	0-30.0	Periodate	K-6503
Total & Ferrous Iron (Fe(II), Fe)	0-6.00	Phenanthroline	K-6203
Total & Soluble Iron (Fe)	0-25.0	Phenanthroline	K-6013
Total Iron	0-30.0, 30-300	Phenanthroline	K-6210D
Sulfide (H_2S/HS^-)	0-6.00	Methylene Blue	K-9523
Sulfide	0-1.0, 1-10	Methylene Blue	K-9510

About 4 L of water from selected wells and the drive-point piezometers at the Veast study site were passed through sterile 0.2 µl filters under vacuum to collect mobile particulates and microorganisms suspended in the aquifer, and filters were frozen at -4℃ for later DNA extraction and sequencing (Knappett et al., 2012).

Water samples were collected using 20 ml scintillation vials (LS Vial, HDPE, Urea Cap Sep, PE Cone Lnr, Wheaton Industries Inc., Millville, NJ) from each monitoring well, drive-point piezometer, and the Meghna River (~10 m away from shore and ~1 m deep). Samples intended for major and trace cation and anion analyses were filtered using a 0.45 µm nylon syringe filter (Ref: S25NY045, Simsii Inc., Irvine, CA) and the vial analyzed for

`

cations was acidified to 0.1% nitric acid while in the field. All water samples were stored in a 4℃ environment after collection. Ion Chromatography (IC) anions and cations) and Dissolved Organic Carbon (DOC) analyses were performed within two weeks of sampling at Texas A&M University (TAMU). Inductively Coupled Plasma Mass Spectrometry (ICP-MS) was performed, also at TAMU within two months of field work.

4.2 Aqueous Geochemical Analysis

Aqueous geochemical analyses were performed in the laboratories at TAMU to quantify and characterize the well water and surface water samples collected in Bangladesh. Ion Chromatography (IC) (Dionex 600, Thermo Fisher Scientific Inc. Waltham, MA) was used to obtain concentrations for anions (F^-, Cl^-, SO_4^{2-}, Br^-, PO_4^{3-}, NO_3^-, and NO_2^-) and cations (NH_4^+, Na^+, K^+, Mg^{2+}, and Ca^{2+}).

A Single Collector Inductively Coupled Plasma Mass Spectrometer (ICP-MS) (Element XR. Thermo Scientific, Waltham, MA) was used to obtain dissolved elemental concentrations. Using a 10 µg/L internal indium standard, elemental concentrations were measured at a high (As and K), medium (Mn, Fe, Si, S, Al, P, Cr, Co, Ni, Cu, Zn, Sr Na, Mg, and Ca), and low resolution (Mo, Cd, Sb, Ba, Pb) at the Radiogenic Isotope Laboratory, Geology and Geophysics, TAMU.

Dissolved Organic Carbon concentrations were measured using high temperature Pt-catalyzed combustion with a Shimadzu TOC-VCSH (Shimadzu Corporation, Houston, Texas, USA) and were measured as non-purgeable carbon (USEPA method 415.1). This procedure involves acidifying the sample (2 M HCl) and sparging for 4 min with C-free air to remove volatile and inorganic C. The water samples analyzed for DOC were filtered using an ashed Whatman GF/F 0.7 µm filter before analysis.

`

4.3 Solid-Phase Geochemical Analysis

4.3.1 Field X-Ray Fluorescence

To study the detailed solid-phase geochemistry, a ~17 m borehole (T7) was drilled 11 m west of T6 monitoring well at the Veast site (Fig. 3). At the Vwest North site, three boreholes (1b, 2b, and 3b) ~15 m deep were drilled and new permanent monitoring wells were installed (Fig. 4). Solid-phase geochemistry was assessed along the length of the three boreholes at Vwest North. The boreholes were drilled using the reverse percussion hand flapper method described in Horneman et al., (2004). Sediment grain sizes were estimated visually at ~0.6 m intervals. A Bruker Tracer III-SD handheld X-ray fluorescence (XRF) spectrometer (Bruker Corporation, Billerica, MA) that contained a Rh target X-ray tube was used to measure solid-phase elemental concentrations from sediment samples within each 0.6 m interval. Light elements (Al, Ca, K, Mg, Na, P, S, and Si) were measured at 15 kV incident energy and heavy elements (As, Ba, Fe, and Mn) were measured at 40 kV. The solid-phase elemental concentrations were converted to weight percent using the element calibration standards described in Rowe et al., (2012).

4.3.2 X-Ray Diffraction

X-ray diffraction (XRD) (Bruker D8 ADVANCE, Coventry, United Kingdom) was used to identify minerals present in soil samples collected from the same four boreholes. As the boreholes were being excavated a soil sample every ~0.6 m was collected, bagged, and brought back to TAMU for further analysis. The procedures used for XRD were from a lab manual written by Dr. Youjun Deng, Dr. White, and Dr. Dixon at TAMU. A range of 11 samples from borehole T7 at Veast, and boreholes 1b, 2b, and 3b at Vwest North were selected to perform bulk XRD analyses. Overall, about 2-3 samples at varying depths from each borehole, some more sandy or silt/clay, and some samples containing a sharp increase in

`

solid-phase As were selected for the bulk XRD run. Bulk XRD is performed by passing a raw air-dried soil sample through the XRD machine without the need for extensive sample preparation or grain separation. To properly run the samples, ~50 g of each sample was air dried for over 24 hours. Next, approximately 2 g of each soil sample were placed into a mortar and pestle. The soil was crushed with the pestle and passed through a 140-180 µm mesh. Each sample was mounted on a labeled round sample holder using a clean slide to evenly fill soil into the sample holder cavity(Fig. 5). The software DIFFRAC.SUITE.EVA V3 (Bruker Coventry, United Kingdom) was used to match XRD peaks with their corresponding minerals. Table 3 shows which samples and their corresponding depths were evaluated using XRD.

Figure 5: Empty round XRD sample holder (left) and an example of ground soil sample in a sample holder (right).

Table 3: Samples evaluated for different XRD size fractionations

XRD Evaluation	Samples & Depths (m)	Quantity
Bulk	T7 0.3, T7 10, T7 13.7, 1b 0.9, 1b 10.6, 1b 21, 2b 2.1, 2b 11.2, 3b 1.5, 3b 11.2, 3b 13.1	11
Sand	T7 13.7, 1b 0.9, 2b 11.2	3
Silt/Clay	T7 13.7, 1b 0.9, 2b 11.2	3
Clay Analysis	1b 0.9	1

`

A mineral's presence is detected by aligning the position of peaks on the graph to known reference materials. The y-axis displays the peak intensity, which represents counts per second. The x-axis is the angle of diffraction (2θ) with respect to the incident beam. The 2θ angle can be converted into interplanar spacings d using Bragg's Law:

$$n\lambda = 2dsin\theta \qquad \text{(Eq. 4)}$$

where λ is the wavelength of the X-ray, θ is the diffraction angle, and n is the order of diffraction. All of the expected peaks for a mineral must be present to determine that it is present in the sample and the greater the intensity is on the peaks means the mineral is more abundant.

4.3.3 Sample Evaluation

After examining the bulk XRD results, samples were placed into three groups based on location, lithology, known mineralogy, and XRF results. One sample from each group: T7 13.7 m, 1b 0.9 m, and 2b 11.2 m were selected for additional XRD analyses in order to identify more minerals possibly being masked by highly abundant minerals.

Before any further XRD analyses, an initial sample evaluation was performed on the three selected samples. The following tests were performed by spreading <1 g sample onto a micro weighing dish and then adding the appropriate reagents for each test. A check for carbonate minerals was performed by adding one drop of 0.5 mL 1M hydrochloric acid (HCl), to a subsample of each selected sample. The subsample fizzes intensely if carbonate minerals are abundant. The oxidizing/reducing components check was performed by adding one drop of 30% hydrogen peroxide which reacts with several oxidizing/reducing agents

`

including Mn oxides, sulfides, and Fe^{2+}. The magnetic minerals check was done by using a magnet.

To perform the next tests, a 5:1 water volume/solid weight ratio, 5 g of each soil sample and 25 mL of deionized water were added to 250 mL Nalgene centrifuge bottles. Each bottle was capped and shaken using a reciprocating shaker for 30 minutes and centrifuged at 2000 rpm for 10 minutes. About 20 mL of the supernatant was isolated to measure the electrical conductivity and the pH using an EC electrode and a pH electrode respectively.

In order to test for gypsum ($CaSO_4$), 1 mL of supernatant was added to a glass test tube followed by a drop of acetone. A cloudy white precipitate indicated the presence of gypsum. The presence of sulfate (SO_4^{2-}) was tested by isolating 1 mL of supernatant and adding one drop of Ba^{2+}. A cloudy white precipitant indicated the presence of SO_4^{2-}. Chloride (Cl^-) anions were tested by adding one drop of Ag^+ to 1 mL of supernatant. A cloudy white precipitant indicated the presence of Cl^-.

4.3.4 Size Fractionation

Abundant minerals such as quartz and feldspar are known to occasionally mask the appearance of other minerals in a bulk XRD run. To find other lesser abundant minerals that may be present the sand, silt, and clay size fractions were separated by size fractionation. About 20 g of each soil sample and 50 mL of pH 10 sodium carbonate (Na_2CO_3) solution, used as the dispersive agent were added to clean 250 mL Nalgene bottles, one for each sample. The bottles were shaken well by hand and centrifuged at 2000 rpm for 10 minutes. The supernatant was pipetted away and the procedure was repeated one more time. To separate the sand from the silt/clay fraction, a funnel with a 53 µm sieve was set up on a ring

`

stand with a plastic 5000 mL beaker under the funnel. Figure 6 shows the sand fractionation set up (left) and sand grains in the sieve (right).

Figure 6: Sample 1b sand fractionation set up (left) with a ring stand, funnel, sieve and Nalgene beaker which catches the silt & clay, and the remaining sand inside of the sieve (right).

Each sample was washed through the sieve with pH 10 Na_2CO_3 solution until the silt/clay had gone through the sieve. The sand particles were rinsed with deionized water, placed in an aluminum dish and placed into an oven set at 105℃ to dry.

Samples T7 at 13.7 m depth and 2b at 11.2 m depth contained too small quantity of silt and clay to continue any size fractionation. Sample 1b at 0.9 m contained mostly silt and clay so the size fractionation procedure was taken further.

For sample 1b at 0.9 m depth, the silt & clay mixture was left to settle for over 24 hours. After settling most of the supernatant was removed using a pipette tip and discarded. The silt & clay mixture was placed into Nalgene centrifuge bottles filled up to the 9 cm mark

`

with 10 pH Na_2CO_3, shaken well, and centrifuged at 750 rpm for 3.2 minutes. The clay containing supernatant was siphoned into a clean 5000 mL plastic beaker. This procedure was repeated 5 more times until the supernatant was relatively clear. The sample on the bottom of the centrifuge bottle is the silt, which was placed in an aluminum dish and placed in a 105^{O} C oven to dry. About 50 g of NaCl was added to the beaker containing the clays to cause flocculation and the beaker was left covered > 48 hours.

The clay particles in solution were obtained using dialysis. The purpose of the dialysis was to clean the sample and remove any remaining electrolytes including NaCl. Before transferring the clay into the dialysis tubing, the volume of suspension was first minimized by removing and discarding most of the supernatant from the beaker using a pipette. The remaining clay mixture was transferred into Nalgene centrifugation bottles, and centrifuged at 1000 rpm for 5 minutes. Tubes of dialysis tubing were appropriately cut from a roll. The dialysis tubing is initially stiff so it was placed in a small beaker of deionized water for 1-2 minutes to help the tube open up. Once the tube opened up, a knot was tied on one end and the clay sample was poured in using a funnel. The other end of the tube was tied off and the dialysis tubes containing the clays were placed in a 4 L beaker filled with deionized water (Fig. 7).

`

Figure 7: Clay dialysis set up for sample 1b. Clay-sized grains inside the dialysis tubes in a beaker full of deionized water which removes the NaCl from the clay.

The deionized water was switched out for fresh deionized water after 2 hours and again the next day. After ~48 hours, the clay samples were removed from the dialysis tubes. Samples containing only sand, silt/clay, and silt fractionations were mounted onto XRD sample holders in the same way as the bulk samples.

4.3.5 XRD Clay Analysis

To perform an in-depth clay analysis on sample 1b at 0.9 m, the appropriate volume of clay suspension containing 50 mg of clay needed to go into a 50 mL centrifuge tube. Before doing this, the quantity of clay in 1 mL of suspension was calculated by oven drying 1 mL of clay suspension and measuring the weight of clay (mg) in 1 mL of clay suspension. After adding at least 50 mg clay, 0.5 M MgCl solution was added to the 15 mL mark and the tube was shaken for 20 minutes at 220 rpm. After 20 minutes, the tube was centrifuged at 2000 rpm for 10 minutes. The supernatant was removed and discarded using a pipette tip following centrifugation. This procedure was repeated two more times. The Mg^{2+} washed clay was then washed three times with deionized water, shaken for 10 minutes, centrifuged at 2000 rpm for 10 minutes, and the clear supernatant was removed and discarded using a pipette tip. The clay was then suspended in 1 mL of deionized water. A glass disc was labeled and mounted onto a sample holder using poster adhesive. The Mg^{2+} washed clay sample was transferred onto the glass disc using a pipette tip covering as much of the disc surface area as possible in a place in the lab where the disc would not be disturbed. The sample was then covered by a watch glass to prevent dust or other particles from settling onto the sample.

The procedure for the K^+ wash was exactly the same as the Mg^{2+} wash but using a 1 M KCl solution and two samples were prepared. Only one of the glass discs was mounted on a sample holder, the other one was for doing XRD analyses after heating to 330℃ and 550℃. For the Mg washed clay sample, the clay film was analyzed by the XRD and then sprayed with 20% glycerol solution and analyzed again by the XRD.

When performing a full clay analysis, Mg^{2+} and K^+ are the most commonly used cations. The use of K^+ is important because the cations large size allows it to migrate into the interlayer of some clay mineral groups such as smectites in an un-hydrated state. This results in the collapse of the interlayer which is heat dependent and also why the clay samples with the K^+ wash are ran through the XRD at 25℃, 330℃, and 550℃. Magnesium is used because it is highly hydrated and its presence in the interlayer stabilizes the complex with two water layers between each 2:1 layer. This complex is less sensitive to layer change and humidity than other cations. Glycerol is used on the Mg^{2+} wash because glycerol solvated swelling minerals, like smectite clays, are less sensitive to layer charge differences than glycerol. This

`

means glycerol allows for easier detection of interstratified components in a mineral. Any differences in XRD patterns for the K^+ and Mg^{2+} washed samples indicate the presence of swelling components in the sample.

4.3.6 Density Separation

To identify possible As containing minerals such as pyrite, the sand sized fractionations from samples T7 at 13.7 m and 2b at 11.2 m (Figs. 3, 4) were prepared for the scanning electron microscope (SEM) first by density separation. Diiodomethane was used for density separation and a laboratory procedure written by Dr. Katharine Huntington at the University of Washington was followed. The density of diiodomethane is ~3.3 g/cm^3, quartz is 2.65 g/cm^3, feldspar is 2.56 g/cm^3, and pyrite is 5.01 g/cm^3. If pyrite is present, it will sink while the quartz and feldspar will float. The sand fractionation for samples T7 at 13.7 m depth and 2b at 11.2 m depth were placed in diiodomethane in a cake-decorating bag set up on a ring stand under a fume hood. All minerals <3.3 g/cm^3 floated and minerals > 3.3 g/cm^3 sank (Fig. 8).

Figure 8: Density Separation set up. The full apparatus (left) consists of a ring stand and funnel to hold the cake decorating bag in place, below it is another funnel with an acetone soaked filter and under vacuum with an Erlenmeyer flask. A close up of the density separation (right) shows the lighter minerals floating and the denser ones on the bottom.

The samples were left for 5-10 minutes and occasionally stirred to ensure separation. The light and heavy grains were washed separately using a funnel with a filter rinsed with acetone over an Erlenmeyer flask under vacuum. The grains were washed thoroughly with acetone changing filters as appropriate.

4.3.7 Scanning Electron Microscope

A scanning electron microscope (SEM) (FEI QUANTA 600F, Thermo Fisher Scientific, Hillsboro, OR) was used to examine two of the selected soil samples and identify potential As containing minerals including Fe oxides and possible authigenic pyrite. The SEM forms a focused beam that scans a sediment sample. When the beam scans the sediment, several signals form including secondary electrons, backscatter electrons, auger electrons, and X-rays. The secondary electrons are used to form the image while the X-rays

`

are recorded as an energy dispersive X-ray spectrum. The X-rays, which are given off by the sample show the chemical composition of the sample which is used to identify specific minerals present.

Only the heavy grains from samples T7 at 13.7 m depth and 2b at 11.2 m depth (Figs. 3, 4) were examined using SEM. A small quantity of each sample was placed onto an SEM stub using conductive tabs 1 cm in diameter. A coating of platinum was applied to both samples. The platinum prevents charge build up and heat from electrons hitting the surface. The results from SEM are usually obtained from experienced use of the instrument and identifying minerals from several locations. Minerals were identified using elemental abundance and mineralogical textures observed with the SEM.

4.4 DNA Analysis & Microbial Community Analysis

In the field, about 1.5-2 L of water from selected wells and drive-point piezometers from Veast were passed through 0.2 μm paper filters under a vacuum using sterile bottles. DNA extractions were performed on water filters from the field in the laboratory at TAMU using a Power Soil DNA Isolation Kit (MO BIO Laboratories, Inc. Carlsbad, CA). Filters were cut into small pieces using a sterile exacto knife and added to the DNA extraction tubes (Knappett et al., 2012). The extraction kit came with all the necessary buffers, equipment, and step-by-step instructions. After the DNA was successfully extracted, the quality and concentration of extracted DNA was measured using a Thermo Scientific NanoDrop 1000 Spectrophotometer (Thermo Scientific, Wilmington, DE).

Extracted DNA from the following Veast samples: T1, T3, T4, T6, T6A, DP2A, DP2B, DP3A, DP3B, and Meghna River (Fig. 3) were sent to Molecular Research Laboratory (Mr. DNA, LP Shallowater, TX). DNA from the 27F-592R region of the 16S

`

rRNA gene was sequenced using universal primers on an Illumina MiSeq platform. DNA libraries were prepared using Nextera DNA sample prep kits to construct individual barcode indices and at least 0.8 gigabases of nucleotide sequence was generated. Samples were amplicon sequenced using MG-RAST metagenome analysis server. The resulting DNA sequences were compared to the BlastX protein databases and predicted genes were classified into functional categories from individual genes to cellular possesses. Gene abundance was calculated for each taxonomic rank by dividing the similarity hits for an individual gene by total hits against any in the database.

The operational taxonomic rank from the genus level was utilized in an open source statistics program PAleontological STatistics (PAST), version 3.15 (Oyvind Hammer, David A. T. Harper, Paul D. Ryan, Paleontological Association) to construct alpha rarefaction curves, multivariate plots including ANOSIM (ANalysis Of SIMilarities), and principal components analysis (PCA).

An analysis of similarities (ANOSIM) is a non-parametric statistical test that measures the significant difference between two or more groups based on a measure of distance (Clarke, 1993). The test is based on calculating and comparing distances between groups. The test statistic R is defined by the following equation:

$$R = \frac{r_b - r_w}{N(N-1)/4} \qquad \text{(Eq. 5)}$$

Where r_b is the mean rank of all the distances between groups and r_w is the mean rank of all distances within groups. The one-tailed significance is calculated by permutation of group membership (N).

`

A principal components analysis (PCA) calculates the directions of a reduced number of Principal Components (PCs) which are orthogonal to each other in multi-variate space. That is, the correlation between two PCs is zero. Each PC is a linear combination of “real” parameter values (Davis, 1986, Harper, 1999). One common application of PCA is to reduce the dimensionality of a multi-variate data set into a small number of PCs which capture a high percentage of the overall variability in the data set. This usually works because many parameters are strongly correlated to each other and therefore, knowing the exact values of each parameter is commonly not as important as knowing the value of that sample plotted along the PC that represents that grouping of real parameters. These values along a PC are known as PC scores. Once the PC scores for the PC which describes the most variability in the data set (PC1) are plotted against the PC describing the next greatest variability in the data set (PC2), groupings of samples commonly appear. The greater the collinearity between the various parameters in a data set, the higher percentage of the overall variability can be explained by the first two or three PCs. This increases the efficacy of this method for visualizing clustering of samples. For this experiment PCA was used for reduction of the DNA sequencing data set to two variables represented by the first two components.

4.5 Geochemical Modeling

A two-endmember mixing model was developed to calculate the remaining groundwater along the discharge flow path within the riverbank aquifer with increasing degrees of mixing with river water as the flow path approaches the river bottom. Eq. 6 calculates the groundwater remaining in the aquifer:

$$f_{gw} = \frac{[TRAC]sample - [TRAC]river}{[TRAC]gw - [TRAC]river} \qquad \text{(Eq. 6)}$$

`

where f_{gw} is the fraction of remaining groundwater, $[TRAC]_{river}$, $[TRAC]_{sample}$, and $[TRAC]_{gw}$ represents the conservative tracer concentrations in the Meghna river, well water sample of interest, and the groundwater endmember respectively. The monitoring well farthest from the river (T1) and the Meghna River samples were used to represent the groundwater endmembers. The numerator in the equation consists of the tracer concentration of the well sample of interest subtracted from the surface water concentration. This is divided by the tracer concentration of monitoring well T1 minus the Meghna River concentration. This calculation was performed on all of the monitoring wells and drive-point piezometers at the Veast and Vwest North study sites.

Once the fraction of groundwater is calculated for each water sample, excess elemental concentrations can be calculated using Eq. 7. This equation quantifies the concentrations of elements and compounds such as As, Fe, or NH_4^+ being removed or released along the groundwater discharge flow path towards the river. Eq. 7:

$$[X]_{excess} = \frac{[X]sample-[X]river}{[X]gw-[X]river} - f_{gw} \qquad \text{(Eq. 7)}$$

where $[X]_{excess}$ is the element concentration in excess within a well along the groundwater flow path, $[X]_{river}$, $[X]_{sample}$, and $[X]_{gw}$ represent the element concentration in the Meghna River, groundwater well along a discharge flow path, and the groundwater endmember at the beginning of the observed discharge flow path respectively. This calculation was applied to all the element concentrations measured by the IC and ICP-MS at both well transects. Using Fe as an example, if the excess element calculation for Fe is a positive number, then Fe is being released. If excess Fe is negative, then Fe is being removed.

`

To further validate these results the calculations in Eq. 6 and Eq. 7 were performed using three conservative and potentially conservative tracers: chloride (Cl^-), silicon (Si), and the sum of four major cations expressed as total cationic charge (meq) (∑[Na^+], [K^+], 2x[Mg^{2+}], and 2x[Ca^{2+}]), which were expected to compare to total alkalinity in areas where weathering rates were nominal (Jung et al., 2015). These calculations were applied to all of the monitoring wells and drive-point piezometers at both study sites. The Si and the sum of major cations fraction of groundwater calculations were more similar to one another than to the Cl^- results. This, in addition to concentration fluctuations in Cl^- along the groundwater flow path at Veast suggested that Cl^- may not be an optimal tracer for these study sites. Silica isn't an optimal choice as a tracer since it's commonly found in most minerals and Si is often left behind when minerals are weathered away. Therefore, for this study the major cation calculations are the best tracers to use. Jung et al., (2015) came to a similar conclusion, working 10 km south of the Veast field site.

Geochemist's Workbench Student Edition, Version 11.0.4 (Aqueous Solutions LLC, Champaign, IL) was used to construct Eh-pH phase diagrams showed what compounds to expect in what phase. The Eh-pH results from the monitoring wells and drive-point piezometers were displayed on the diagrams to show which elemental phases were likely occurring at each well. Eh values were calculated by adding 200 mV to the ORP values obtained from the field (YSI Environmental).

PH Redox EQuilibrium (PHREEQC) software, Version 3.3.7-11094 (United States Geological Survey, Reston, VA) was used to calculate expected mineralogy and saturation indices (SI) given measured solution concentrations and assuming thermodynamic

`

equilibrium, using four databases in the PHREEQC environment: minteq, minteq.v4, phreeqc, and wateq4f. The purpose of this model was to show how the chemical environment fluctuates at each well and drive-point piezometer for minerals potentially present. Eq. 8 was used to calculate pe values for the model:

$$pe = \frac{Eh*F}{2.303*R*T} \quad \text{(Eq. 8)}$$

where Eh is the electron activity [mV], F is Faraday's constant [cal/V], R is the gas constant [cal/degree], and T is temperature [K]. Since PHREEQC models thermodynamics and not kinetics, it may not be able to predict the dominant reactions or species of reactive ions across a riverbank aquifer with rapidly changing redox conditions in time and space. Whereas PHREEQC may not predict actual reactions, since many reactions do not reach equilibrium, it will predict the prevailing thermodynamically favorable reactions at a given point along the flow path, which can inform possible mechanisms responsible for observed elements being released or removed along the flow path (Eq. 7). Lastly, the kinetics of the reactions are strongly affected by the *in-situ* bacteria that mediate redox transformations, or produce local increases or decreases in pH that induce weathering, which is not considered in the basic PHREEQC models. In order to gain an understanding of the role of microorganisms in the geochemical transformations along the Veast aquifer transect, specific bacteria known to facilitate reduction and oxidation of As and Fe were analyzed along the flow path to gain further insight into biogeochemical controls on release or removal rates of elements within the mixing zone.

The PhreeqC database didn't have the option to input dissolved As concentrations. The minteq and minteq.v4 databases calculated a pH of 10, which is not an accurate

`

representation of the study sites, therefore these results were not considered further. The wateq4f database had the option to input aqueous As concentrations and calculated the pH to be 7, which more accurately reflects measured groundwater pH at the study sites. Thus, the wateq4f database fit best with the environmental parameters at the study sites and was used in this project.

`

5. RESULTS

5.1 Results from the Field

5.1.1 Aqueous Geochemistry

Geochemical profiles were constructed from two well transects, Veast and Vwest North (Figs. 2, 3, 4) perpendicular to the Meghna River. Table 4 shows the concentrations of dissolved elements and compounds along the groundwater discharge flow path at Veast, monitoring well T1 is located furthest from the river, 86 m away from the shoreline during low, neap-tide in the dry season. Drive-point piezometers DP 3A and DP 3B were installed 11 m from the low, neap-tide river edge, in the river (Figs. 3, A1). The pH remained near neutral and the water temperature varied 21-27℃ with distance from the river. At Veast, alkalinity increased from 51 to 315 mg/L with distance from the river. Dissolved oxygen measurements were likely overestimated, perhaps due to extra air getting into the peristaltic pump and from air getting pushed down when the drive-point piezometers were installed. However, even the act of filing a vial for analysis likely introduced oxygen.

Total As varied from 0-0.5 mg/L in concentration, generally decreasing closer to the river in the drive-point piezometers. Arsenic was not detected in the river water. Iron concentrations consistently decreased in the monitoring wells along the deeper aquifer flow path with proximity to the river (15-26 mg/L), but Fe concentrations suddenly increased up to 28 mg/L in some of the drive-point piezometers near the groundwater discharge point at the river's edge. Manganese concentrations varied from 2.4 to 1.6 mg/L in the monitoring wells but had some sudden concentration increases, up to 5.8 mg/L in the drive-point piezometers at the . Some measurements for phosphate, nitrate, and sulfate were taken in the field, but not enough to create a complete geochemical profile.

Table 4: Aqueous geochemistry results measured in the field at Veast. N/A = not analyzed.

Well Name	Well Depth (m)	Temperature (° C)	Specific Conductivity (µS/cm)	pH	Oxidative Reductive Potential (mV)	Alkalinity (mg/L)	Arsenic (mg/L)	Iron (mg/L)
T1	16.8	26.4	699.0	6.9	-160.9	315.0	0.5	26.7
T2	16.8	26.7	577.0	7.0	-179.7	352.0	0.5	24.7
T3	16.8	26.9	601.0	7.0	-193.2	292.0	0.5	23.2
T4	16.2	27.0	560.0	7.0	-197.2	261.0	0.5	21.4
T5	14.6	26.9	527.0	7.1	-198.5	252.0	0.3	17.3
T6	13.7	26.9	528.0	7.1	-218.3	206.0	0.5	15.5
T6A	6.0	27.0	471.2	6.9	-183.0	N/A	0.3	21.3
DP 2A	1.2	23.4	483.0	6.9	-154.8	187.0	0.3	11.6
DP 3A	1.2	24.1	452.2	6.8	-52.5	243.0	0.2	15.5
DP 2B	3.2	26.8	364.4	6.6	-34.6	170.0	0.2	28.1
DP 3B	3.2	24.0	231.3	6.8	-61.5	100.0	0.2	1.8
River	0.0	21.3	108.2	7.6	26.7	51.0	0.0	0.0

Well Name	Ammonia (mg/L)	Sulfides (mg/L)	Manganese (mg/L)	Dissolved Oxygen (mg/L)	Nitrate (mg/L)	Phosphate (mg/L)	Sulfate (mg/L)
T1	0.4	0.2	1.6	0.12	6.5	N/A	N/A
T2	7.0	0.1	1.7	0.06	10.7	N/A	N/A
T3	7.4	0.1	2.4	0.09	9.5	N/A	N/A
T4	0.0	0.2	1.8	0.4	19.8	3.0	49.2
T5	1.4	0.1	1.9	0.13	26.0	3.1	44.8
T6	N/A	0.1	2.0	0.49	N/A	N/A	N/A
T6A	N/A	0.2	1.4	0.07	N/A	N/A	N/A
DP 2A	0.3	0.2	5.8	0.02	N/A	3.6	28.0
DP 3A	4.8	0.2	2.3	0.03	4.6	0.4	N/A
DP 2B	0.8	0.2	2.9	0.03	8.3	1.8	N/A
DP 3B	3.6	0.1	2.2	0.12	6.5	1.6	N/A
River	0.0	0.2	0.4	7.83	7.6	N/A	9.6

Aqueous geochemical tests were obtained from the field at Vwest North (Table 5). Monitoring well 3b is furthest from the river, 78 m away from the shoreline during the dry season (Fig. 4). The pH values were near neutral and the water temperature was consistently 26°C until the river water which was 21°C. Arsenic concentrations remained at 0.3 mg/L until the river water where As was not detected. Iron concentrations varied from 0.3-4.5 mg/L and then increased to 12.1 mg/L in the drive-point piezometer. Manganese concentrations did not change substantially (0-1.8 mg/L) in the Vwest North transect.

Table 5: Aqueous geochemistry results collected from the field at Vwest North. The compound concentrations were measured using field test kits. N/A = not analyzed.

Well Name	Well Depth (m)	Temperature (° C)	Specific Conductivity (µS/cm)	pH	Oxidative Reductive Potential (mV)	Alkalinity (mg/L)	Arsenic (mg/L)	Iron (mg/L)
DP 1	3	26.2	228.2	6.9	-84.3	203.0	0.0	12.1
1a	7	26.4	300.6	6.9	-99.0	120.0	0.3	1.0
1b	15	26.5	463.8	6.9	-37.7	255.0	0.3	4.5
2a	7	26.6	295.0	6.9	-27.0	155.0	0.3	0.3
2b	15	26.5	459.1	6.9	21.3	232.0	0.3	1.6
3b	15	26.1	344.2	6.8	-8.2	171.9	0.3	1.1
Well Name	**Ammonia (mg/L)**	**Sulfides (mg/L)**	**Manganese (mg/L)**	**Dissolved Oxygen (mg/L)**	**Nitrate (mg/L)**	**Phosphate (mg/L)**	**Sulfate (mg/L)**	
DP 1	0.6	0.1	1.3	1.7	5.6	N/A	N/A	
1a	1.2	0.2	0.8	4.1	2.1	N/A	N/A	
1b	1.8	0.2	0.0	0.8	2.7	N/A	N/A	
2a	1.3	0.1	0.8	1.9	2.1	N/A	N/A	
2b	1.5	0.1	0.9	3.0	2.3	N/A	N/A	
3b	1.0	0.0	1.8	1.9	2.3	N/A	N/A	

Important spatial trends were observed in some of the chemical field parameters including alkalinity, ORP, and SC (Fig. 9) at the Veast well transect. The concentration values are shown in the y-axis and the x-axis displays the well distance away from the river. Drive-point piezometers DP 2A and DP 2B were located at the low, neap-tide, river shoreline so their distance from the river is reported as zero. Drive-point piezometers DP 3A and DP 3B were reported ~10 m from the shoreline.

Along the entire groundwater discharge flow path at Veast, alkalinity decreased with proximity to the river. Concentrations varied from 51-352 mg/L (Fig. 9c). The same spatial

`

trend was seen with the temperature (Fig. 9b) and the SC (Fig. 9d). Along the deeper groundwater flow path, the SC for the monitoring wells varied from 471 µS/cm to 699 µS/cm; whereas concentrations along the discharge point in the drive-point piezometers varied from 108 µS/cm to 483 µS/cm. Oxidative reductive potential measurements for the monitoring wells varied from -218 mV to -161 mV and ranged from -155 mV to 27 mV for the drive-point piezometers and the river water.

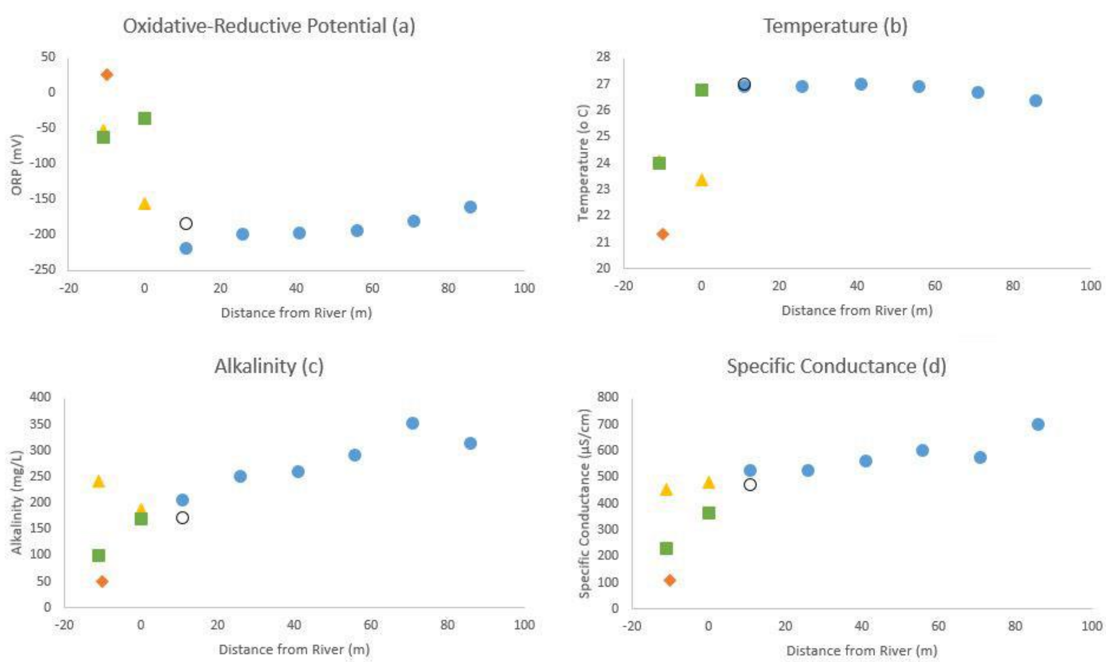

Figure 9: Physical-chemical parameters measured in the field from Veast. The blue circles, hollow circles, green squares, yellow triangles, and orange diamond represent 15 m monitoring wells, 7 m monitoring well, 3 m and 1 m drive-point piezometers, and river water respectively.

Strong spatial trends in alkalinity, ORP, and SC were observed at Vwest North (Fig. 10). Alkalinity increased with proximity to the river in the deeper groundwater flow path in

`

the 15 m monitoring wells (172-255 mg/L), but decreased with proximity to the river in the shallower 7 m wells and the 3 m drive-point piezometer (120-203 mg/L). The temperature remained consistent at 26℃ until the river (21℃) (Fig. 10b). Specific conductance concentrations in the deeper 15 m monitoring wells (463-344 µS/cm) were greater than the shallower 7 m monitoring wells (295-300 µS/cm). Oxidative-reductive potential decreased with proximity to the river (-99-21 mV) compared to 27 mV in bulk river water collected several meters from shore.

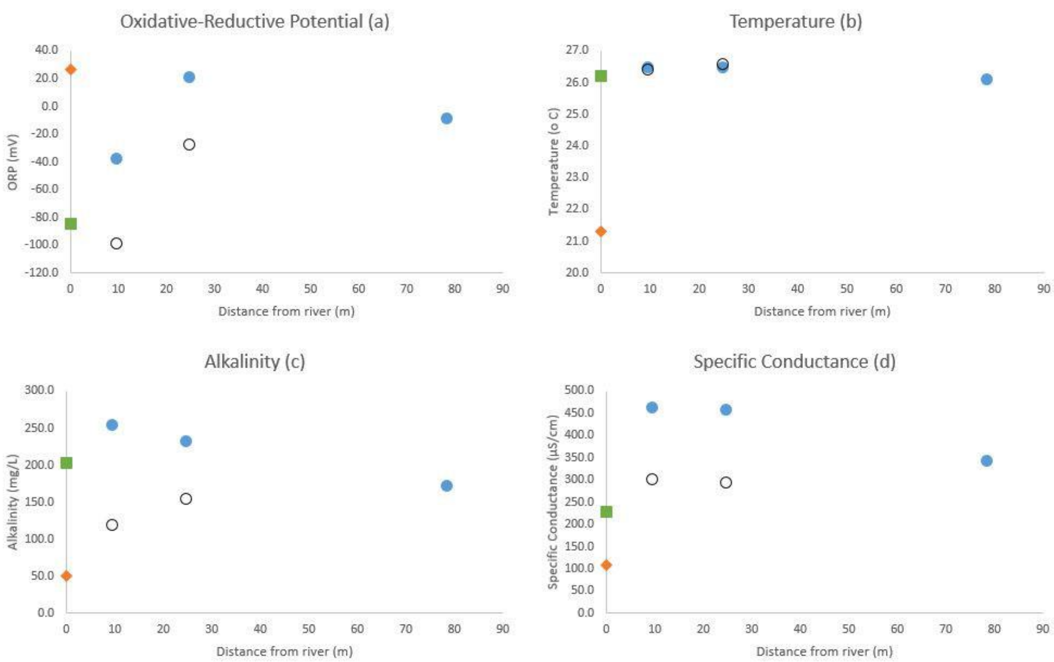

Figure 10: Physical-chemical parameters measured in the field from Vwest North. The blue circles, hollow circles, green square, and orange diamond represent 15 m monitoring wells, 7 m monitoring wells, 3 m drive-point piezometer, and river water respectively.

`

5.1.2 Field-based Solid-phase Geochemical Analyses

A 17 m borehole (T7) was drilled at the Veast study site to describe the general, bulk solid-phase geochemistry of the aquifer adjacent to the river. Concentrations of solid-phase As, Fe, and Mn varied with lithology and depth (Fig. 11). At borehole T7 increases in As, Fe, and Mn concentrations were observed at 3 and 12 m depths. Whereas the former concentration increase occurred in a clay layer, the latter occurred within a medium coarse sand layer.

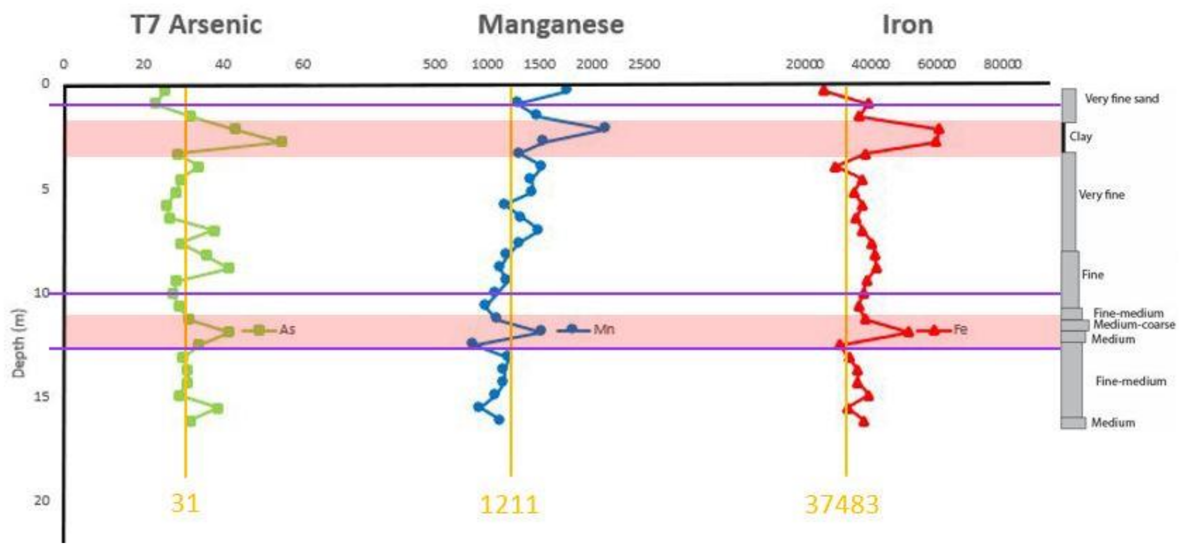

Figure 11: XRF results from borehole T7 at Veast. The green squares, blue circles, and red triangles represent As, Mn, and Fe concentrations (mg/kg) respectively. The vertical yellow lines and numbers (mg/kg) represent the median concentration for the borehole. The horizontal purple lines represent the depths at which sediments underwent XRD. The shaded red boxes indicate important sharp increases in As, Mn, and Fe concentrations.

Solid-phase geochemistry was studied on three boreholes were excavated at Vwest North, however these boreholes were excavated to install new monitoring wells (Fig. 4). Borehole 1b had exhibited extensive variation in As, Fe, and Mn concentrations (Fig. 12).

`

Extensive variation in lithology including clay, silt, and sand layers was also observed. An increase in As, Mn, and Fe concentrations were observed in the >1 m clay layer lining the upper surface of the riverbank and in a silt/clay layer at 0.9 m depth (Fig. 12).

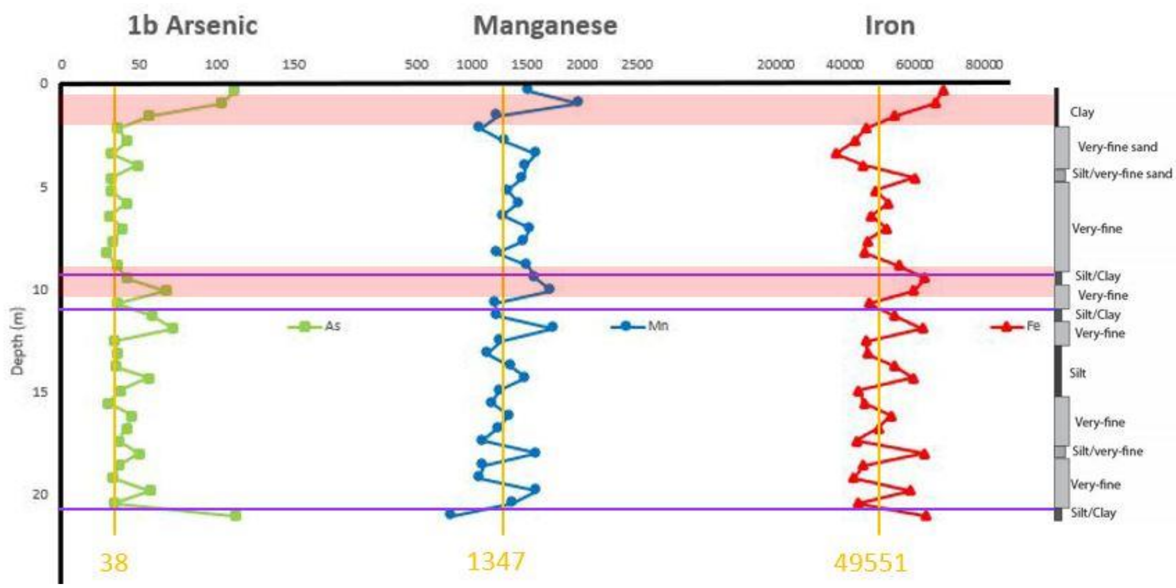

Figure 12: XRF results from the newly installed 1b monitoring well at Vwest North. The green squares, blue circles, and red triangles represent As, Mn, and Fe concentrations (mg/kg) respectively. The vertical yellow lines and numbers (mg/kg) represent the median concentration for the borehole. The horizontal purple lines represent the depths at which sediments underwent XRD. The shaded red boxes indicate important sharp increases in As, Mn, and Fe concentrations.

Borehole 2b, which is positioned further away from the river than 1b and possessed less variability in sediment and As, Fe, Mn concentrations than borehole 1b (Fig. 13). Borehole 2b contained mostly very fine sand with some silt/clay layers. Increases in As, Fe, and Mn concentrations were observed at 9 m depth in a silt/clay layer and at 13.5 m in a very fine sand layer shortly before a silt/clay layer. Borehole 2b on average had the highest As, Fe, and Mn concentrations out of the four excavated boreholes (refer to the yellow median concentrations in Figs. 11, 12, 13, 14).

`

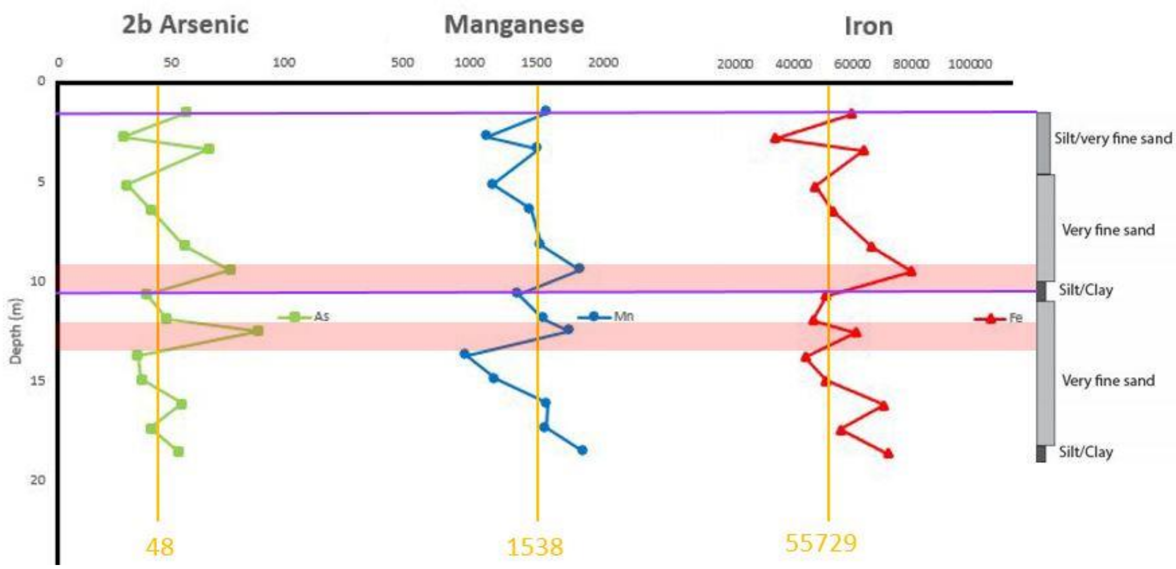

Figure 13: XRF results from the newly installed 2b monitoring well at Vwest North. The green squares, blue circles, and red triangles represent As, Mn, and Fe concentrations (mg/kg) respectively. The vertical yellow lines and numbers (mg/kg) represent the median concentration for the borehole. The horizontal purple lines represent the depths at which sediments underwent XRD. The shaded red boxes indicate important sharp increases in As, Mn, and Fe concentrations.

Of the three boreholes drilled at Vwest North, borehole 3b was the most homogeneous (Fig. 14). Thus, there is a trend of increasing heterogeneity and decreasing sediment layer thickness towards the river. An increase in As, Fe, and Mn concentrations was observed in the very fine sand with organic particles at approximately 3 m depth within borehole 3b. Detrital organic particles consisting of leaf and wood litter were observed at borehole 3b at depths 3.4 m, 5.8 m, 7.9-9.1 m, 18 m, and 20.4 m. Increases in As, Fe, and Mn concentrations were observed at approximately 8 m depth in a very fine sand layer containing organic particles, 11 m in the very fine sand, and at 18 m in a very fine sand layer containing organic particles.

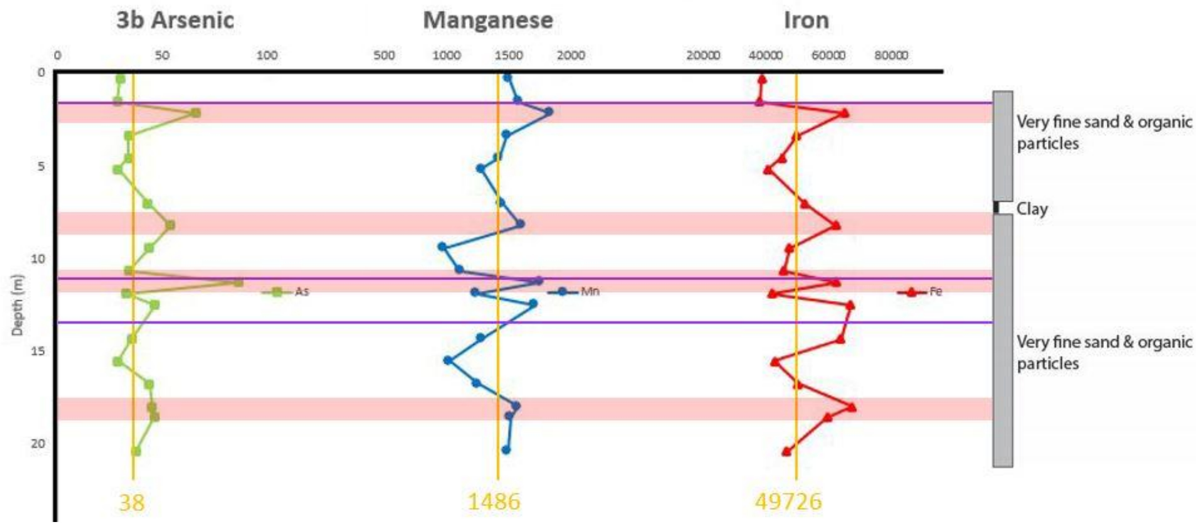

Figure 14: XRF results from the newly installed 3b monitoring well at Vwest North. The green squares, blue circles, and red triangles represent As, Mn, and Fe concentrations (mg/kg) respectively. The vertical yellow lines and numbers (mg/kg) represent the median concentration for the borehole. The horizontal purple lines represent the depths at which sediments underwent XRD. The shaded red boxes indicate important sharp increases in As, Mn, and Fe concentrations.

Borehole lithology at Vwest North became increasingly heterogeneous <1 km with proximity to the river. On average borehole 2b contained the highest As, Mn, and Fe concentrations. At boreholes 1b and 3b, the median As, Mn, and Fe concentrations ranges were 38 mg/kg, 1,347-1,486 mg/kg, and 49,551-49,726 mg/kg respectively. Borehole 2b contained higher median As, Mn and Fe concentrations (48 mg/kg, 1,538 mg/kg, and 55,729 mg/kg respectively). Borehole T7 at the Veast study site contained the lowest median As, Mn, and Fe concentrations of 31 mg/kg, 1,211 mg/kg, and 37,483 mg/kg respectively. All four boreholes at both study sites contained an increase in As, Mn, and Fe concentrations within a clay layer 0-3 m in depth. Most of the significant increases in As, Mn, and Fe concentrations occurred in silt/clay layers and one in a medium coarse sand layer in the T7

`

borehole at Veast. Increases in As, Mn, and Fe concentrations occurred in very fine sand lithology containing organic particles.

5.2 Aqueous Geochemical Results

5.2.1 Aqueous Geochemistry

Water samples collected from wells, drive-point piezometers and river water. Cation and anion concentrations were analyzed for aqueous phase constituents, to complement geochemical data obtained from aquifer solids. Cation and anion concentrations were obtained from Ion Chromatography (IC) (Table 6) for the Veast well transect. Fluoride concentrations from Veast were low and did not change much (0.2-0.4 mg/L) with proximity to the river.

`

Table 6: IC aqueous geochemistry anion and cation results from Veast. BDL = Below Detection Level.

Well Name	Fluoride (mg/L)	Chloride (mg/L)	Bromide (mg/L)	Nitrate (mg/L)	Nitrite (mg/L)	Sulfate (mg/L)	Phosphate (mg/L)
T1	0.4	20.0	BDL	5.6	2.8	BDL	BDL
T2	0.3	4.5	BDL	BDL	7.2	BDL	BDL
T3	0.4	8.4	BDL	BDL	3.4	BDL	BDL
T4	0.3	10.7	BDL	BDL	2.7	BDL	BDL
T5	0.3	11.0	BDL	BDL	2.5	BDL	BDL
T6	0.4	7.3	BDL	0.1	2.8	BDL	BDL
T6A	0.3	16.5	BDL	0.1	5.3	BDL	BDL
DP 2A	0.3	34.3	BDL	BDL	4.9	BDL	BDL
DP 3A	0.2	9.4	BDL	0.4	1.9	BDL	BDL
DP 2B	0.3	18.4	BDL	BDL	3.9	BDL	BDL
DP 3B	0.2	5.4	BDL	0.3	1.3	BDL	BDL
River	0.2	4.1	BDL	1.4	0.2	8.1	BDL

Well Name	Sodium (mg/L)	Ammonium (mg/L)	Potassium (mg/L)	Magnesium (mg/L)	Calcium (mg/L)
T1	14.3	19.7	6.2	22.5	67.5
T2	7.5	11.0	4.9	20.4	63.2
T3	8.2	10.5	5.2	21.4	67.0
T4	7.4	11.3	5.2	19.0	60.4
T5	7.1	10.9	5.2	18.2	62.7
T6	6.9	9.2	4.6	18.1	62.3
T6A	8.2	9.5	3.9	16.3	44.9
DP 2A	12.4	5.9	4.6	15.1	49.9
DP 3A	8.9	7.9	3.8	11.2	61.3
DP 2B	14.3	5.2	3.4	11.2	29.8
DP 3B	7.5	6.1	2.9	8.1	21.0
River	7.3	0.0	2.3	4.3	11.0

The fluoride concentrations at Vwest North did not change much with proximity to the river (0-0.3 mg/L) and were low (Table 7). Sulfate concentrations were higher with proximity to the river at 3-7 m depths (13-14 mg/L) and lower further away from the river at 15 m depths (0.2-4 mg/L). Phosphate concentrations were higher at the 7 m depths (3.6-4.2 mg/L) than at the 15 m depths (1.7-3.2 mg/L).

`

Table 7: IC aqueous geochemistry anion and cation results from Vwest North. BDL = Below Detection Level.

Well Name	Fluoride (mg/L)	Chloride (mg/L)	Bromide (mg/L)	Nitrate (mg/L)	Nitrite (mg/L)	Sulfate (mg/L)	Phosphate (mg/L)
DP1	0.2	8.0	BDL	BDL	2.1	14.6	BDL
1a	0.2	10.7	BDL	BDL	0.8	14.0	3.6
1b	0.3	7.3	BDL	BDL	2.0	0.2	1.7
2a	0.3	9.4	BDL	BDL	0.8	13.2	4.2
2b	0.2	2.7	BDL	BDL	6.5	0.2	2.6
3b	0.0	2.7	BDL	0.3	4.1	4.0	3.2

Well Name	Sodium (mg/L)	Ammonium (mg/L)	Potassium (mg/L)	Magnesium (mg/L)	Calcium (mg/L)
DP 1	9.4	0.9	3.1	6.6	19.2
1a	7.9	1.5	3.6	9.7	41.2
1b	10.3	2.1	4.4	15.4	68.0
2a	7.6	1.5	3.5	9.7	41.2
2b	9.2	1.8	4.3	15.3	68.6
3b	8.6	1.3	3.8	12.2	49.2

The As, Fe, and Mn concentrations at Veast obtained using the ICP-MS (Table 8) were similar to those found in the field. The As concentrations were higher (0.4-0.6 mg/L) in the monitoring wells, decreased in the drive-point piezometers (0.1-0.2 mg/L) and was not detected in the river water. Iron concentrations decreased with proximity to the river in the monitoring wells (8.9-19.5 mg/L) and concentrations suddenly increased up to 20 mg/L in the drive-point piezometers. Manganese concentrations ranged 1.5-2.4 mg/L at the 7-15 m depths and increased up to 4.1 at the 3 m depth.

`

Table 8: ICP-MS aqueous geochemistry results for Veast.

Well Name	Fe56 (mg/L)	Mn55 (mg/L)	As75 (mg/L)	Co59 (μg/L)	Ni60 (μg/L)	Cu63 (μg/L)	Zn66 (mg/L)
T1	18.6	1.5	0.4	0.6	1.7	0.2	0.1
T2	19.5	1.7	0.4	0.7	0.8	0.3	0.1
T3	16.0	2.4	0.5	0.7	1.7	0.4	0.3
T4	0.0	1.8	0.1	0.5	0.6	0.1	0.0
T5	10.8	1.7	0.6	0.6	1.1	0.9	0.1
T6	8.9	1.8	0.5	0.5	0.5	0.1	0.1
T6A	15.0	1.6	0.2	0.4	0.6	0.3	0.1
DP 2A	10.2	4.1	0.2	0.1	0.2	0.5	0.1
DP 3A	10.4	1.9	0.2	0.1	0.2	0.1	0.2
DP 2B	20.1	2.7	0.1	0.1	0.1	1.1	0.1
DP 3B	8.2	1.3	0.2	0.3	0.7	0.1	0.1
River	0.0	0.0	0.0	0.0	2.3	1.3	0.1

Well Name	Na23 (mg/L)	K39 (mg/L)	Mg26 (mg/L)	Si30 (mg/L)	Ca43 (mg/L)	S32 (mg/L)	P31 (mg/L)
T1	11.9	4.0	18.0	22.0	57.6	0.07	0.7
T2	6.1	6.4	16.8	16.5	56.9	0.09	0.6
T3	7.0	4.7	18.0	17.3	61.7	0.15	0.2
T4	6.6	14.4	17.1	16.4	57.5	0.07	0.0
T5	5.8	0.0	15.2	16.0	56.1	0.13	0.1
T6	5.6	2.8	14.8	12.6	55.4	0.09	0.2
T6A	6.6	2.6	13.4	24.5	40.3	0.09	1.0
DP 2A	9.0	3.2	12.0	15.2	49.5	0.10	1.7
DP 3A	6.6	2.6	8.7	15.7	51.0	0.08	0.9
DP 2B	8.3	2.3	9.0	20.9	27.2	0.08	0.9
DP 3B	5.1	1.9	6.5	16.7	18.3	0.08	0.8
River	5.7	1.3	3.5	4.1	8.7	2.96	0.0

Well Name	Mo98 (μg/L)	Cd111 (μg/L)	Sb121 (μg/L)	Ba137 (μg/L)	Pb208 (μg/L)	U238 (μg/L)	Al27 (μg/L)	Cr52 (μg/L)
T1	1.0	0.0	0.1	37.0	0.6	0.0	5.0	0.1
T2	2.0	0.0	0.1	40.0	0.1	0.0	58.7	0.1
T3	2.6	0.0	0.0	34.9	0.1	0.0	0.0	0.1
T4	2.3	0.0	0.1	16.3	0.0	0.0	0.0	0.0
T5	2.8	0.0	0.1	28.0	0.2	0.0	15.9	0.2
T6	4.1	0.0	0.0	23.0	0.0	0.0	32.0	0.1
T6A	0.8	0.0	0.1	20.8	1.9	0.0	50.6	0.2
DP 2A	0.4	0.0	0.1	35.8	0.1	0.0	8.8	0.2
DP 3A	0.3	0.0	0.0	28.7	0.0	0.0	10.9	0.1
DP 2B	0.5	0.0	0.1	22.6	0.1	0.0	11.4	0.1
DP 3B	0.7	0.0	0.0	11.0	0.0	0.0	13.2	0.1
River	0.2	0.0	0.1	4.3	0.1	0.1	7.4	0.1

Trace metal and cation results at Vwest North (Table 9) revealed As concentrations of 0-0.2 mg/L. Iron concentrations were higher in the 15 m monitoring wells (0.8-3.7 mg/L) than the shallower 7 m wells (0.3-0.8 mg/L) whereas the highest Fe concentration (9.2 mg/L) was observed at the 3 m depth in the drive-point piezometer. Manganese concentrations were higher in the deeper 15 m monitoring wells (0.6-0.7 mg/L) than the shallower 7 m wells (0.4-0.5 mg/L).

Table 9: ICP-MS aqueous geochemistry results for Vwest North.

Well Name	Fe56 (mg/L)	Mn55 (mg/L)	As75 (mg/L)	Co59 (µg/L)	Ni60 (µg/L)	Cu63 (µg/L)	Zn66 (mg/L)	
DP 1	9.2	1.2	0.0	0.2	0.6	0.1	0.1	
1a	0.8	0.4	0.1	0.3	0.3	0.3	0.1	
1b	3.7	0.6	0.2	0.2	0.2	0.3	0.1	
2a	0.3	0.5	0.2	0.4	0.4	0.2	0.1	
2b	1.5	0.7	0.2	0.3	0.3	0.2	0.1	
3b	0.8	0.6	0.1	0.3	0.3	0.1	0.1	
Well Name	**Na23 (mg/L)**	**K39 (mg/L)**	**Mg26 (mg/L)**	**Si30 (mg/L)**	**Ca43 (mg/L)**	**S32 (mg/L)**	**P31 (mg/L)**	
DP 1	7.4	1.9	5.3	15.8	16.5	4.93	1.6	
1a	5.8	2.5	7.7	17.8	39.8	4.68	1.9	
1b	7.7	3.2	12.2	16.5	57.7	0.17	1.9	
2a	5.6	2.4	7.9	17.9	39.8	4.68	2.0	
2b	7.0	3.0	11.9	17.1	57.5	0.14	2.0	
3b	6.7	2.6	9.9	15.6	48.1	1.31	0.0	
Well Name	**Mo98 (µg/L)**	**Cd111 (µg/L)**	**Sb121 (µg/L)**	**Ba137 (µg/L)**	**Pb208 (µg/L)**	**U208 (µg/L)**	**Al27 (µg/L)**	**Cr52 (µg/L)**
DP 1	0.6	0.0	0.0	15.4	0.1	0.0	4.0	0.1
1a	2.8	0.0	0.0	20.5	0.4	0.1	22.0	0.1
1b	3.4	0.0	0.1	29.6	0.0	0.1	7.4	0.1
2a	2.6	0.0	0.0	23.8	0.2	0.2	8.0	0.1
2b	3.6	0.0	0.0	28.5	0.2	0.4	4.2	0.1
3b	2.1	0.0	0.1	27.4	0.1	0.5	1.5	0.0

`

The DOC concentrations range at Veast were 2.7-7.9 mg/L and the concentration decreased with proximity to the river (Table 10). Total dissolved nitrogen (TDN) concentrations decreased from 12 to 0.5 mg/L with proximity to the river at Veast. The 7-15 m monitoring wells at Vwest North contained DOC concentrations that ranged from 2.1 mg/L to 3.3 mg/L and the TDN concentrations ranged from 0.4-1.4 mg/L (Table 11).

Table 10: DOC and TDN results for Veast.

Well Name	Dissolved Organic Carbon (mg/L)	Total Dissolved Nitrogen (mg/L)
T1	6.1	12.3
T2	6.5	6.7
T3	7.6	6.6
T4	7.9	7.0
T5	7.1	6.9
T6	5.8	5.8
T6A	5.1	6.1
DP 2A	5.3	4.7
DP 2B	4.7	4.9
DP 3A	2.5	3.9
DP 3B	3.0	3.7
River	2.7	0.5

Table 11: DOC and TDN results for Vwest North.

Well Name	Dissolved Organic Carbon (mg/L)	Total Dissolved Nitrogen (mg/L)
DP 1	2.1	0.4
1a	3.3	0.9
1b	2.2	1.4
2a	3.3	0.9
2b	3.1	1.1
3b	3.2	0.8

`

Within the Veast transect As (Fig. 15a) concentrations were highest in the deeper 15 m monitoring wells (0.3-0.5 mg/L) and lowest in the drive-point piezometers and river water (0-0.2 mg/L). Similarly, Fe (Fig. 15b) concentrations decreased with proximity to the river. Manganese (Fig. 15c) concentrations, however, were stable across the groundwater flow path (1.5-2.4 mg/L) in the 7-15 m monitoring wells, but increased sharply to 4.1 mg/L in one of the 1 m drive-point piezometers. Chloride (Fig. 15d) concentrations were highest in well T1 and two of the drive-point piezometers (18-34 mg/L). Elemental silicon (Si) (Fig. 15e) concentrations declined along the deeper 15 m flow path with proximity to the river (12.6-22 mg/L), but abruptly increased in concentration to 21-24 mg/L in the 7 m well and one of the 3 m drive-point piezometers. Dissolved organic carbon (Fig. 15f) concentrations in the 7-15 m deep monitoring wells were higher (5-8 mg/L) than the 1-3 m drive-point piezometer depths (2-5 mg/L).

`

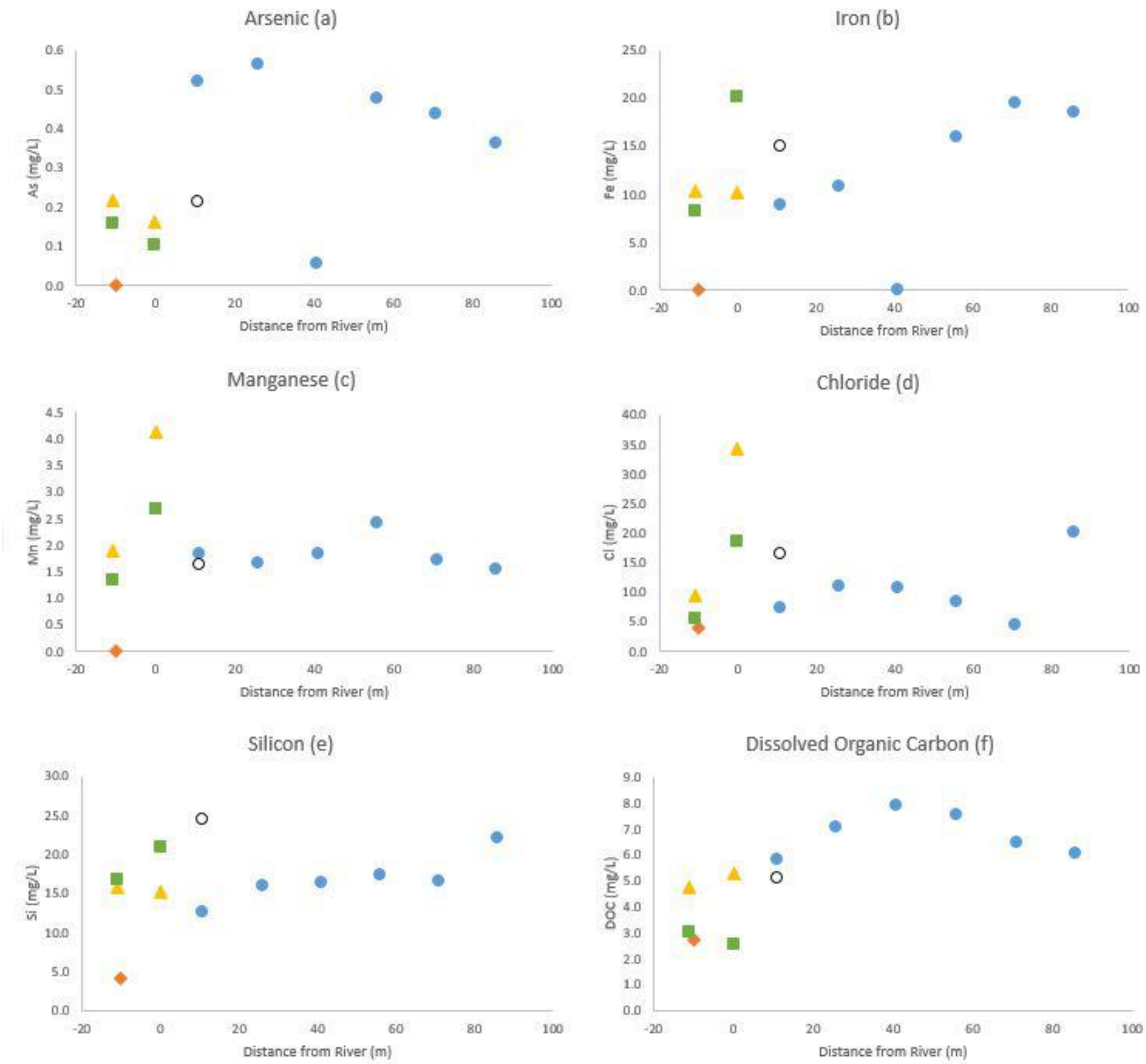

Figure 15: IC, ICP-MS, & DOC results from Veast. The blue circles, hollow circles, green squares, yellow triangles, and orange diamond represent 15 m monitoring wells, 7 m monitoring well, 3 m and 1 m drive-point piezometers, and river water respectively.

At the Veast transect, Ca^{2+} (Fig. 16a) and Mg^{2+} (Fig. 16b) concentrations both decreased with proximity to the river, although Ca concentrations abruptly increased in the 1 m drive-point piezometers. Sodium (Fig. 16c) and K^{+} (Fig. 16d) showed a similar trend to Ca^{2+} and Mg^{2+}; the concentrations were stable, but Na^{+} concentrations abruptly increased at the groundwater discharge point in some of the drive-point piezometers (Fig. 16c). Ammonium (NH_4^+) (Fig. 16e) concentration consistently decreased closer to the river. Nitrite (NO_2^-) (Fig. 16f) was relatively stable along the 15 m deep groundwater flow path but concentrations suddenly increased near the discharge point within the 7 m monitoring well, and the drive-point piezometers.

`

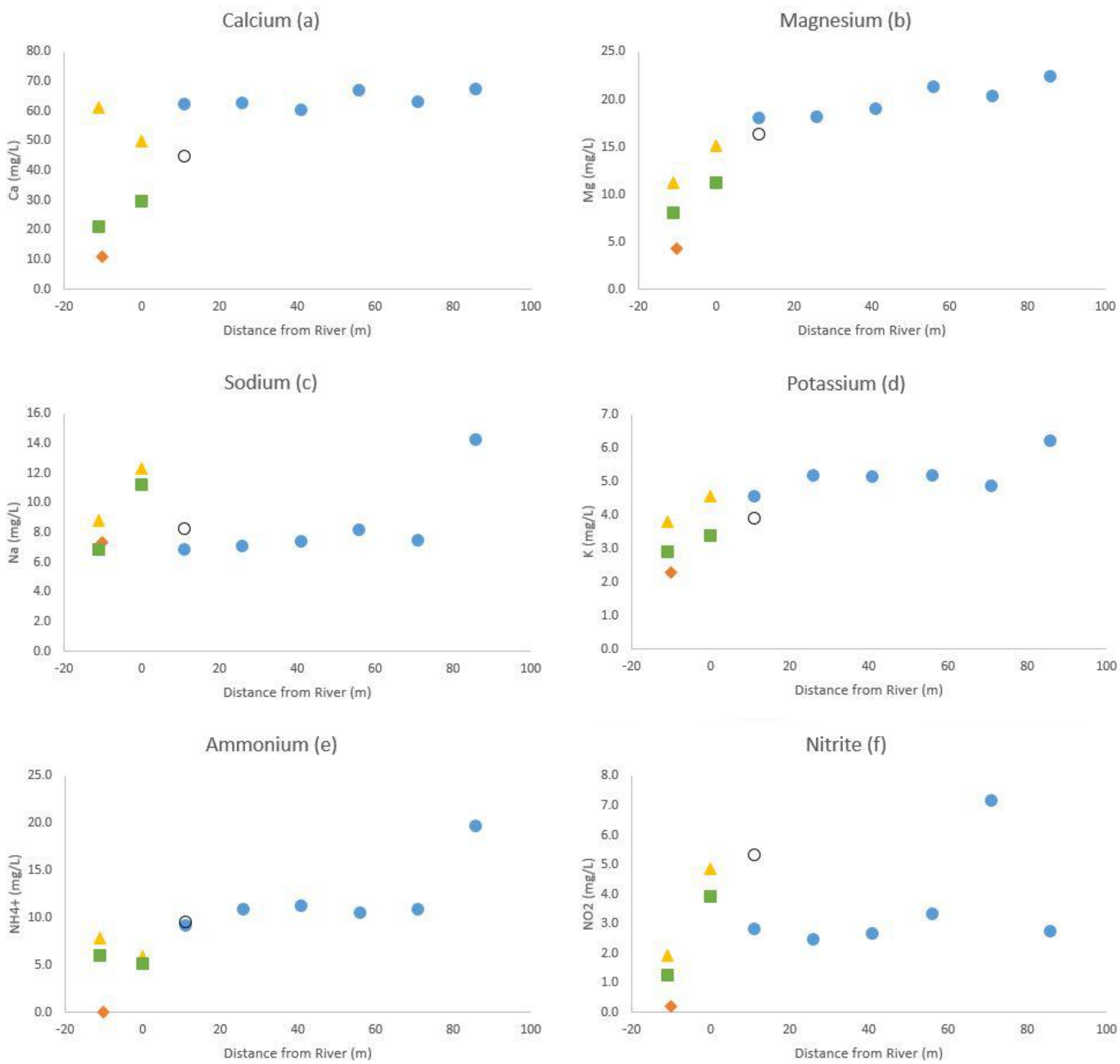

Figure 16: IC results from Veast. The blue circles, hollow circles, green squares, yellow triangles, and orange diamond represent 15 m monitoring wells, 7 m monitoring well, 3 m and 1 m drive-point piezometers, and river water respectively.

Along the Vwest North well transect (Fig. 17), As concentrations were stable (0.2-0.3 mg/L) further away from the river (Fig. 17a). The drive-point piezometer and river water had little to no As detected, similar to the Veast site. Iron (Fig. 17b) concentrations were 0.3-3.7

`

mg/L in the 7-15 m monitoring wells and increased to 9 mg/L in the drive-point piezometer. Manganese (Fig. 17c) concentrations were stable (0.4-0.7 mg/L) until the 3 m drive-point piezometer where the Mn concentration increased to 1.2 mg/L. Chloride (Fig. 17d) concentrations increased towards the river. Silica (e) concentrations were fairly stable (15-17 mg/L) with proximity to the river and depth. DOC (Fig. 17f) concentrations were constant but started to decrease near the discharge point.

`

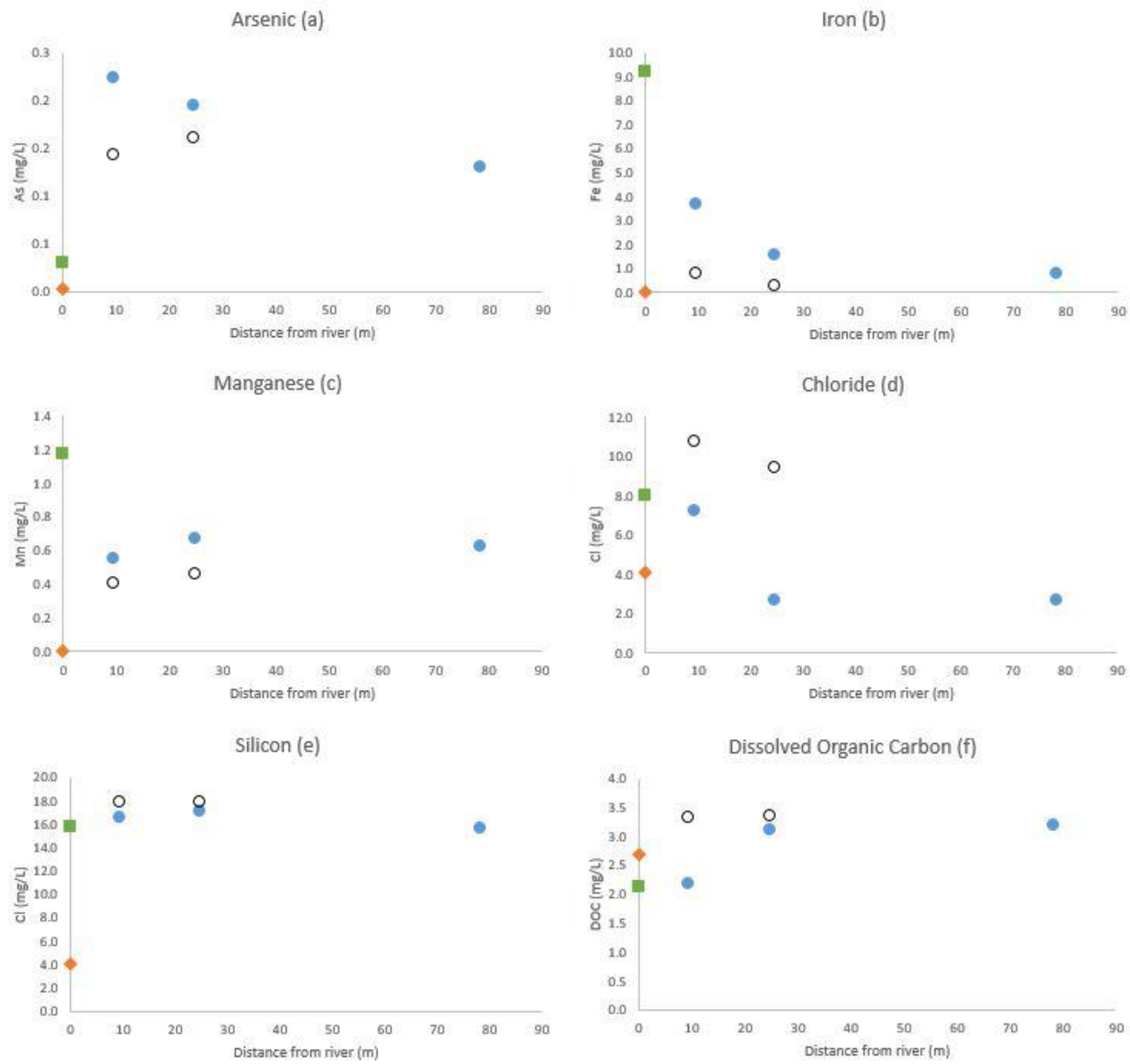

Figure 17: IC, ICP-MS, & DOC results from Vwest North. The blue circles, hollow circles, green square, and orange diamond represent 15 m monitoring wells, 7 m monitoring wells, 3 m drive-point piezometer, and river water respectively.

Within Vwest North, major cations: Ca^{2+} (Fig. 18a), Mg^{2+} (Fig. 18b), Na^{+} (Fig. 18c), and K^{+} (Fig. 18d) concentrations varied substantially with depth (15 m, 7 m, 3 m), but remained stable laterally. Major cation concentrations were highest in the 15 m deep wells,

`

lower in the shallower depths (7 m) and lowest in the drive-point piezometers (3 m). Calcium, Mg^{2+}, Na^+, and K^+ concentrations ranged from 19.2-68 mg/L, 6.6-15.3 mg/L, 7.6-10.3 mg/L, and 3.1-4.4 mg/L, respectively. This is consistent with depth-dependent mixing with the river, which had the lowest major cation concentrations of all. In contrast, ammonium (Fig. 18e) concentrations increased with proximity to the river at the 15 m depths (8.6-10.3 mg/L), but NH_4^+ concentration decreased within the shallower 7 m depths (1.5 mg/L). Nitrite (Fig. 18f) concentration decreased with proximity to the river (0.8-6.5 mg/L).

`

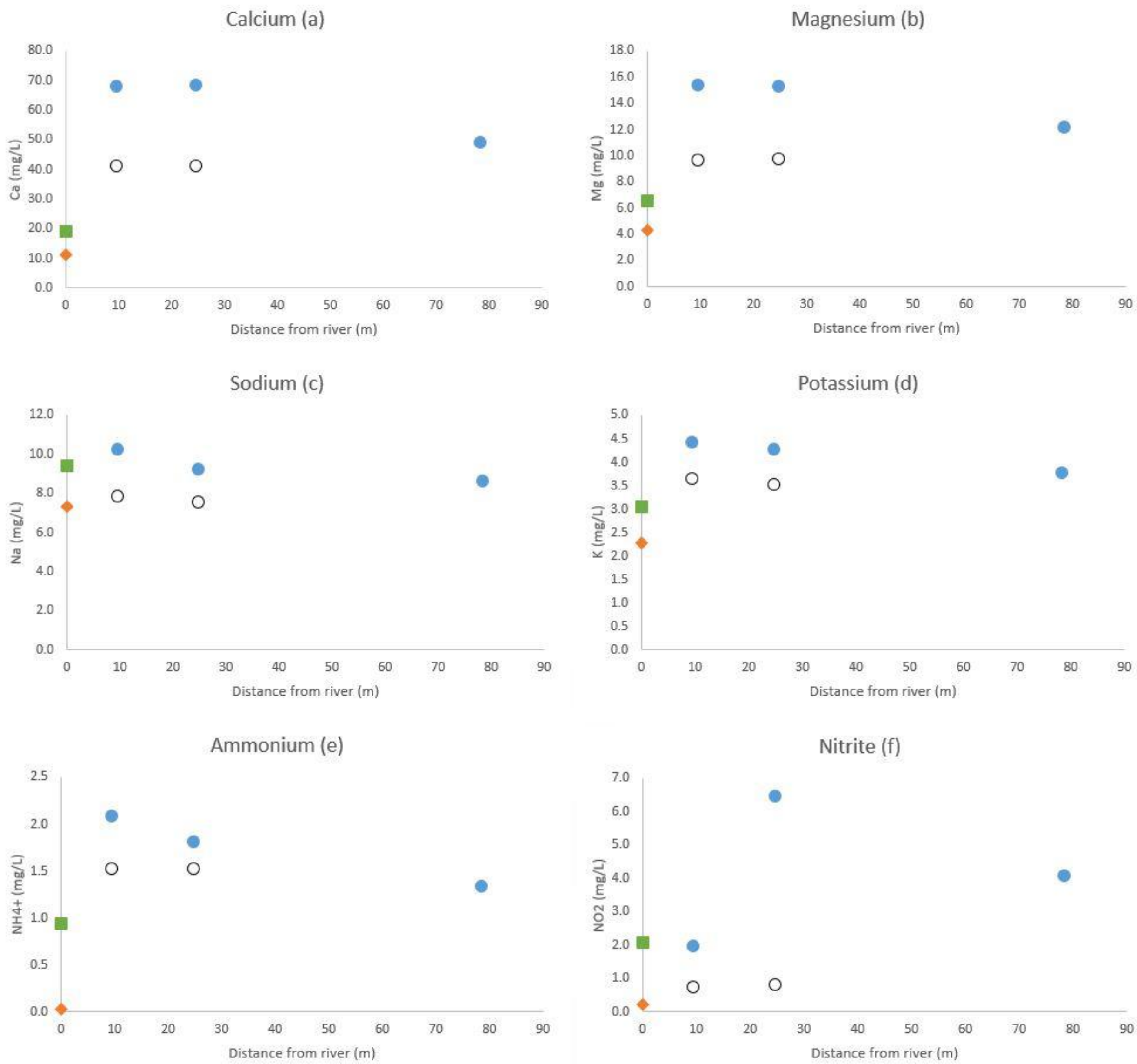

Figure 18: IC results from Vwest North. The blue circles, hollow circles, green square, and orange diamond represent 15 m monitoring wells, 7 m monitoring wells, 3 m drive-point piezometer, and river water respectively.

All of the aqueous geochemistry data collected from the field, IC, and ICP-MS was converted from mg/L to mM (see Tables A1-A6 in appendix). The total cations (Ca^{2+}, Mg^{2+}, Na^{+}, and K^{+}) were further converted from mmol/L to Meq/L and graphed in Figures 19 and 20 for Veast and Vwest North respectively.

`

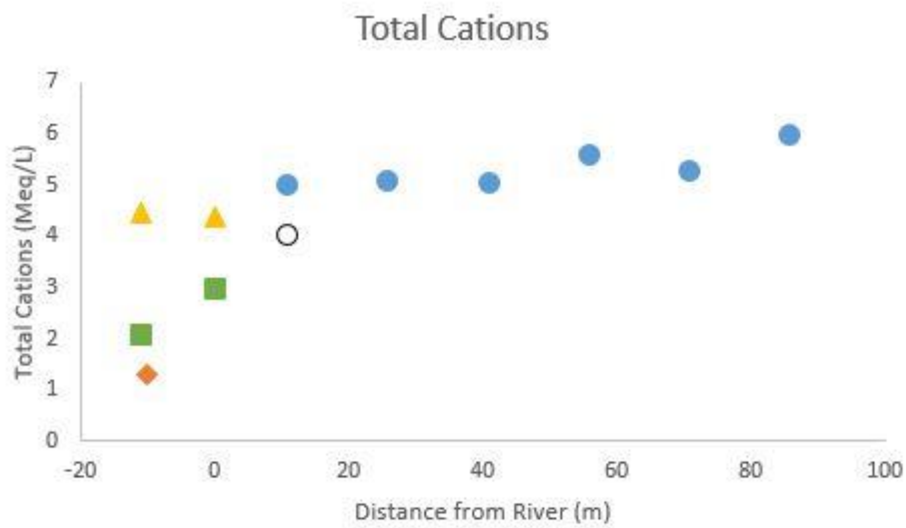

Figure 19: Total cation charge within the Veast monitoring well transect. The blue circles, hollow circles, green squares, yellow triangles, and orange diamond represent 15 m monitoring wells, 7 m monitoring well, 3 m and 1 m drive-point piezometers, and river water respectively.

Figure 19 shows that the total cation charge was constant along the deeper 15 m monitoring wells at Veast. Cation charge within the 1 m drive-point piezometers (4.4-4.5 Meq/L) were similar to those of the deep 15 m wells (5-5.9 Meq/L), whereas cation charge was much lower in the 7 m well (4 Meq/L), the 3 m drive-point piezometers (2-2.9 Meq/L), indicating mixing with the river. It is noteworthy that the 1 m drive-point piezometers were screened within the fine silt layer capping the riverbank aquifer, whereas the 3 m drive-point piezometers were installed below this layer (Fig. 3).

`

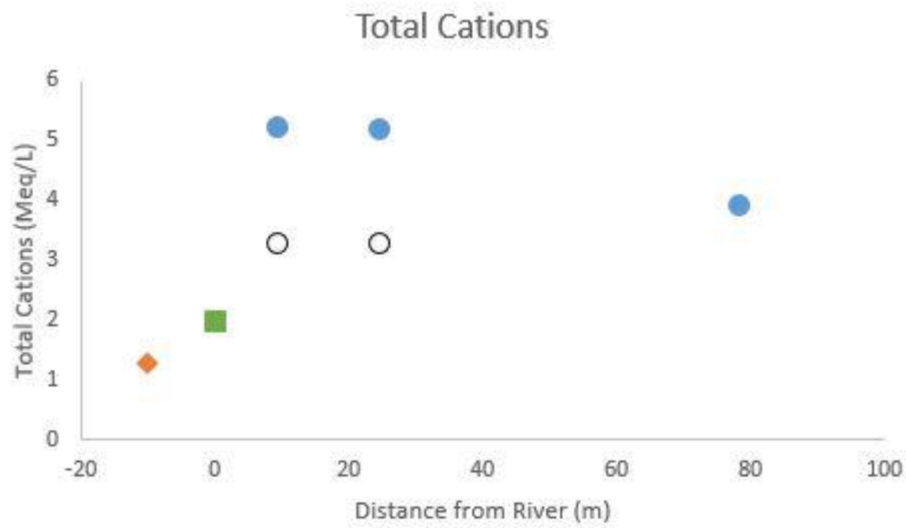

Figure 20: Total cation charge within the monitoring well transect Vwest North. The blue circles, hollow circles, green square, and orange diamond represent 15 m monitoring wells, 7 m monitoring wells, 3 m drive-point piezometer, and river water respectively.

The total cation charge somewhat increased with proximity to the river in the deeper 15 m monitoring wells at Vwest North. Total cation charge was much lower in the 7 m monitoring wells (3.3 Meq/L) than in the 15 m deep wells (3.9-5.2 Meq/L), and decreased even more in the 3 m drive-point piezometer (1.9 Meq/L) towards the level observed in the river. Together, these results suggest the groundwater is progressively diluted by river water with elevation, but not with proximity to the river along the 15 m flow path as with Veast.

5.2.2 Solid-phase Geochemistry

Mineralogy analyses were performed on sediment samples using X-Ray Diffraction (XRD). The y-axis is the number of counts which measures the level of intensity and the x-axis is the diffraction angle (2θ). Figures 21, 22, 23, and 24 show a mineralogical analysis of borehole cutting from T7 at Veast, and 1b, 2b, and 3b from Vwest North respectively. Abundant quartz was identified in all four boreholes along with albite ($NaAlSi_3O_8$), a

`

plagioclase feldspar and kaolinite ($Al_2Si_2O_5(OH)_4$), a clay mineral resulting from albite weathering. Amphibole is a group of inosilicate minerals containing Fe and/or Mg in their structures, hornblende ($(Ca,Na)_{2-3}(Mg,Fe,Al)_5(Al,Si)_8O_{22}(OH,F)_2$) being the most common. Mica ($KAl_3Si_3O_{10}(OH)_2$) , a group of phyllosilicate minerals were also identified in some of the soil samples. Pyrite (FeS_2) was possibly identified in some of the soil samples but this finding could not be confirmed.

In borehole T7 abundant quartz was identified along with some albite (Fig. 21). Some small peaks were identified as pyrite at 13.7 m however, due to the peaks being so small this finding could not be confirmed. Borehole 1b mainly contained quartz with some albite. A small peak for mica was identified at 0.9 m depth (Fig. 22). Borehole 2b at Vwest North was mainly comprised of quartz and albite. A small peak identified as mica was identified at 11.2 m depth (Fig. 23). Borehole 3b mineralogy results showed mostly quartz and albite (Fig. 24). Mica, amphibole, and kaolinite were identified at 11.2 m. The XRD bulk results for boreholes T7, 1b, 2b, and 3b yielded similar mineralogy despite different locations and distances from the Meghna River.

`

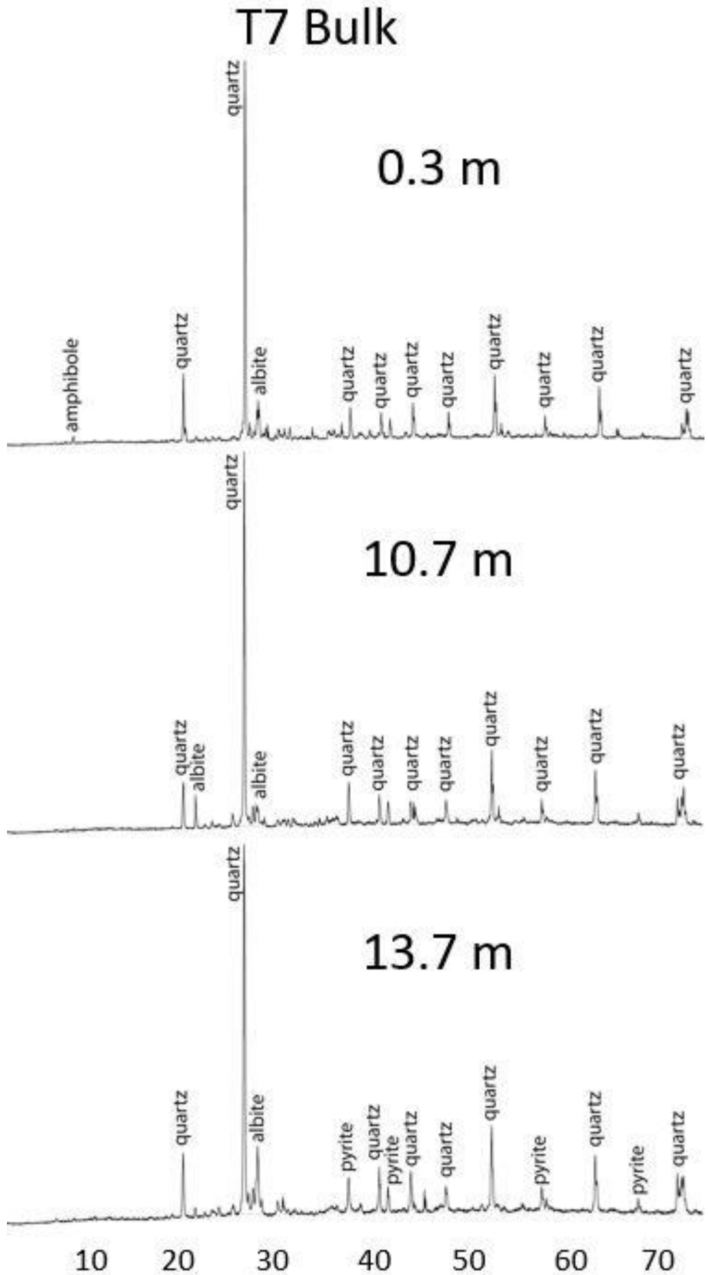

Figure 21: X-ray diffraction results for Veast borehole T7. Only major peaks are labeled.

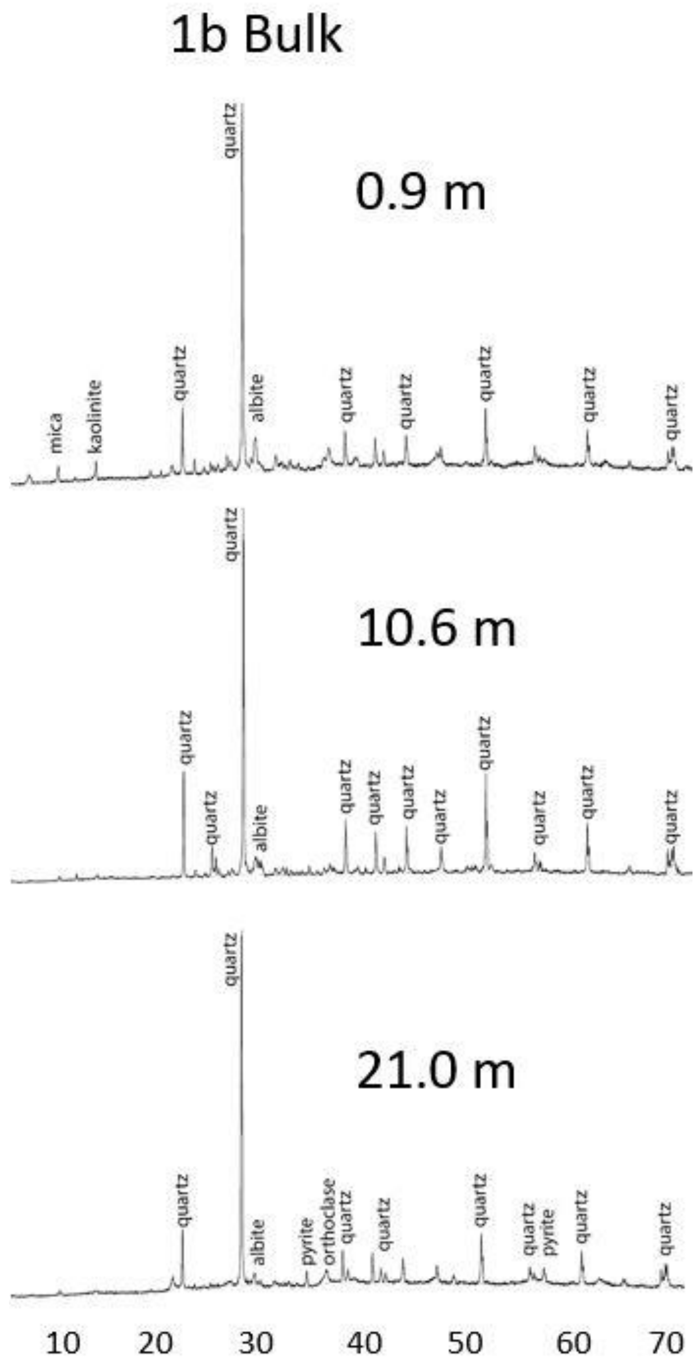

Figure 22: X-ray diffraction results for Vwest North borehole 1b. Only major peaks are labeled.

`

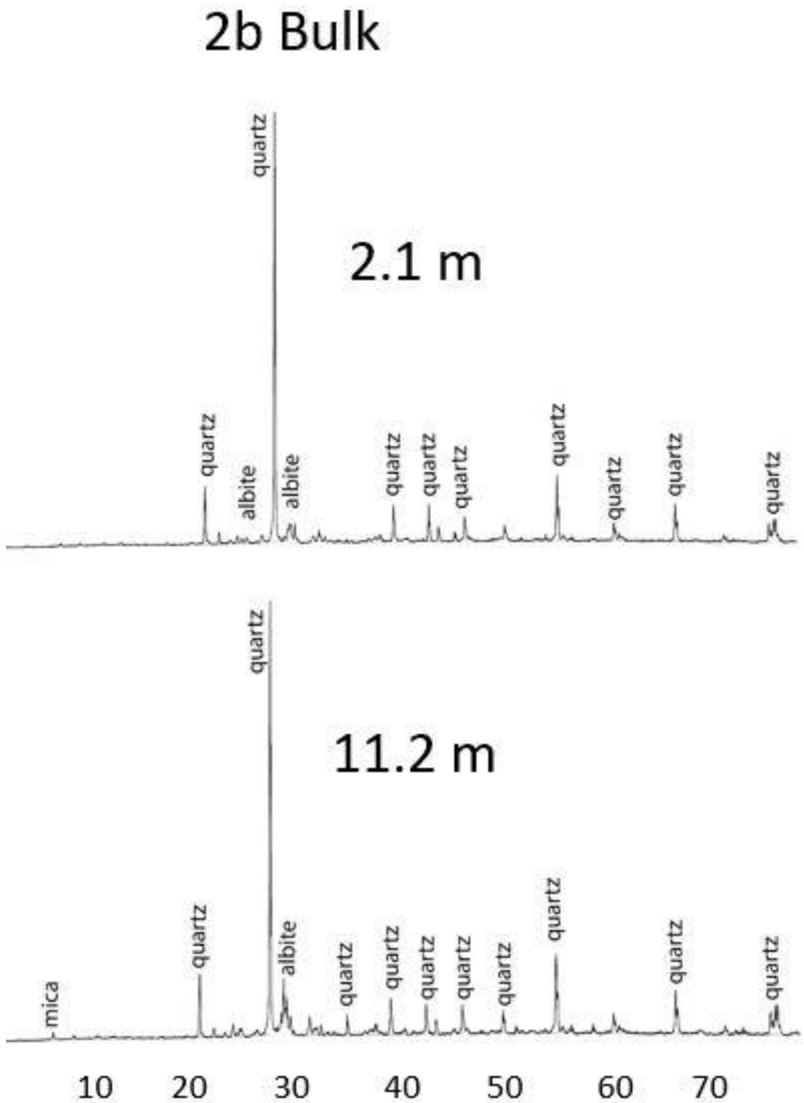

Figure 23: X-ray diffraction results for Vwest North borehole 2b. Only major peaks are labeled.

`

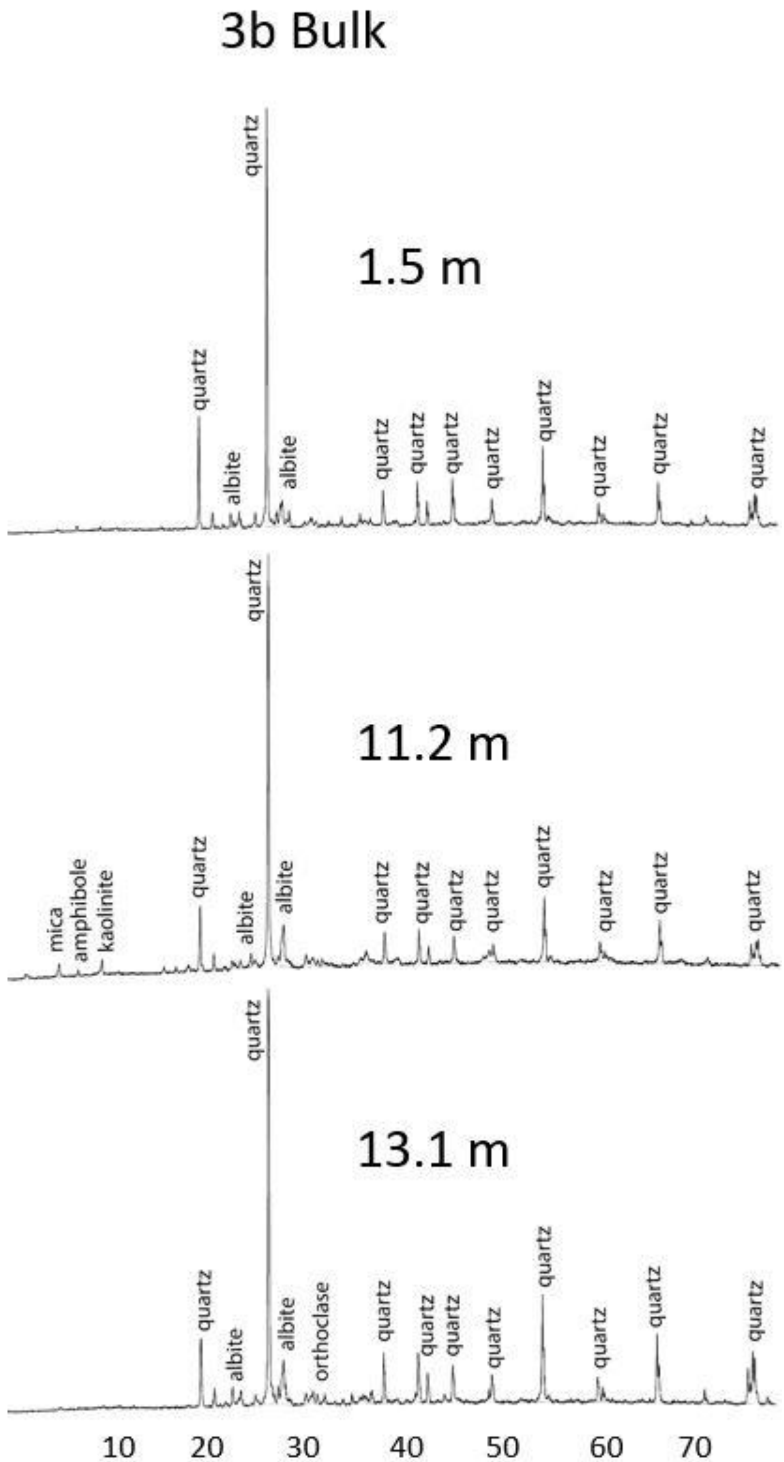

Figure 24: X-ray diffraction results for Vwest North borehole 3b. Only major peaks are labeled.

`

Two sandy samples, borehole T7 at 13.7 m depth and borehole 2b at 11.2 m depth and a clay sample, borehole 1b at 0.9 m depth were selected for further XRD analysis. First an initial sample analysis was performed on the three samples selected before further XRD analysis to get a better idea what minerals could be present in the samples (Table 12).

Table 12: Initial sample evaluation test results indicate whether the sample had no reaction (0) to the reagent or specific test or a strong reaction (5). The different tests tested for the presence and abundance of specific mineral groups.

	Reaction with:			Tests with:				
Sample	**1M HCl**	**30% H_2O_2**	**Magnetic Minerals**	**Acetone**	**$BaCl_2$**	**$AgNO_3$**	**EC (µS/cm)**	**pH**
T7 13.7	0	0	3	1	2	2	50.5	6.592
1b 0.9	0	3	2	0	1	1	38.16	6.501
2b 11.2	0	0	3	1	2	3	32.95	6.691

None of the samples reacted with hydrochloric acid (HCl), demonstrating a lack of significant calcite content in the bulk samples. Borehole T7 at 13.7 m depth and borehole 2b at 11.2 m depth did not react with hydrogen peroxide meaning there was little to no oxidizing/reducing components present. However, in borehole 1b at 0.9 m depth the sediment had some reaction to the hydrogen peroxide (Table 12) indicating some oxidizing/reducing components were present. A magnet indicated that some magnetic minerals were present in all three samples. The acetone test indicated that little to no evaporite minerals such as halites, sulfates, and nitrates were present in all three samples. The sulfate anion check ($BaCl_2$) indicated that boreholes T7 at 13.7 m depth and 2b at 11.2 m depth contained a moderate presence of sulfate anions while borehole 1b at 0.9 m depth contained a low quantity of sulfate anions (Table 12). The chloride anion check ($AgNO_3$)

`

indicated that boreholes T7 at 13.7 m depth and 2b at 11.2 m depth contained some chloride anions while borehole 1b at 0.9 m depth fewer chloride anions. The electrical conductivity (EC) measurements were within normal ranges for sandy soils and the pH values are near neutral.

The abundance of a single mineral, such as quartz can mask the presence of other minerals so performing a size fractionation with grain size is an efficient way to view other minerals present. Figure 25 shows the XRD results of just the sand sized grains for the three samples. Mostly quartz was identified along with albite and orthoclase ($KAlSi_3O_8$), a potassium-containing feldspar. The three samples are lined up together to show that the mineralogy at Veast and Vwest North are similar.

`

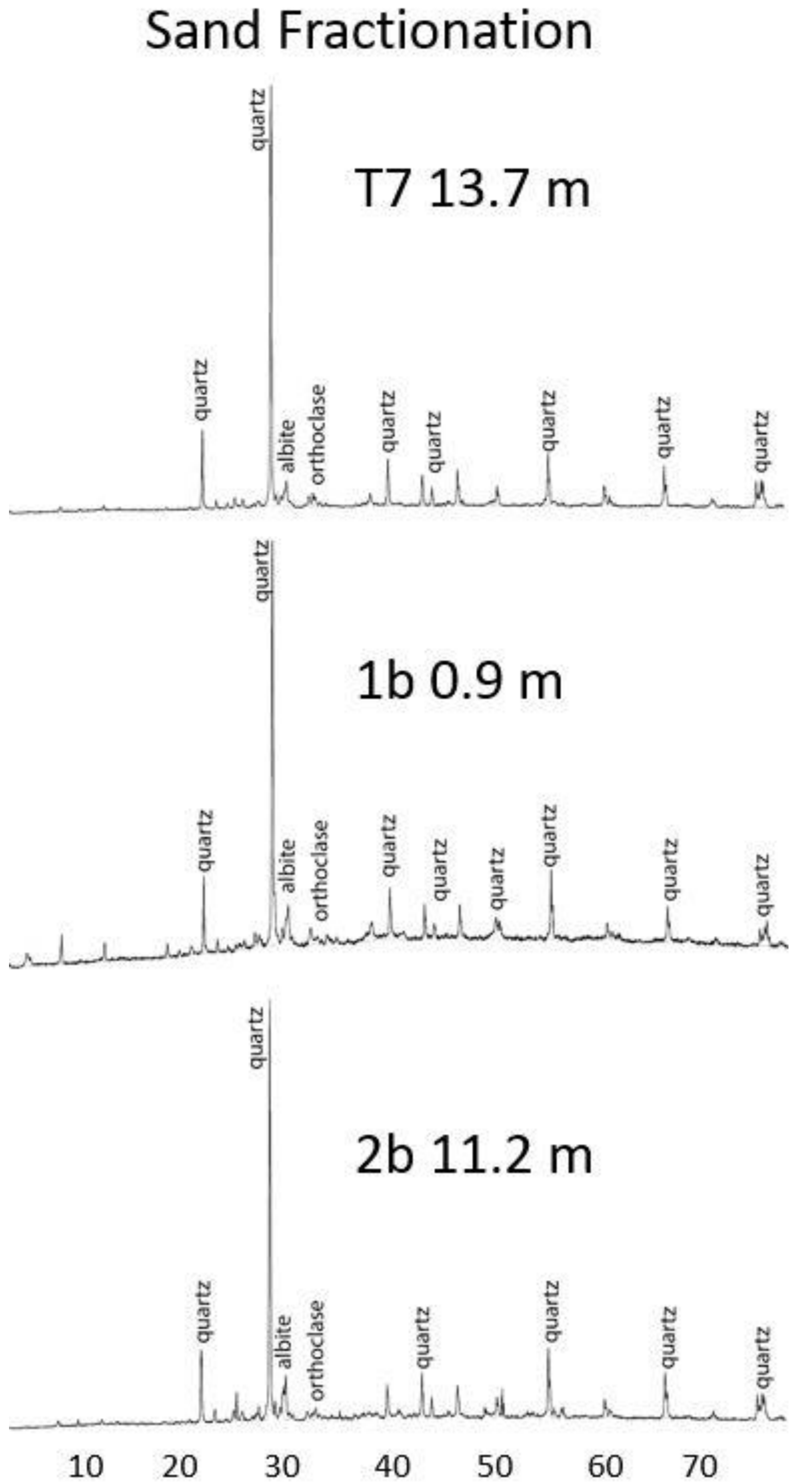

Figure 25: X-ray diffraction sand-sized grains results for borehole T7 at the Veast transect, and boreholes 1b and 2b from transect Vwest North at selected depths. Only major peaks are labeled.

`

Figure 26 shows the silt and clay XRD results for borehole T7 within the Veast transect at 13.7 m depth, borehole 1b at 0.9 m depth, and borehole 2b at 11.2 m depth from the Vwest North transect (Figs. 3, 4). Once the majority of the quartz had been removed, more minerals were identified. Albite and kaolinite were identified in all three samples. The peaks for amphibole, mica, and chlorite ($(Mg,Fe,Li)_6AlSi_3O_{10}(OH)_8$) are taller meaning these minerals are relatively more abundant than the others present. All three of these minerals were observed in the three boreholes. Figure 26 further shows that the silt and clay mineralogy at both Veast and Vwest North are quite similar.

`

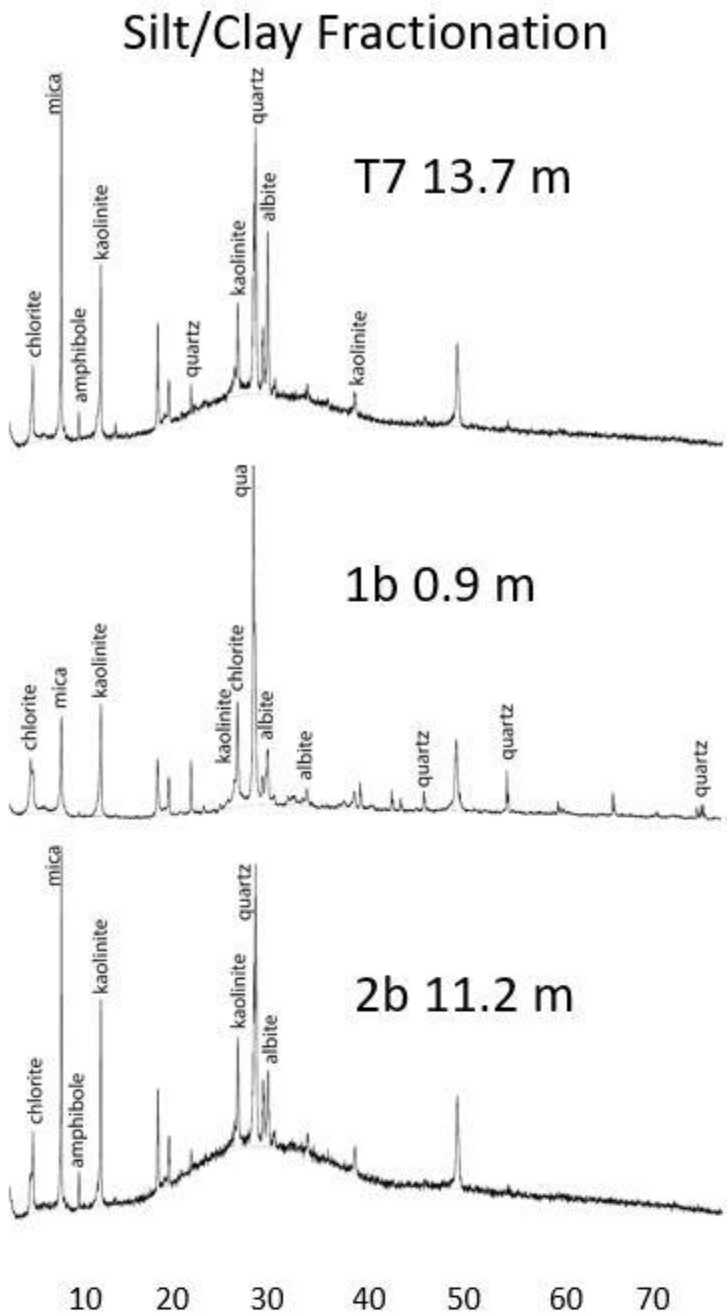

Figure 26: X-ray diffraction silt/clay sized grains results on samples for borehole T7 from the Veast transect, and boreholes 1b and 2b from the Vwest North transect at selected depths. Only major peaks are labeled.

`

Samples from borehole T7 at 13.7 m depth and borehole 2b at 11.2 m depth did not contain enough silt/clay to separate and do a full clay analysis so no more XRD was performed on those samples. The sample from borehole 1b at 0.9 m depth contained mainly silt and clay. Therefore, a full clay analysis could be performed. The mineralogical results with the primary peaks labeled are displayed in Figure 27. Mostly the same mineralogy identified in the silt/clay XRD results were identified such as chlorite, kaolinite, mica and quartz. Smectites ($(Na,Ca)_{0-3}(Al,Mg)_2Si_4O_{10}(OH)_2 \cdot n(H_2O)$, a group of phyllosilicate mineral species showed up as well.

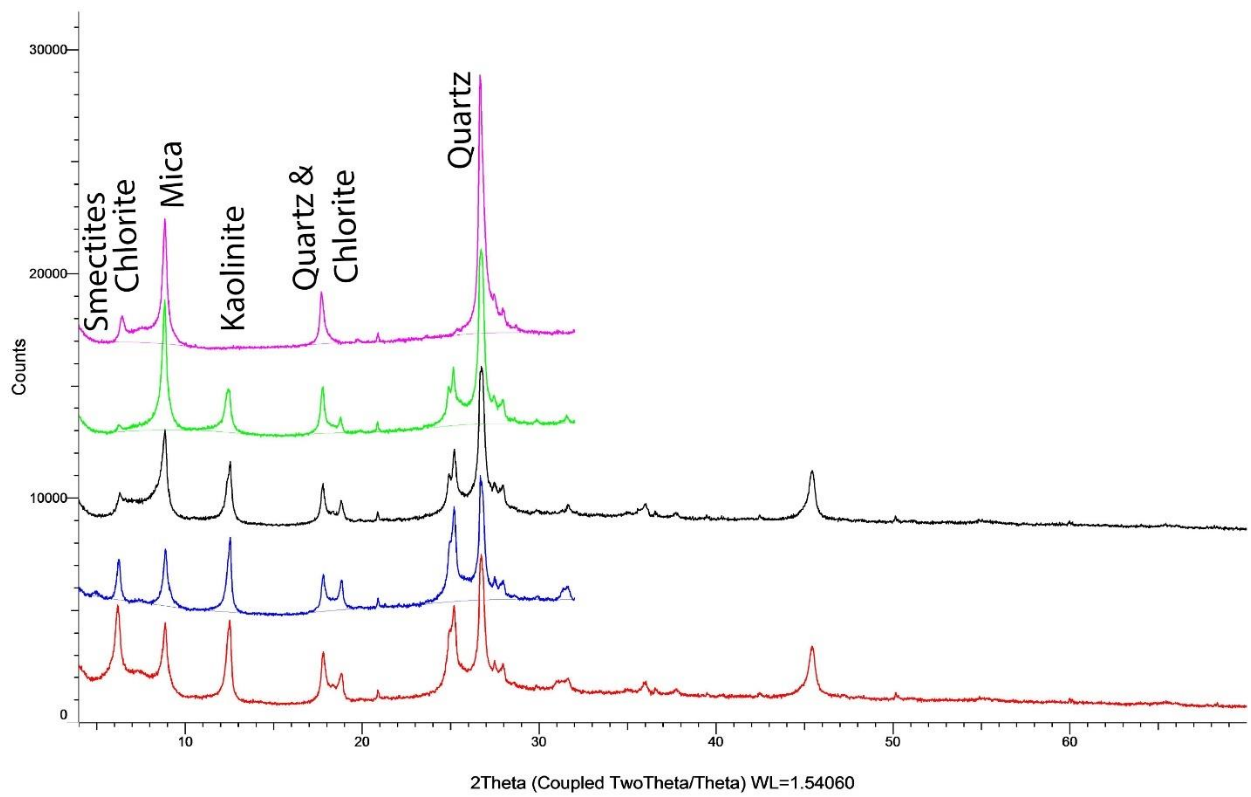

Figure 27: Clay analysis for the sample from borehole 1b at 0.9 m depth at Vwest North. The red and blue show the Mg wash and Mg glycerol results respectively. The black, green, and pink show the K wash, K at 330º C, and K at 550º C results respectively. Only major peaks are labeled.

`

With the goal of identifying the presence of minerals commonly identified in As cycling such as pyrite, the dense minerals from samples from borehole T7 at 13.7 m depth and borehole 2b at 11.2 m depth were observed under a Scanning Electron Microscope (SEM). However, no pyrite could be identified with SEM.

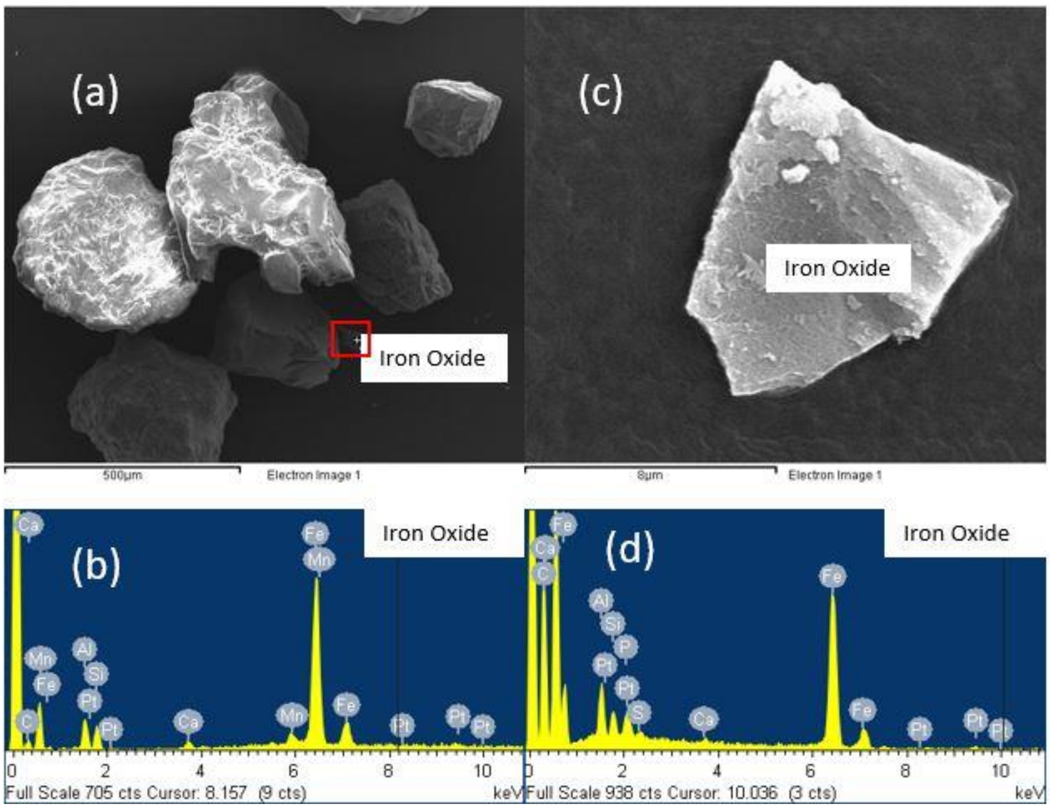

Figure 28: Selected SEM results for heavy sand minerals from borehole T7 at 13.7 m depth. (a) and (c) show the SEM area along with a size scale. (b) and (d) show the elemental abundance for their corresponding SEM image. The elemental peaks indicate elemental presence and abundance.

From the dense sand for the sample taken from borehole T7 at 13.7 m depth, a small piece of iron oxide was identified (Fig. 28a, c) by the strong Fe peak at 6.5 keV. Fig. 28a shows a zoomed-out SEM image and Fig. 28b shows the corresponding elemental

`

abundance. In Fig. 28c the image is 16 μm across; the Fe oxide found is very small and must not be abundant since none was detected by the XRD.

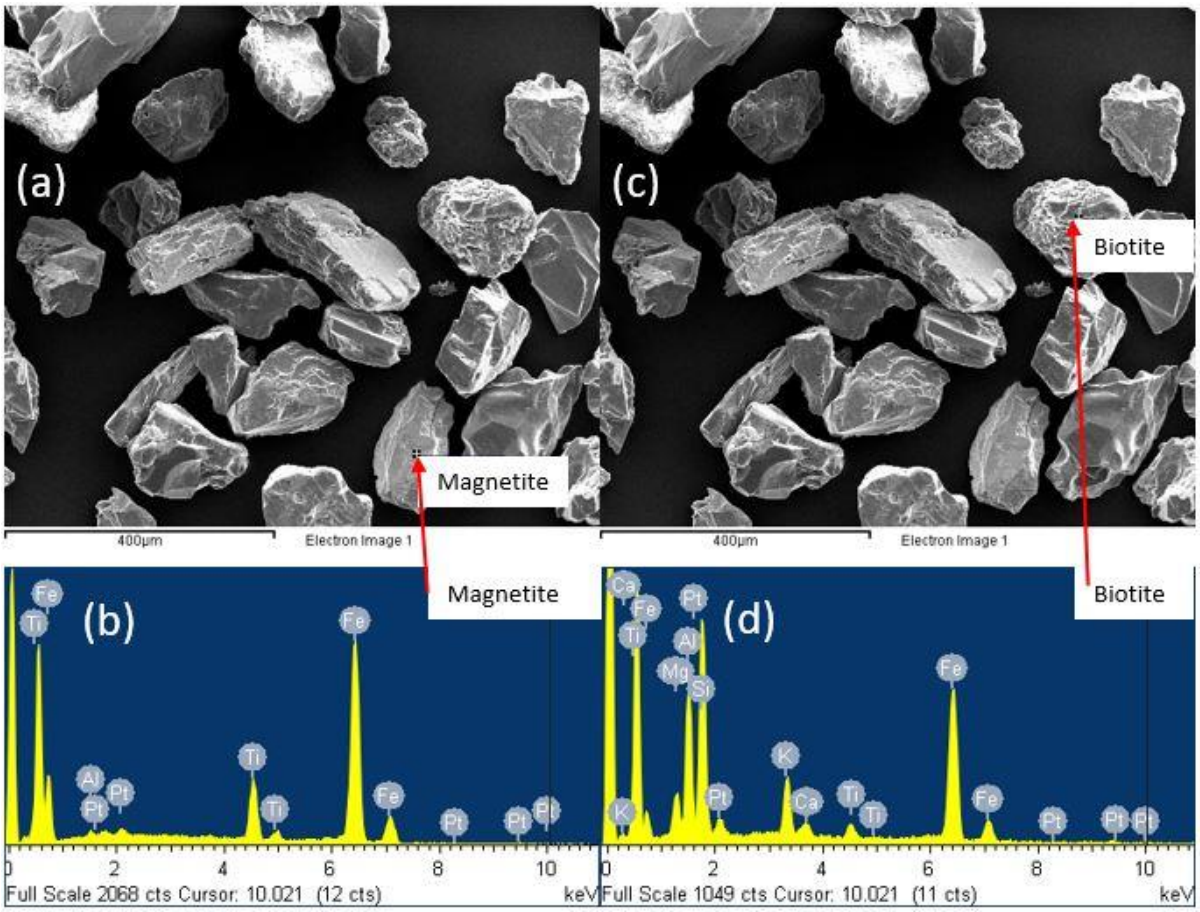

Figure 29: Selected SEM results for heavy sand minerals from borehole 2b at 11.2 m depth. (a) and (c) show the SEM area along with a size scale. (b) and (d) show the elemental abundance for their corresponding SEM image. The elemental peaks indicate elemental presence and abundance.

Figure 29 shows some of the heavy mineralogical results from borehole 2b at 11.2 m depth. The labeled mineral in Fig. 29a was identified to be magnetite by the abundance of elemental Fe, some titanium (Ti), and aluminum (Al) (b). The labeled mineral the red arrow

`

points to in Fig. 29c was identified to be biotite by the presence of elemental Fe, Ca, K, Si, Mg, and Al (Fig. 29d).

5.3 Modeling

5.3.1 Aqueous Geochemistry

The fraction of groundwater remaining within the aquifer along the flow path within each monitoring well and drive-point piezometer was calculated using Equation 1. To seek the most conservative tracer, this calculation was performed three times utilizing three different tracers: chloride, silicon, and the sum of four major cations (Na^{+}, K^{+}, Mg^{2+}, and Ca^{2+}) (Fig. 30). Calculated fractions of groundwater using silica and the major cation charge were more alike than those calculated using chloride. Furthermore, cation charge and silicon declined smoothly towards the river similar to alkalinity and SC, whereas the spatial variation of chloride along the flow path was highly variable. This suggests that silicon and cation charge were more accurate tracers. However, because the sum of the major cations was determined to be the best tracer to use at these study sites to avoid possible interference by silicon release or precipitation into the groundwater along the flow path.

`

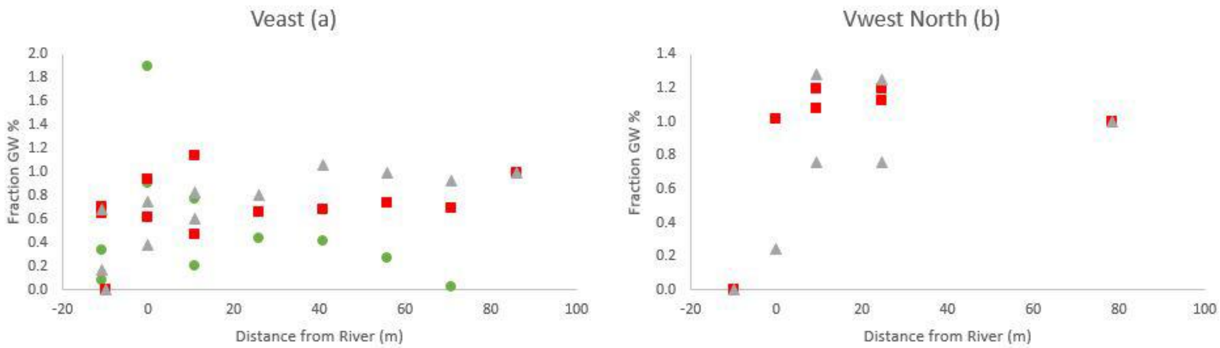

Figure 30: Fraction of groundwater calculated using three different tracers. The green circles, red squares, and grey triangles represent the conservative and semi-conservative tracers chloride, silicon and the sum of four major cation charge, respectively. The chloride tracer results for Vwest North were inconclusive and are therefore not shown.

Once the relative proportion of groundwater had been calculated along the groundwater flow path, Equation 2 was used with cation charge as the tracer to calculate the excess element concentrations at each monitoring well and drive-point piezometer, relative to what would be expected if no elements were being released as the groundwater was diluted with river water (Fig. 31). Along the groundwater discharge flow path at the Veast transect, As (Fig. 31a) is being released in along the deeper 15 m flow path but sharply removed from solution as the groundwater discharges in the shallow sediments bordering the river. Iron (Fig. 31b) is somewhat removed from solution along the deeper flow path, but is released at some of the monitoring wells further from the river and the 3 m drive-point piezometers which are installed within sandy material in contrast to the 1 m drive-point piezometers. In contrast, Mn (Fig. 31c) is released along the entire flow path to the river, first gradually and then sharply near the river at the depths of the shallow 1 and 3 m drive-point piezometers. Calcium (Fig. 31d) is removed from solution with proximity to the river. Silicon (Fig. 31e) is

`

removed from solution with proximity to the river. Nitrite (Fig. 31f) is released along the entire flow path to the river.

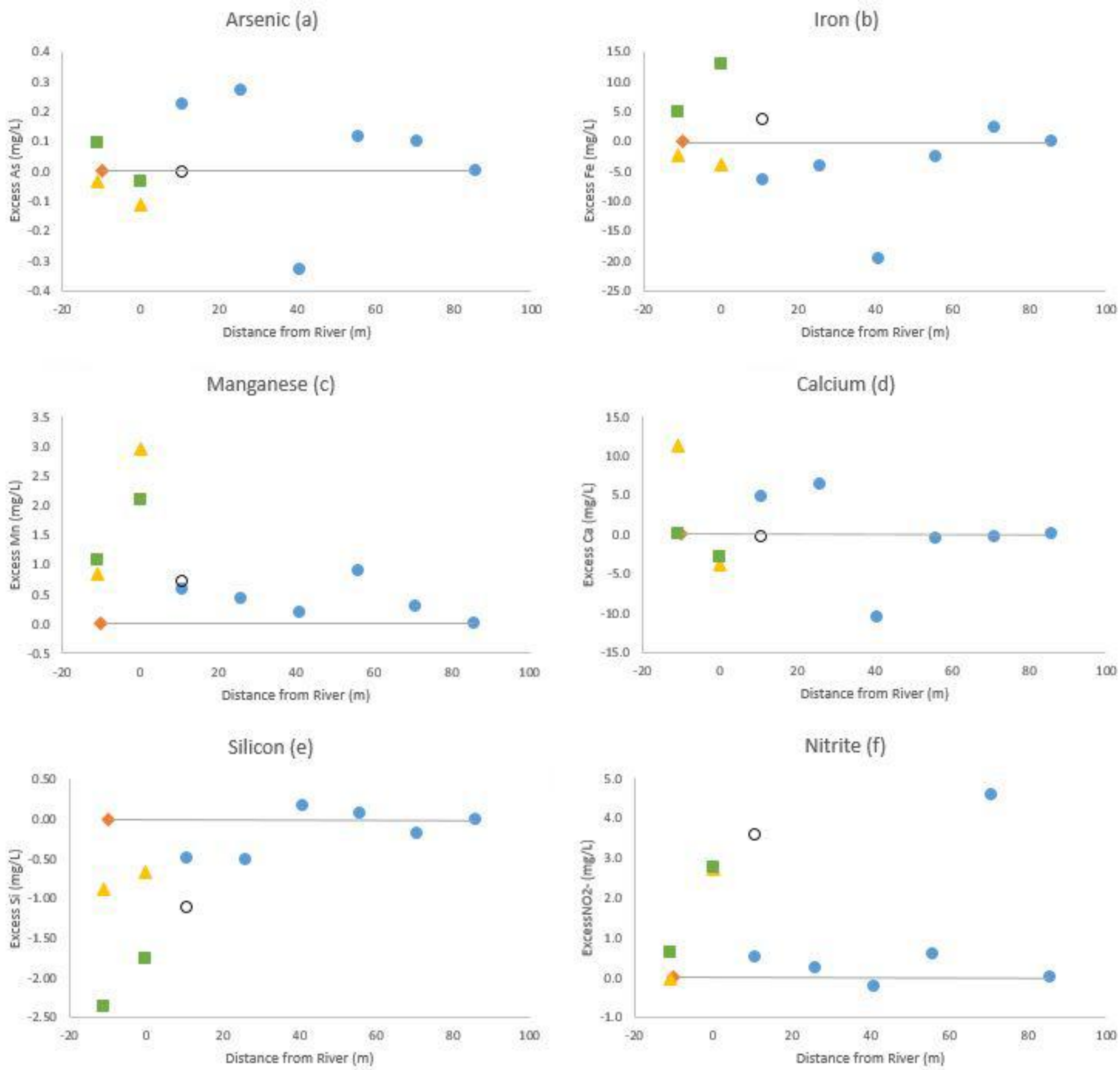

Figure 31: Excess elemental concentration calculations for Veast using the major cations as the tracer. The blue circles, hollow circles, green squares, yellow triangles, and orange diamond represent 15 m monitoring wells, 7 m monitoring well, 3 m and 1 m drive-point piezometers, and river water respectively.

`

Figure 32 shows the excess element calculations for Vwest North. Arsenic (Fig. 32a) is released along the deeper 15 m and the shallower 7 m flow paths and removed from solution as the river discharges in the shallow sediments bordering the river. Iron (Fig. 32b) is increasingly released along the 15 m flow path and the 3 m drive-point piezometer. Manganese (Fig. 32c) is removed from solution along the deeper 15 m and shallower 7 m flow paths, but is released as the river discharges in the shallow sediments bordering the river. Calcium (d) is released into solution along the 15 m and 7 m flow paths. Silicon (Fig. 32e) is released along the shallower 7 m flow path and removed from solution at the deeper 15 m flow path. Nitrite is removed from solution along the groundwater flow paths at Vwest North.

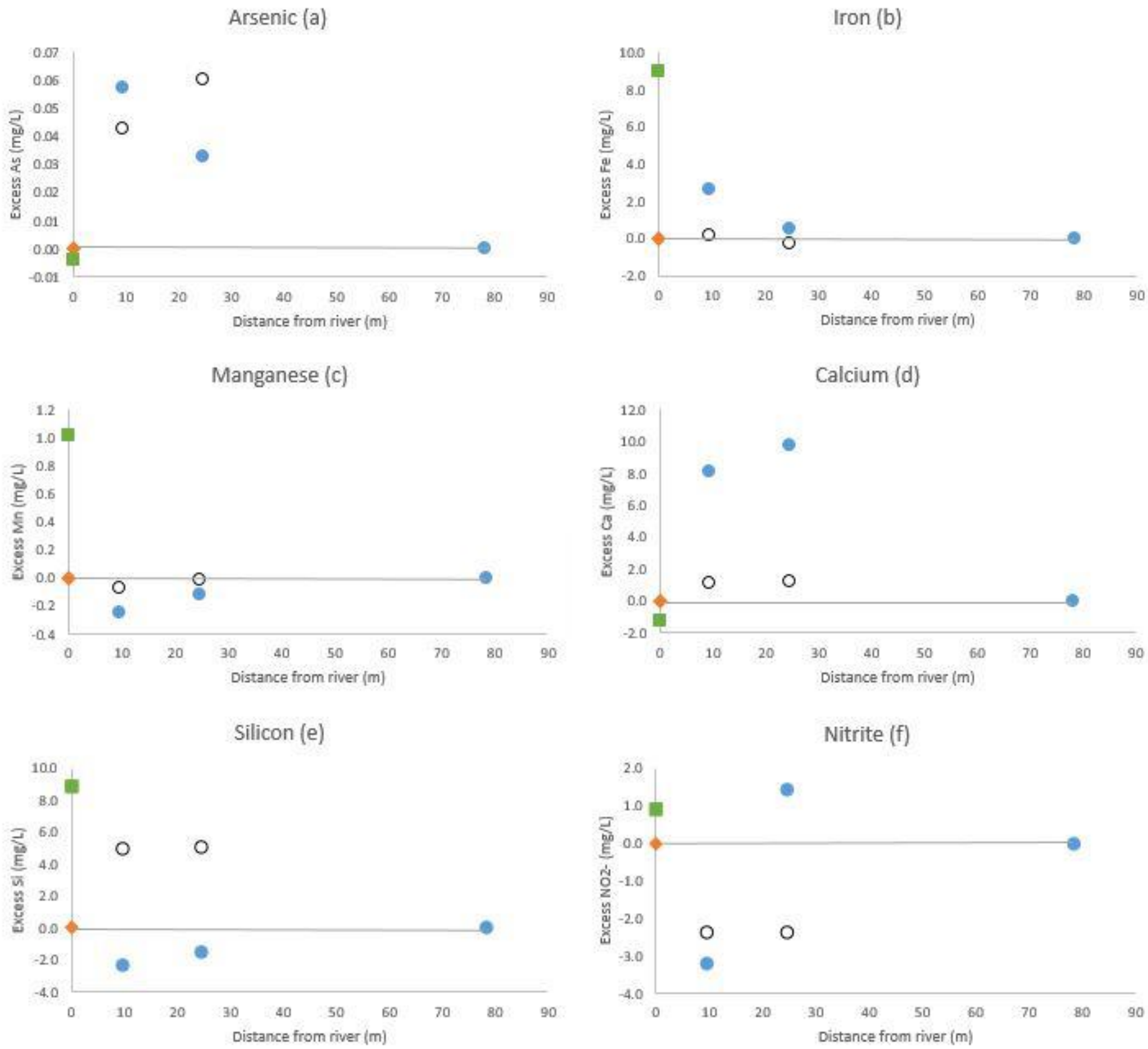

Figure 32: Excess elemental concentration calculations for Vwest North using the major cations as the tracer. The blue circles, hollow circles, green square, and orange diamond represent 15 m monitoring wells, 7 m monitoring wells, 3 m drive-point piezometer, and river water respectively.

Eh-pH diagrams were constructed using Geochemist's Workbench which showed which species and minerals were favored by thermodynamics along the flow paths at Veast and Vwest North riverbank aquifer sites. Figure 33 shows an Eh-pH diagram showing As and Fe phases and the Eh and pH values for each well, drive-point piezometer and river water at

Veast. The deeper 15 m well transect (T1-T6) samples sit on the As(III) and As(V) stability boundary which means the shallow groundwater aquifer could be a suitable environment for either compound to occur naturally. Clearly, as the groundwater discharges through the riverbank at 1-3 m depth, As(V) is favored.

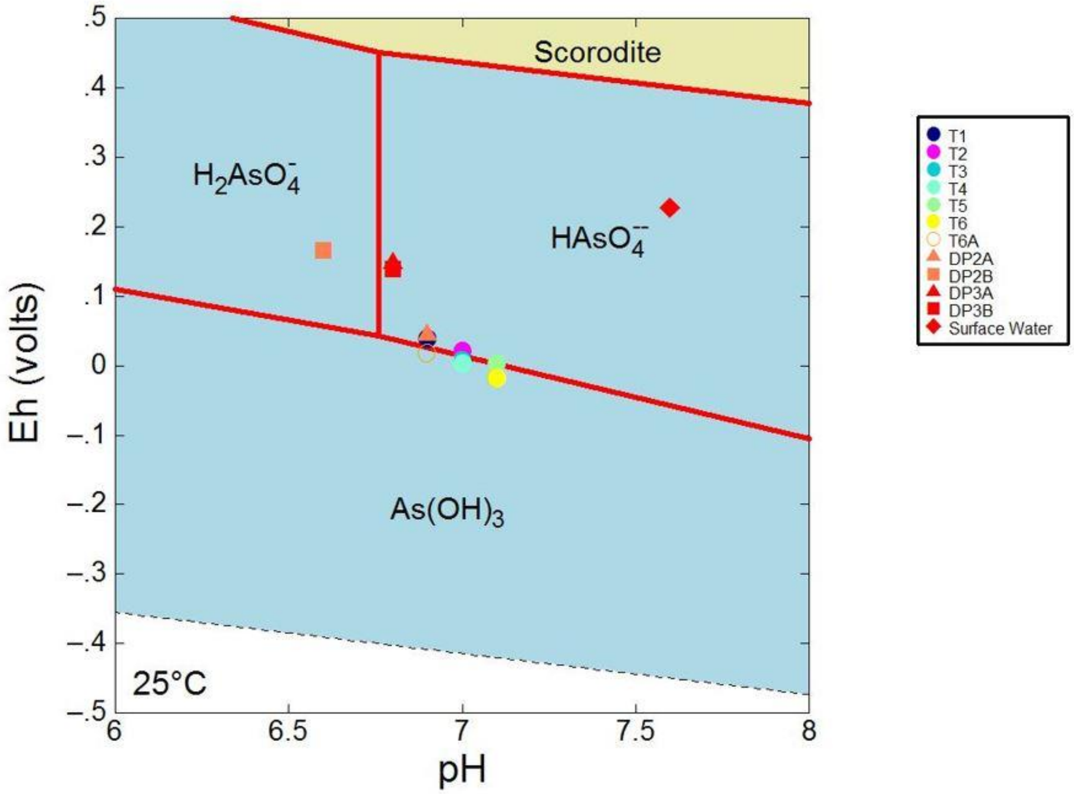

Figure 33: Diagram $As(OH)_4$, T = 25°C, P = 1.013 bars, a [main] = 10^{-6}, a[H_2O] = 1, a[Fe^{2+}] = 10^{-4} Veast. This model shows each well and drive-point piezometer graphed with respect to their measured pH and Eh values at Veast. The graph is on top of a phase diagram which shows the expected phases of iron and arsenic at the Eh-pH range at Veast. The warmer colors are closest to the river.

Figure 34 shows an Eh-pH diagram using As, Fe, SO_4^{2-}, and HCO_3^- phases and the Eh and pH values for each well, drive-point piezometer and river water at Veast as the input.

`

Figure 34 shows what compounds and their phases, dissolved (blue) or precipitated (orange) could be occurring in the water at each well and drive-point piezometer. These results indicate that the part of the aquifer that the deeper 16 m wells are tapping into may not be reducing enough to precipitate As-sulfur minerals such as realgar and orpiment.

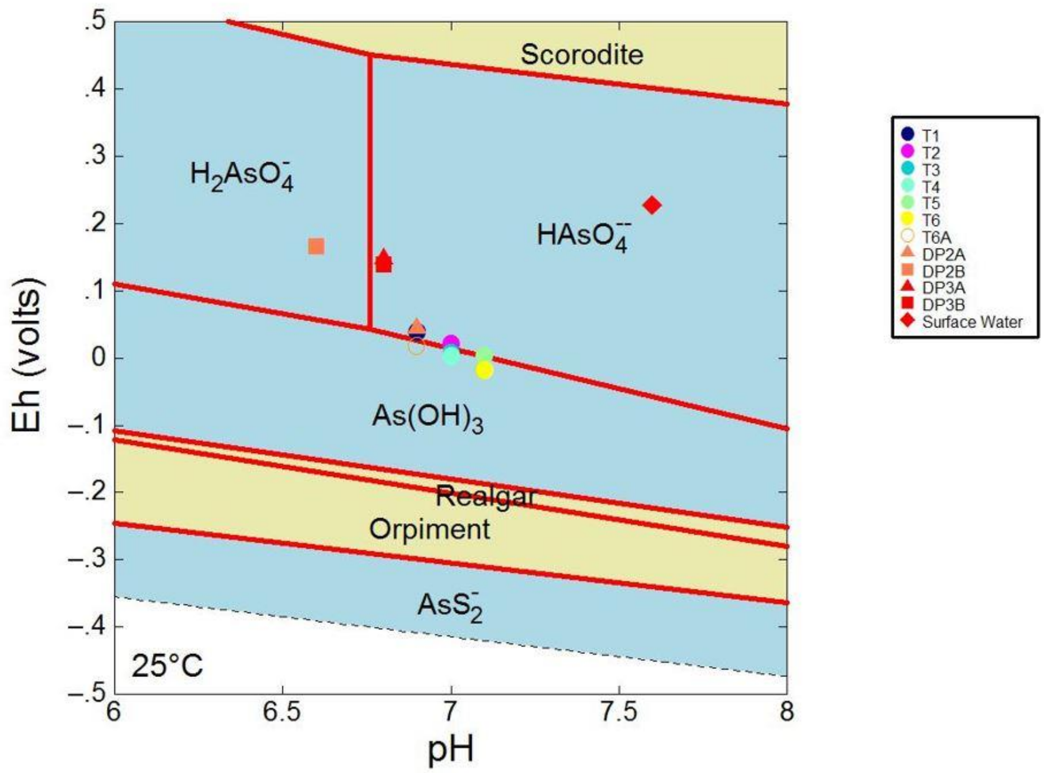

Figure 34: Diagram $As(OH)_4$, T = 25°C, P = 1.013 bars, a[main] = 10^{-6}, a[H_2O] = 1, a[Fe^{2+}] = 10^{-4}, a[HCO_3] = 1, a[SO_4^{2-}] = 10^{-5} Veast. This model shows each well and drive-point piezometer graphed with respect to their measured pH and Eh values at Veast. The graph is on top of a phase diagram which shows the expected phases of As, Fe, SO_4^{2-}, and HCO_3^- at the Eh-pH ranges at Veast. The warmer colors are closest to the river.

Figure 35 shows an Eh-pH diagram showing only the Fe phases and the Eh and pH values for each well, drive-point piezometer and river water at Veast. The minerals hematite,

`

goethite, and magnetite were suppressed in the model since there would be too little time at Veast for them to precipitate. This model shows what dissolved (blue) and precipitated (blue) Fe phases could be occurring at each well, drive-point piezometer and river. The results indicate that some wells will contain primarily aqueous Fe(II) in solution or precipitated Fe oxides. As the groundwater discharges through the HZ, $Fe(OH)_3$ precipitation is clearly favored. This thermodynamic prediction conflicts, however, with the calculated releases of Fe along the end of the groundwater discharge flow path at Veast.

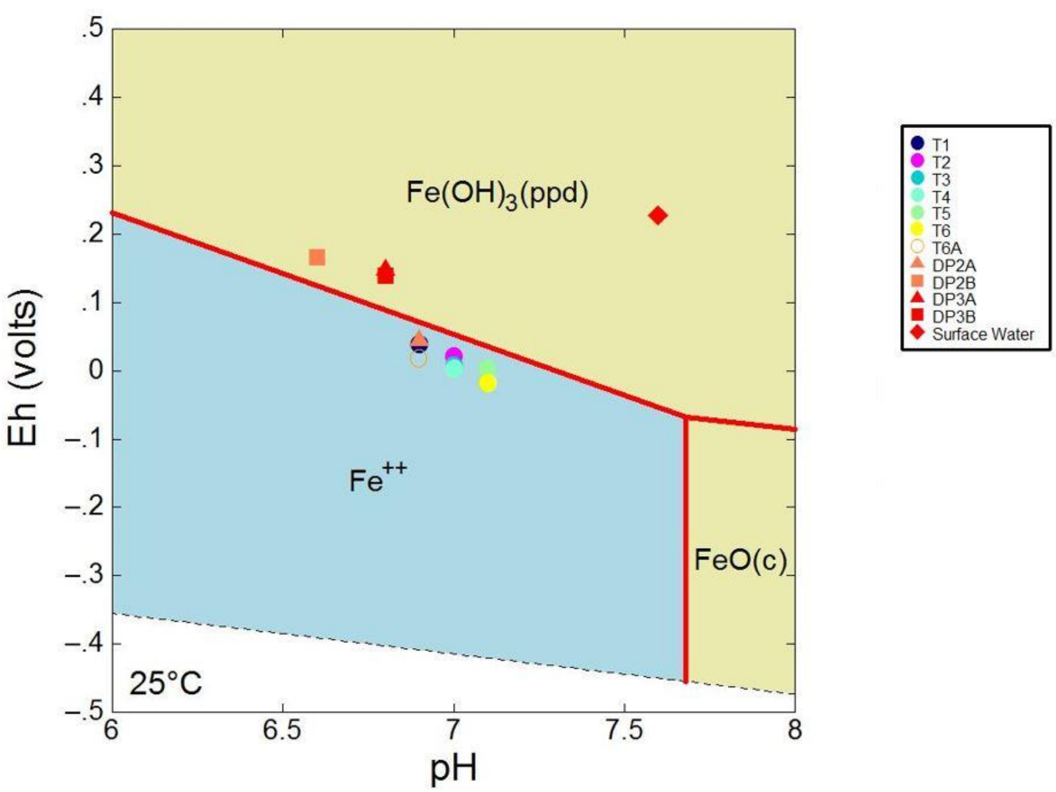

Figure 35: Diagram Fe^{2+}, T = 25°C, P = 1.013 bars, a[main] = 10^{-4}, a[H_2O] = 1; Suppressed: Goethite, Hematite, Magnetite; Veast. This model shows each well and drive-point piezometer graphed with respect to their measured pH and Eh values at Veast. The graph is on top of a phase diagram which shows the expected phases of only Fe^{2+} at the Eh-pH range at Veast. The warmer colors are closest to the river.

`

Eh-pH diagrams were constructed for the wells at Vwest North (Figues 36, 37, and 38) as well using the same parameters as Figures 33, 34, and 35 at Veast. In Figure 36, the wells and drive-point piezometer fall in the same phase, the As (III) stability zone.

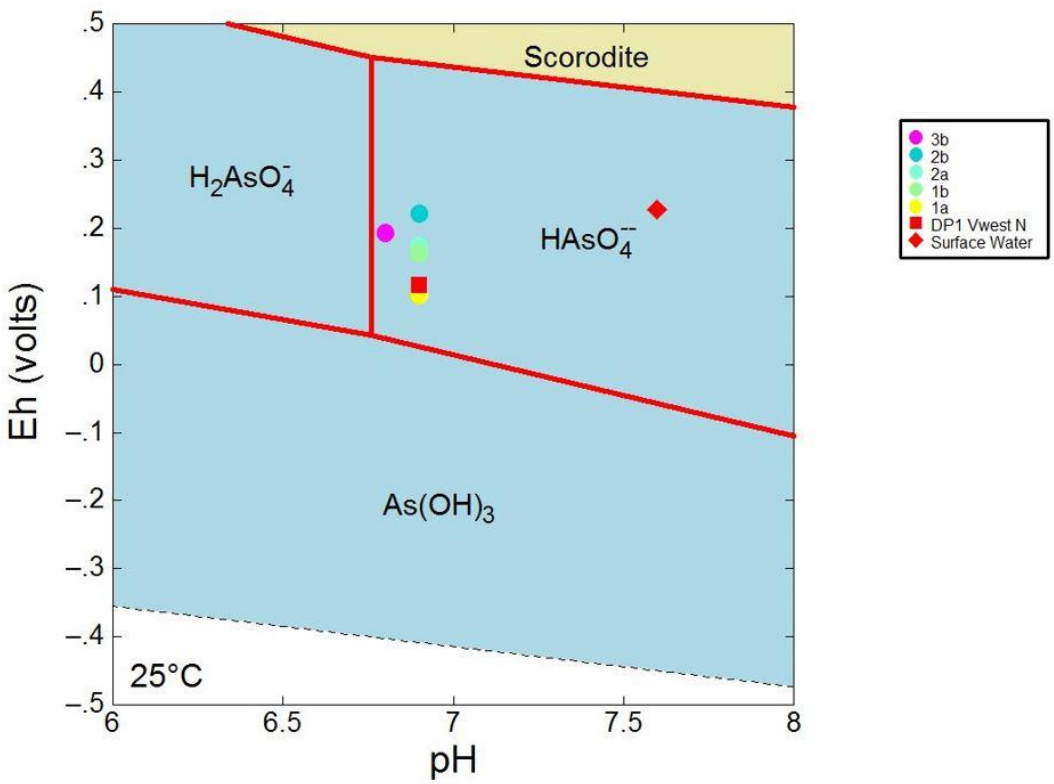

Figure 36: Diagram $As(OH)_4$, T = 25ºC, P = 1.013 bars, a [main] = 10^{-6}, a[H_2O] = 1, a[Fe^{2+}] = 10^{-4} Vwest North. This model shows each well and drive-point piezometer graphed with respect to their measured pH and Eh values at Vwest North. The graph is on top of a phase diagram which shows the expected phases of iron and arsenic at the Eh-pH range at Vwest North. The warmer colors are closest to the river.

Once again, in figure 37 the wells and drive-point piezometer at Vwest North all fall into the aqueous As(III) stability zone when the As, Fe, SO_4^{2-}, and HCO_3^- phases are all factored into the model. It also shows that the shallow aquifer at Vwest North isn't in a

`

reduced enough environment to precipitate As containing minerals such as realgar and orpiment. These results agree with the XRD and SEM results since no As containing minerals were detected in either.

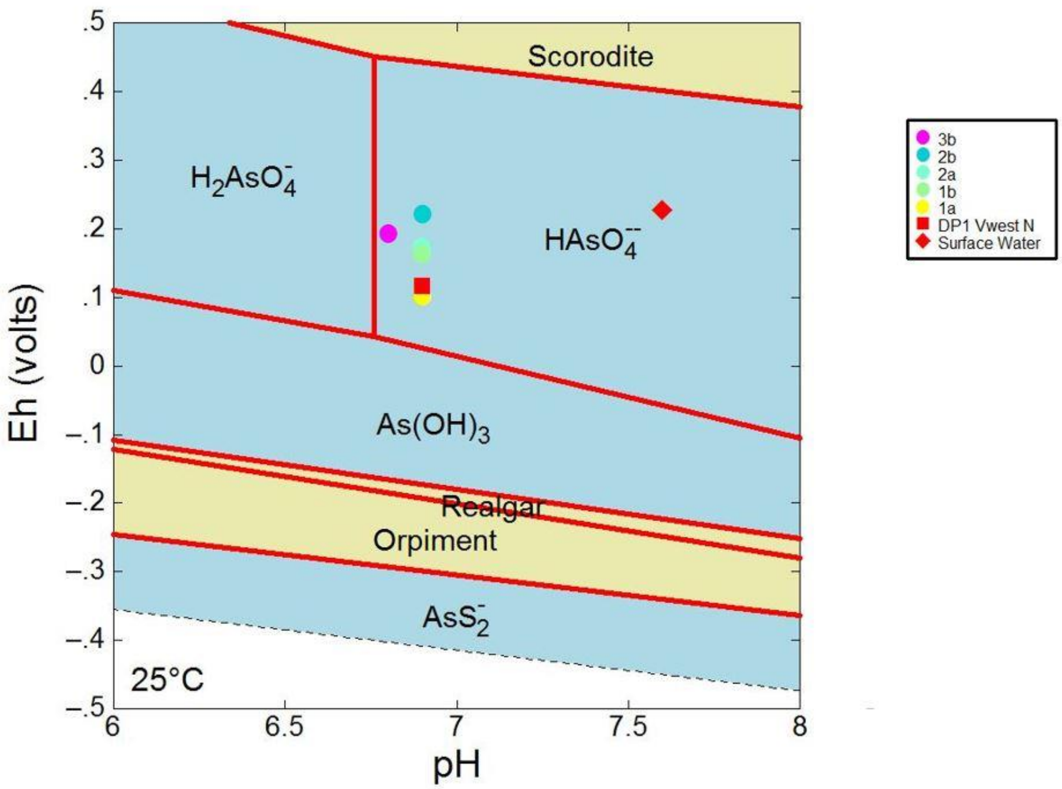

Figure 37: Diagram $As(OH)_4$, T = 25ºC, P = 1.013 bars, a[main] = 10^{-6}, a[H_2O] = 1, a[Fe^{2+}] = 10^{-4}, a[HCO_3] = 1, a[SO_4^{2-}] = 10^{-5} Vwest North. This model shows each well and drive-point piezometer graphed with respect to their measured pH and Eh values at Vwest North. The graph is on top of a phase diagram which shows the expected phases of As, Fe, SO_4^{2-}, and HCO_3^- at the Eh-pH ranges at Vwest North. The warmer colors are closest to the river.

Figure 38 shows an Eh-pH diagram showing only the Fe phases and the Eh and pH values for each well, drive-point piezometer and river water at Vwest North. The minerals hematite, goethite, and magnetite were suppressed in the model since there would be too little

`

time at this site for them to precipitate. This model shows what dissolved (blue) and precipitated (blue) iron phases could be occurring at each well and drive-point piezometer. The results indicate that thermodynamically, Fe oxide precipitation is favorable. Indeed, compared with Veast, the dissolved Fe concentrations in both 15 and 7 m depth wells at Vwest North were quite low (Fig. 15), but increased towards the river and were especially high in the drive-point piezometer at 3 m depth (9.2 mg/L). It's noteworthy that Fig. 38 shows the redox conditions in wells closer to the river (1a, 1b, DP1) approach the domain where dissolved Fe is stable.

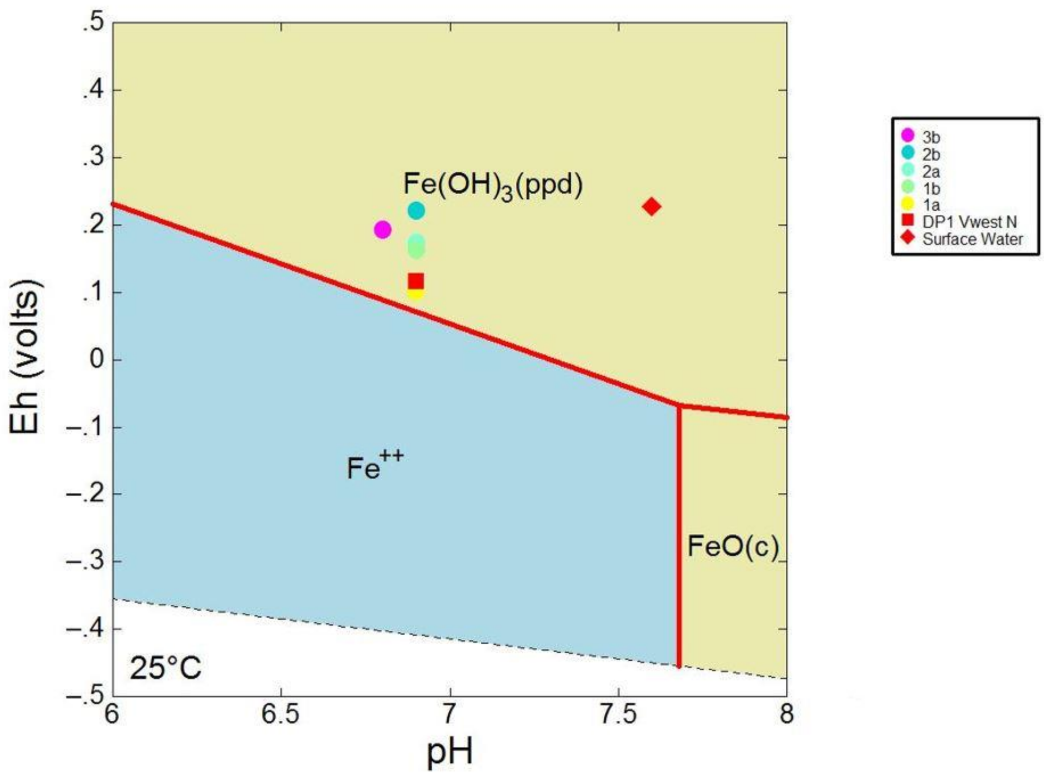

Figure 38: Diagram Fe^{2+}, T = 25°C, P = 1.013 bars, a[main] = 10^{-4}, a[H_2O] = 1; Suppressed: Goethite, Hematite, Magnetite; Vwest North. This model shows each well and drive-point piezometer graphed with respect to their measured pH and Eh values at Vwest North. The graph is on top of a phase diagram which shows the expected phases of only iron at the Eh-pH range at Vwest North. The warmer colors are closest to the river.

`

Saturation indices (SI) and mineralogy were calculated for each well and drive-point piezometer at both study sites using PHREEQC. This model utilizes multiple aqueous geochemistry parameters as an input and uses thermodynamics to calculate expected mineralogy and their corresponding SI. If a mineral has a SI less than zero, then it is under saturated and likely dissolving. If a mineral has a SI greater than zero, then it is supersaturated and likely precipitating. Some of the SI for selected minerals are shown in Figures 39 and 40 for Veast and Vwest North respectively.

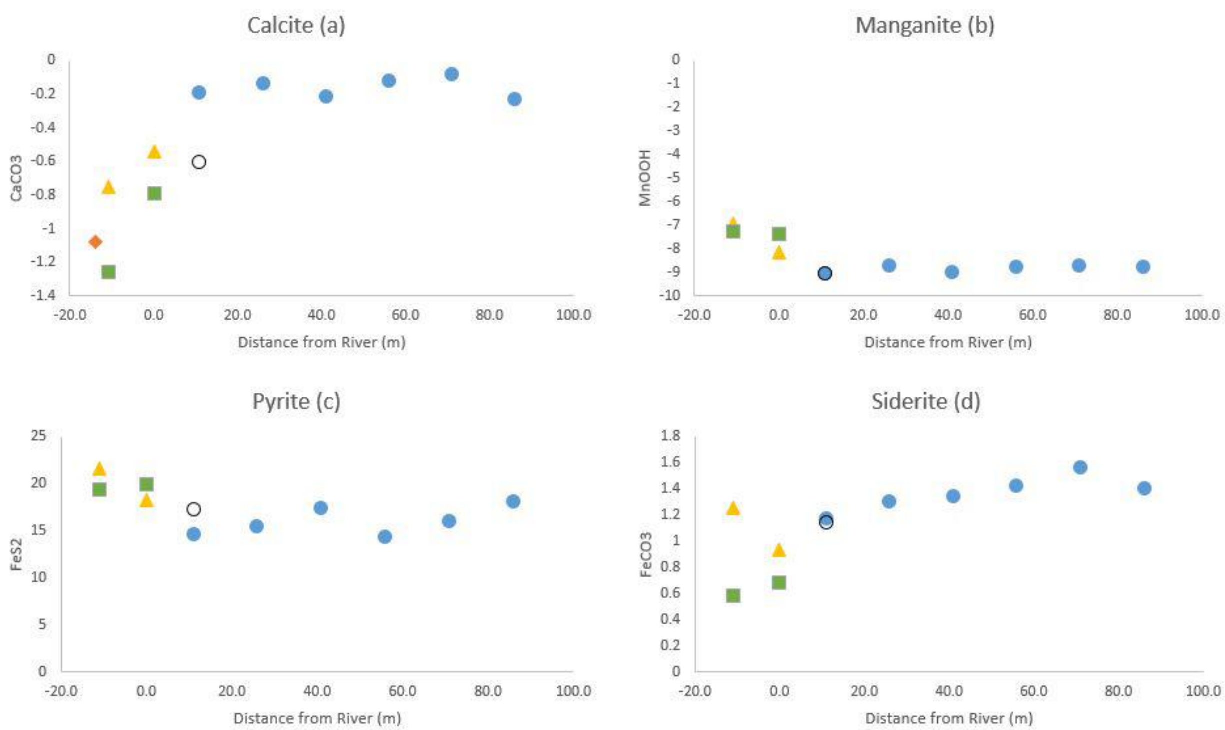

Figure 39: Saturation Indices calculated by PHREEQC for Veast. The blue circles, hollow circles, green squares, yellow triangles, and orange diamond represent 15 m monitoring wells, 7 m monitoring well, 3 m and 1 m drive-point piezometers, and river water respectively.

`

The SI values for the mineral calcite at Veast (Fig. 39a) are near zero near the beginning of the monitored section of the flow path, but become more negative towards the river meaning calcite is under saturated along the flow path and is expected to dissolve, if present, closer to the river. This trend also suggests that calcite may be controlling alkalinity concentrations upgradient of the groundwater discharge pathway. Manganite (MnOOH) (Fig. 39b) is greatly under saturated as well which may mean it would dissolve, if present, as well. Pyrite (Fig. 39c) and siderite (Fig. 39d) are both supersaturated which means they're expected to be in a precipitated form. However, the presence of pyrite and siderite were not necessarily detected with XRD or SEM.

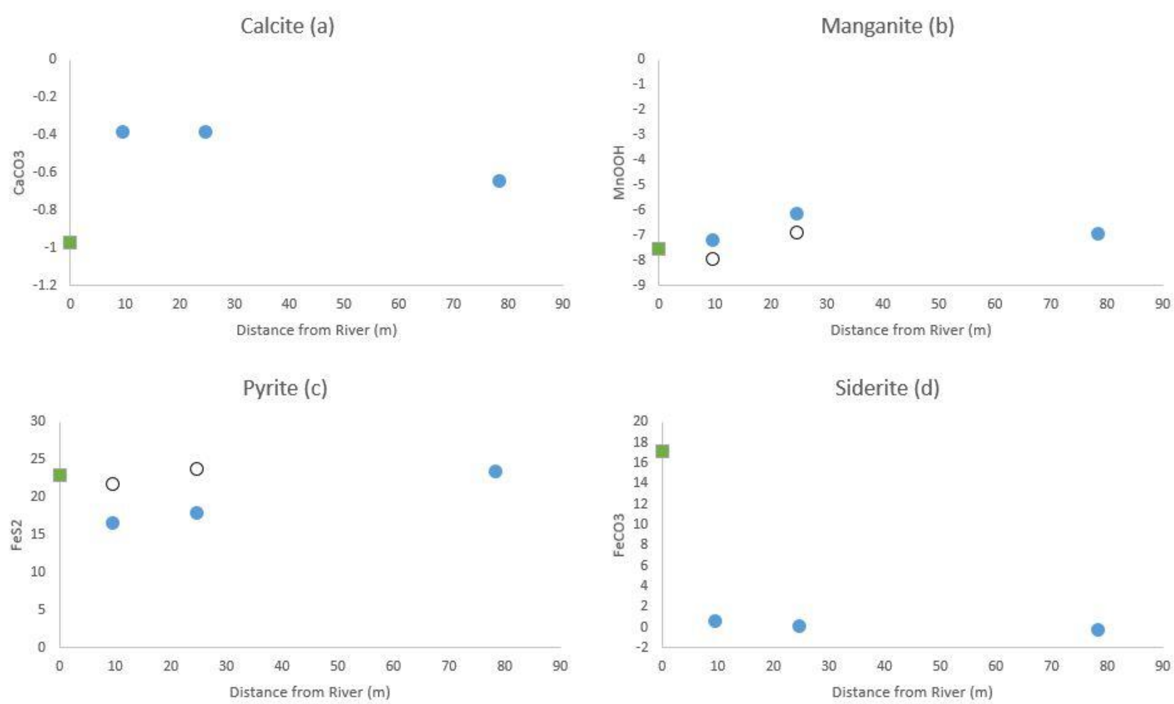

Figure 40: Saturation Indices calculated by PHREEQC for Vwest North. The blue circles, hollow circles, and green square represent 15 m monitoring wells, 7 m monitoring wells, and 3 m drive-point piezometer respectively.

`

The SI values for calcite (Fig. 40a are negative suggesting calcite is under saturated along the flow path at Vwest North, meaning it is expected to dissolve if present. The SI values for manganite (Fig. 40b) are negative and is under saturated along the groundwater flow paths at Vwest North, meaning it will dissolve if present. Pyrite (Fig. 40c) is supersaturated since the SI's are positive meaning it would occur in a precipitated form if present. Siderite (Fig. 40d) SI's in the deeper 15 m groundwater flow path are roughly zero meaning they're in equilibrium, but siderite is supersaturated when the groundwater discharges in the shallow sediments bordering the river, meaning it is expected to be in a precipitant phase. However, it is noteworthy to mention that pyrite or siderite were not identified by XRD or SEM at Vwest North.

5.3.2 Bacterial Diversity Analysis

Over 800 bacterial genera were identified from the selected DNA sequence samples from the Veast study site. Individual rarefaction curves were constructed for each sample (Fig. 41). For each sample, the number of individuals were tabulated into rows (taxa) and multiple columns (samples) (Fig. 41) (Harper, 1999). Each curve represents one sample. Curves which level off at a higher number of genera indicate greater overall bacterial diversity. The fact that each curve levels out means each monitoring well and drive-point piezometer measured were well sampled for a communal diversity profile.

`

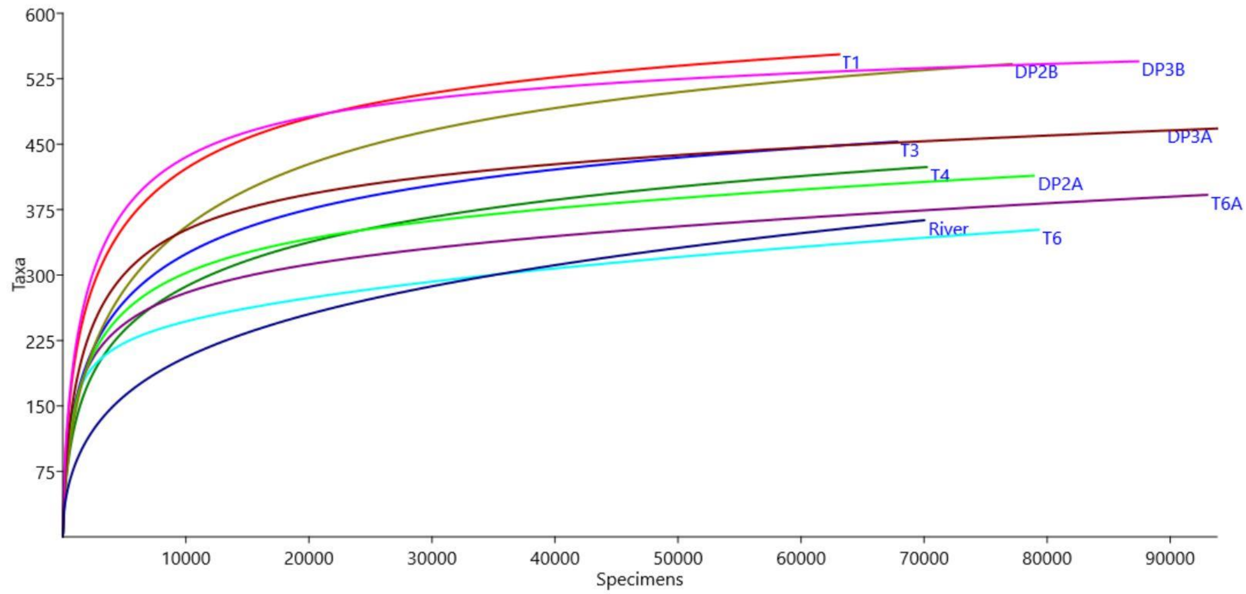

Figure 41: A representation of sampling depth and minimum estimates for alpha diversity are demonstrated by rarefaction curves constructed for 10 samples at Veast. Each labeled curve represents the well identifier that the water sample was drawn from. The y-axis represents the number of taxa identified at the generic (genus) level present and the x-axis represents the sampling depth.

Figure 41 reveals that the 15 m monitoring well furthest from the river (T1) contained the most taxonomic diversity at the genus level. This generic-level analysis represents a total communal diversity profile of DNA from both living and dead organisms present at the time of sampling. Some of the genera showing up could have been from a cone of depression that forms in the water table due to groundwater pumping from the irrigation well located only 1 m away from well T1. This pumping occurs late in the dry season each year, and had not yet begun when well T1 was sampled in January, 2016.

The two 3 m drive-point piezometers (DP 2B and DP 3B) contained the most taxonomic diversity following T1. These drive-point piezometers were installed in sand which indicated strong dilution with river water (Fig. 3). In contrast, the 7 m (T6A), the 15 m

`

monitoring wells closest to the river (T6), and the river water contained the lowest bacterial diversity.

Figure 42 shows bacteria that have been studied in the past, mostly to study geochemical and biological transformations of As in surface sediments (Gorny et al., 2015). Figure 42 indicates which wells these bacteria are present (left) and color codes which wells these selected bacteria were found in (right).

Bacterium Genus	As Reducing	Fe Reducing	As Oxidizing	Fe Oxidizing	Wells Genus is Present
Shewanella	X	X			DP2A, DP3A, DP3B
Sulfurospirillum	X				DP2B, DP3B
Acidithiobacillus				X	DP2B
Acidovorax				X	T1, T3, T4, T6, T6A, DP2A, DP2B, DP3A, DP3B, River
Alcaligenes			X		DP2B, DP3B, River
Agrobacterium			X		T1, DP2B
Dechlorospirillum				X	None
Gallionella				X	T1, T3, T4, T6, T6A, DP2A, DP2B, DP3A, DP3B, River
Leptothrix				X	T1, T3, T4, T6, T6A, DP2A, DP2B, DP3A, DP3B, River
Pseudomonas				X	T1, T3, T4, T6, T6A, DP2A, DP2B, DP3A, DP3B, River
Rhizobium			X		T1, T3, T4, T6, T6A, DP2A, DP2B, DP3A, DP3B, River
Thiobacillus				X	T6A, DP3B

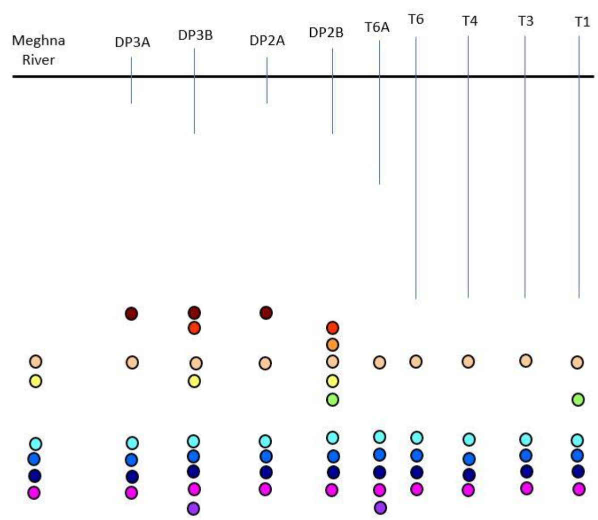

Figure 42: Bacterium genera studied in the past along with their functions, a list of wells they're found in and an illustration showing which wells they're present in by the legend beside each genus. The blue vertical lines represent each well and drive-point piezometer (wells and distances not drawn to scale).

The 3 m drive-point piezometers (DP2B and DP3B) contained the greatest taxonomic diversity at the generic level with 9 of the 12 genera identified from the list of genera known to be involved in As and Fe redox reactions in the table in Fig. 42. The 15 m well furthest

`

from the river (T1), the 7 m well (T6A), the 1 m drive-point piezometers (DP2A, DP3A), and the Meghna River contained 6 of the expected genera involved in As and Fe redox reactions, whereas the rest of the 15 m monitoring wells contained only 5. Interestingly, well T1 contained both Fe and As oxidizing bacteria, but no reducing bacteria. The following 15 m monitoring wells T3, T4, T6, and 7 m monitoring well T6A contained mostly Fe oxidizing bacteria and one of the three As oxidizing bacteria. The 1 m drive-point piezometers DP2A and DP3A contained *Shewanella*, a bacterium capable of As and Fe reduction and some As and Fe oxidizing bacteria. The 3 m drive-point piezometers DP2B and DP3B contain *Sulfurospirillum*, an iron reducing bacteria as well as some As and Fe oxidizing bacteria. The river water sample contained some As and Fe oxidizing bacteria, ones found in all the other monitoring wells and drive-point piezometers.

Table 13: Studied genera and their abundance at each well sequenced for DNA at Veast. The table is heat-mapped, green indicates no bacterial presence and red indicates high bacterial presence. The left column shows the same genera listed in fig. 42 and the numbers correspond to their abundance within each monitoring well and drive-point piezometer.

	T1	T3	T4	T6	T6A	DP2A	DP2B	DP3A	DP3B	River
Shewanella	0	0	0	0	0	1	0	30	22	0
Sulfurospirillum	0	0	0	0	0	0	8	0	6	0
Acidithiobacillus	0	0	0	0	0	0	8	0	0	0
Acidovorax	22	14	5	1	1	14	176	54	130	27
Alcaligenes	0	0	0	0	0	0	2	0	4	4
Agrobacterium	6	0	0	0	0	0	5	0	0	0
Dechlorospirillum	0	0	0	0	0	0	0	0	0	0
Gallionella	607	9	6	1	8	0	1	3	1	1
Leptothrix	15	5	0	0	1	0	54	38	21	29
Pseudomonas	64	37	33	413	512	559	677	414	384	69
Rhizobium	81	201	201	580	74	476	327	442	220	8
Thiobacillus	0	0	0	1	12	0	6	0	11	3

`

Shewanella, a bacterium capable of As and Fe reduction is most abundant in the drive-point piezometers that were located in the river and *Sulfurospirillum*, an Fe reducing bacterium was present only in the 3 m drive-point piezometers. *Acidovorax*, an Fe oxidizing bacterium was highly abundant in the 3 m drive-point piezometers installed in the sandy HZ. *Leptothrix*, and Fe oxidizing bacterium was most abundant in the 3 m drive-point piezometers and one of the 1 m drive-point piezometers, where the groundwater flow path discharges into the river. *Pseudomonas*, another Fe oxidizing bacterium was most abundant in wells close to and drive-point piezometers at the point of groundwater discharge to the river.

An ANOSIM (ANalysis Of SIMilarities), a non-parametric statistical test that measures significant differences between two or more groups was performed using a statistical program called PAST. Group 1 consisted of the deep 15 m depth and shallow 7 m depth monitoring wells and group 2 consisted of the 1-3 m depth drive-point piezometers and the river water. This statistical test was applied to the generic-level classification results to determine whether significant differences occur between the diversity of groups 1 and 2. The resulting *p* value was low (0.0079) indicating that there was a significant difference between the two groups with 95% confidence.

PAST was also used to do principal components analysis (PCA) which assigns components to account for variance in multivariate data. Figure 43 shows that the 15 m monitoring wells T1, T3, T6, and the 3 m drive-point piezometers DP2B and DP3B contained similar taxonomy. The 1 m drive-point piezometers DP2A and DP3A contained similar taxonomy which was not surprising since they were found at the same depths in

`

sandy material that was well mixed with river water (Fig. 3). One of the 15 m monitoring wells (T4, Fig. 3) and the 7 m monitoring well (T6A, Fig. 3) contained similar taxonomy to each other and not to the rest of the 15 m monitoring wells. Note that the river water sample did not group with the monitoring wells or drive-point piezometers.

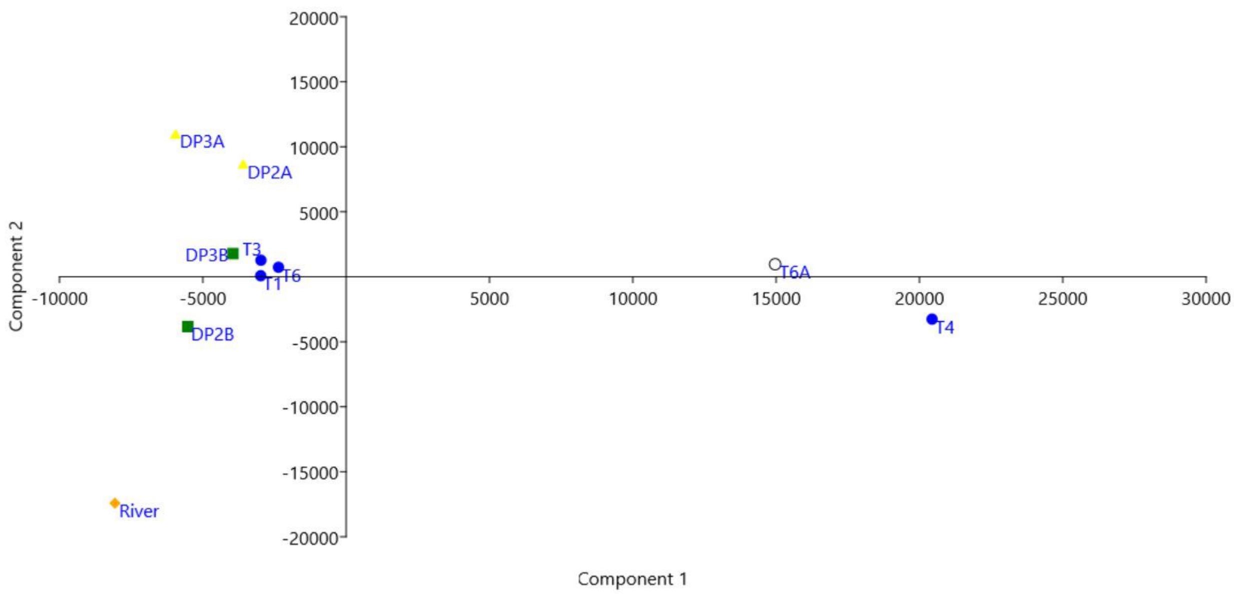

Figure 43: PCA of generic-level taxa identified in wells at Veast. The blue circles, hollow circles, green squares, yellow triangles, and orange diamond represent 15 m monitoring wells, 7 m monitoring well, 3 m and 1 m drive-point piezometers, and river water respectively.

`

6. DISCUSSION

6.1 Two Water Mixing Zones

The overall objective of this project was to study the fate of As at two study sites in a tidally influenced riverbank aquifer along the Meghna River in Bangladesh. More specifically, cations and anions were measured with varying well depths and proximity to the river to investigate any dilution going on within each well transect. Solid-phase geochemistry was studied to identify minerals part of As and Fe cycling and to locate an NRB. Finally, a DNA analysis was done on water samples from selected wells to identify As and Fe oxidizing and reducing bacteria and where they're located along the groundwater discharge flow path.

The decreased concentrations in major cation charge, alkalinity, and SC with proximity to the river at Veast indicate that dilution is occurring near the riverbanks due to groundwater and surface water mixing. This is especially pronounced near the riverbanks at the 1-3 m depth, however river water mixing is diluting the groundwater even at 15 m depth, 85 m away from the river (Fig. 9). In contrast, ORP values are stable along the 15 m and 7 m depths and only increase sharply at 1-3 m depth close to the river. Temperature follows the same pattern. Together, these findings suggest that more recent river water mixing occurs at shallow depths, closer to the river, but that river water mixing is impacting groundwater chemistry 15 m vertically and 85 m laterally into the riverbank aquifer.

Similar to Veast, the riverbank aquifer at Vwest North also displays some evidence of dilution with proximity to the river; however, in this case the dilution occurs with vertical proximity to the river edge, not with lateral proximity. This is in stark contrast to the aqueous geochemistry at Veast where practically every dissolved ion decreased in concentration

`

towards the river laterally along the groundwater discharge flow path (Figs. 15-18). At Vwest North, alkalinity concentrations actually increased in the 15 m deep monitoring wells with proximity to the river. Whereas, the opposite trend is seen at the 7 m depth with alkalinity concentrations decreasing towards the river, the overall differences in alkalinity are greater with change in depth rather than with change in proximity to the river (Fig. 10c). A similar pattern was observed in the SC (Fig. 10d). Although distinctive lateral trends may be hindered by the quantity of wells at that study site, the heterogeneity in the aquifer chemistry is likely caused by the presence of more fine layers as can be seen in the lithology observations in borehole 1b in Fig. 12 and in the Vwest North study site (Fig. 4). The fine silt/clay horizontal layers could be dividing the aquifer into different mixing zones which may or may not be connected to the river.

At each site two zones are evident based on the spatial patterns of temperature, ORP, specific conductance and total cation charge (Figures 9, 10, 19, 20). The 7-16 m monitoring wells at both study sites are tapping into a Reduced Aquifer Zone (RAZ) containing warmer, shallow groundwater. The drive-point piezometers are tapping into a Suboxic Mixing Zone (SMZ) where the warmer, reducing groundwater is mixing with cooler, oxidizing surface water.

At the Veast riverbank aquifer, redox sensitive elements such as As, Fe, and Mn are abundant along the 15 and 7 m deep groundwater flow path (Fig. 15). Arsenic concentrations decreased sharply, however, within the HZ. In contrast, water samples from drive-point piezometers driven into the HZ shows more erratic patterns in Fe and Mn concentrations. The ICP-MS and excess elemental calculations show that As is being captured within the HZ

`

(Figs. 15a, 31a). While this is true for Fe and Mn, some is getting released as indicated by the excess elemental calculations for some of the drive-point piezometers (Fig. 31b, c). These geochemical results indicate that As is being captured by a natural reactive barrier (NRB) near the river banks.

At Vwest North As, Fe, and Mn concentrations demonstrate greater variability in the vertical direction than the horizontal direction (Fig. 17). This may be due to the presence of fine silt/clay layers which separate the aquifer into different mixing zones which results in different geochemical processes occurring at 3, 7, and 15 m depths. It is noteworthy that dissolved As and Fe concentrations increase towards the river, whereas ORP declines. This trend is most simply explained through reductive dissolution of FeOOH driven by fresh DOC from the river or river sediments, releasing As. The direction of the chemical gradient towards the river suggests that the river water or sediments immediately below the river are acting as a source, but only if the river is in losing conditions. Unfortunately, the lateral and vertical hydraulic gradients at the Vwest North site are not well constrained throughout the year. It is possible, then, that the river is at least seasonally losing here which may explain the chemical gradients of As and Fe towards the river as observed by Stahl et al., (2016). Alternatively, the observed gradient could represent As and Fe that had been remobilized into the aquifer following deposition during the last dry season within an NRB. The Meghna River tends to be gaining in the dry season, but losing in the early monsoon (Berube et al., In Review). A slight increase in ORP is also noticeable along the 15 m deep flow path at Veast. These increases may reflect more labile DOC produced from fresh river water or sediment.

`

The dissolved As concentrations at Veast are similar to those found by Jung et al., (2015) whereas the average dissolved As concentrations at Vwest North are somewhat low when compared to Jung et al., (2015). At both study sites, dissolved Mn concentrations farther from the river are low when compared to Jung et al., (2015) but are similar in the HZ.

6.2 Locating an NRB with XRD & XRF

The XRF results showed some concentration increases in As, Fe, and Mn at certain depths within borehole T7 excavated at Veast (Fig. 11) and at boreholes 1b, 2b, and 3b at Vwest North (Figs. 12, 13, 14). At Veast the sharp increases in As, Fe, and Mn concentrations occur at silt/clay and medium coarse sand lithologies. At Vwest North, the XRF results from boreholes 1b, 2b, and 3b at Vwest North (Figs. 12, 13, 14) showed some spikes in As, Fe, and Mn concentrations in clay, silt/clay, and fine-grained sand lithologies. While some increases in elemental concentrations might not mean anything, some could be evidence of a NRB near the river banks, where redox sensitive elements are being captured. However, As concentrations at sub-surface (1-3 m) at Veast and Vwest North are low compared to the concentrations Datta et al., (2009) obtained from the riverbanks of the Meghna River. The solid-phase As concentrations at our study sites are low compared to the concentrations obtained by Jung et al., (2015) from the riverbanks of the Meghna River.

The XRD results suggested the presence of chlorite and mica in the silt/clay fractions in the T7 borehole at Veast and the 1b, 2b, and 3b boreholes at Vwest North. SEM identified biotite in borehole 2b. The weathering of chlorite and mica, more specifically biotite could release redox sensitive elements into the shallow aquifer (Masuda et al., 2012, Seddique et al., 2008). The mica identified in the XRD results could more specifically be biotite. The

`

bulk and sand results suggested a possibility of pyrite present in boreholes T7 and 1b, however this could not be confirmed.

The solid-phase As concentrations found at Veast (31 mg/kg As) and Vwest North (41 mg/kg As) are lower compared to previous studies such as Datta et al., (2009) (100-20000 mg/kg As) and Jung et al., (2015) (99-119 mg/kg As) an NRB may not be present at the location of boreholes T7, 1b, 2b, and 3b. Solid-phase As concentrations at our sites were not much higher than that typically observed in Bangladesh soil. Typically, at maximum 15-20 mg/kg As is found in Bangladesh sediments (Zheng et al., 2005). However, Berube et al., (In Review) studied sediment cores within 50 m of the Veast well transect closer to the Meghna river than the excavated boreholes used for this study. Berube et al., (In Review) possibly found an NRB located in the HZ.

6.3 Modeling the Two Water Mixing Zones

The excess elemental calculations from Veast (Fig. 31) indicate that As is being released from the RAZ and mostly removed from solution in the SMZ, prior to groundwater discharge into the Meghna River which contains little to no detectable aqueous As. Iron is removed from solution within the deeper 15 m monitoring wells and the 1 m drive-point piezometers, but is released within the 7 m monitoring well and 3 m drive-point piezometers. Manganese is being released across the entire groundwater flow path at Veast. The excess elemental calculations show that there’s an environmental change at the HZ when groundwater discharges in the shallow sediments bordering the river.

The excess elemental calculations from Vwest North (Fig. 32) suggest As is released along the deeper 15 m groundwater flow path but is removed within the HZ. Iron is being released along the deeper 15 m flow path and into the HZ, but appears to have suddenly

`

increased in concentrations within the 7 m monitoring well. Manganese is removed from solution within all the monitoring wells and released within the HZ when the groundwater discharges in the shallow sediments bordering the river. Different geochemical processes are going on in the 15 and 7 m groundwater flow paths. Another change in geochemical processes is going on at the HZ where groundwater discharges in the shallow sediments bordering the river.

The purpose of the Eh-pH diagrams is to calculate the expected dominant ion species of As in the aquifer adjacent to each well using thermodynamically derived values. At Veast, the monitoring well samples from RAZ sit on the As(III) and As(V) stability boundary (Figs. 33, 34), implying that the shallow groundwater aquifer could be a suitable environment for either to occur naturally. Further, some wells should contain primarily aqueous Fe(II) in solution or precipitated Fe oxides (Fig. 35). Higher Fe concentrations were detected with XRF, however, no Fe oxide minerals were identified with XRD or SEM. Importantly, figure 34 shows that the Veast site doesn't have the necessary environmental parameters to precipitate As-sulfur minerals. No As-bearing minerals were detected with XRD or SEM.

As for Vwest North, all of the samples are in the aqueous As(V) zone meaning As(V) can occur naturally (Fig. 36). Further, all of the samples sit in the precipitated Fe phase meaning the site should contain precipitated Fe oxides (Fig. 38). This agrees with the relative low concentrations of dissolved Fe observed at the Vwest North site. The plotting of the points of wells from the Vwest North site that are closer to the river, closer to the dissolved Fe^{2+} stability region also agrees with the observed increases in dissolved Fe with proximity to the river (Fig. 15b). Finally, figure 37 suggest the environment at Vwest North is not

`

favorable to precipitate As-sulfur minerals such as realgar and orpiment. No As-bearing minerals were detected with XRD or SEM, further validating the results from figure 37.

6.4 Bacterial Diversity across two Mixing Zones

The purpose behind the metagenomics work was to perform a community diversity profile for Veast and to determine where As and Fe oxidizing and reducing bacterium are located along a groundwater discharge flow path with transient redox zones. The individual rarefaction curves (Figure 41) showed that the 15 m monitoring well furthest from the river, T1 contained the most taxa meaning it had the greatest bacterial genera diversity. After T1, the 3 m drive-point piezometers contained the most bacterial genera diversity. An irrigation well 1 m away from well T1 (Fig. 3), and screened across the same shallow aquifer is pumped by farmers each dry season to irrigate agricultural crops. Monitoring well T1 was sampled for this project in the middle of the dry season before the irrigation well had started being used for the year. The greater amount of bacterial diversity in the well could be due to water mixing caused by pumping in past years.

It is important to note, that although well T1 contained the greatest overall genus diversity, few of the genera known to reduce or oxidize As or Fe were found at T1. In contrast, the great diversity present in the 3 m drive-point piezometers was accompanied by the highest number of genera involved in redox reactions with As and Fe amongst all the waters sampled at Veast. This is consistent with the aqueous geochemistry data which indicated this part of the HZ is very well mixed with recent river water. Tidal and seasonal fluctuations in the river, further ensure, the oxidizing zone will expand and contract regularly, allowing bacterial genera which mediate oxidation reactions to flourish with those mediating reduction reactions in the same spot. The waters with the least bacterial diversity

`

were found within wells T6, T6A, and river water. The high surface area of sediments in HZs are well known to promote bacterial growth in contrast to river water (Nagorski and Moore, 1999).

The monitoring wells were put into group 1 and the drive-point piezometers into group 2, an ANOSIM test was performed to determine if there's a significant difference between the bacterial communities between groups 1 and 2. The ranked distances for group 1 are on average less than that for group 2 which means there is more diversity in the drive-point piezometers versus the deeper monitoring wells. This is another line of evidence for there being two distinct water mixing zones at Veast: a younger, transiently oxidized mixing zone (SMZ) and an older, permanently reducing zone (RAZ). Since the SMZ has greater groundwater/surface water mixing, and likely widely-different transient redox conditions, the bacterial community is more diverse than in the RAZ. Sutton et al., (2009) did a study on bacterial diversity between deep tube wells and shallow tube wells from five villages in Bangladesh in the Munshiganj and Jessore districts. They found that the shallow tube wells contained a greater bacterial diversity than the deep tube wells. Whereas Sutton et al., (2009) were not working along a transiently fluctuating HZ, the seasonally fluctuating water table in Bangladesh would have a similar effect allowing both reducing and oxidizing genera to thrive along the water table.

The Columbia River experiences ~1 m seasonal fluctuations in the water table. Lin et al., (2012) performed a bacterial diversity study on this river in Washington State by sampling three study sites, each of which contained three monitoring wells at 10 m, 13 m, and 17 m in depth. They performed a two-way nested ANOSIM on bacterial results from barcoded pyrosequencing (Lin et al., 2012) from each monitoring well and found a significant difference in bacterial diversity with respect to depth, especially across the 13 m and 17 m wells (Lin et al., 2012). The Columbia River experiences much lower seasonal fluctuations than the Meghna River and Lin et al., (2012) used deeper wells than the drive-point piezometers driven into the HZ along the Meghna River in this thesis, but Lin et al., (2012) still found significant differences between bacterial communities varying with depth which was found at the Meghna River. This was likely related to the fact that that the aquifer adjacent to the Columbia River has a high hydraulic conductivity (K) (Lin et al., (2012) which allows the HZ to greatly expand (Wondzell and Swanson, 1996).

The phase diagrams for Veast (Figures 33-35) show the 7-16 m monitoring wells on the equilibrium line between the As(III) and As(V) phases. This means both aqueous As(III) and As(V) can exist naturally. However, if the environment continuously fluctuates between aqueous As(III) and As(V) stability, it may make the deeper 15 m groundwater flow path a more difficult environment for bacteria to survive in. This could be another reason the 15 m depth monitoring wells contained less bacterial diversity than the 1-3 m drive-point piezometers.

6.5 Comparing Veast & Vwest North Study Sites

The average SC and alkalinity measurements for Veast and Vwest North are similar (Tables 4, 5; Figs. 9, 10). Both show evidence of dilution occurring with proximity to the river banks, even though at Vwest North that mixing seems to occur more in the vertical than the lateral direction as at Veast. This is affected by the abundant horizontal clay and silt layers near the river at Vwest North breaking up the aquifer into separate, vertically-stacked-zones. These same patterns are evident in the major cations charges at both study sites (Figs.

`

19, 20). This is evidence that there are different water mixing zones near the riverbanks of the Meghna River: a young, recent mixing zone and a deeper mixing zone, whose depth and lateral extent is controlled by vertical and lateral K, respectively.

The aqueous geochemistry results at Veast and Vwest North have quite different trends, though the trends at Vwest may be harder to see due to the lack of quantity of wells. Arsenic concentrations are highest in the deeper monitoring wells and concentrations decrease closer to the ground surface and are nonexistent in the Meghna River. Iron has some spikes in concentrations at Veast but the trend seems to simply increase at Vwest North. The increase in Fe concentrations at Vwest North could be the same spikes in concentration seen at Veast. The major cations follow the same trends at both sites as well as nitrite, ammonium, silica, and DOC. Both sites show evidence of geochemical changes going on at shallower depths near the riverbanks which is evidence of two distinct water mixing zones.

The borehole XRF results showed that all four boreholes had spikes in As, Fe, and Mn concentrations in clay and silt/clay lithologies. There was a distinct spike in As, Fe, and Mn concentrations at some medium coarse sand in borehole T7, but there was no medium coarse sand in any of the boreholes at Vwest North so there's nothing to compare it with. The XRD results showed that the mineralogy for all four boreholes were very similar despite being at different locations and having different lithologies. Mostly quartz and feldspars are present in the sand sized grains and some chlorite and mica was found in the silt/clay sized grains.

Some of the excess elemental calculations for As are similar at both sites. At Veast and Vwest North As is mainly released from the deeper 15 m monitoring wells and is

`

released at some points within the SMZ and removed from solution at others. Manganese is being released within all the wells and drive-point piezometers at Veast. However, at Vwest North, Mn is removed from solution within the RAZ and released within the SMZ. Iron is mostly removed from solution within the RAZ and the SMZ at 1 m depth and released within the RAZ at 7 m depth and the SMZ at 3 m depth at Veast. However, Fe is released within both the RAZ and the SMZ at Vwest North.

The excess elemental calculations for Fe correspond with the thermodynamics shown in the Eh-pH diagrams. Fe exists in a precipitated form only at Vwest North (Figure 38) and Fe exists in both aqueous and solid phases at Veast (Figure 35). Figures 34 and 37 suggest the environments at both Veast and Vwest North are not reduced enough to precipitate As-sulfur minerals such as realgar and orpiment which agrees with the XRD and SEM results. The saturated indices (SI) calculated by PHREEQC were similar for Veast and Vwest North. Both calcite and manganite are under saturated at Veast and Vwest North. Siderite and pyrite are supersaturated at Veast and Vwest North.

The two study sites Veast and Vwest North have some similarities but also some differences. The study sites are not far from one another and experience the same seasonal tidal fluctuations. Aqueous geochemistry trends may be more difficult to see at Vwest North due to the lack of quantity of monitoring wells and drive-point piezometers. Though the basic lithology at both sites are similar, Vwest North contains multiple <1 m thick silt/clay layers which could be responsible for the differing aqueous geochemical results from that observed at Veast.

`

6.6 Comparing this Project with Other Research Projects in southeast Asia

It is worth noting the aqueous and solid-phase geochemical results other research projects that have studied the fate of As in a riverbank aquifer in southeast Asia observed and compare to the results observed in this project. Aqueous geochemistry results for As concentrations ranged from 0.2 to 0.5 mg/L in the monitoring wells and drive-point piezometers at both study sites. Shaefer et al., (2016) performed a multiyear study within an aquifer adjacent to the Yangtze river in China and on average measured 0.062 mg/L concentrations for As, lower than As concentrations observed in this study. Jung et al., (2015) performed their study ~25 km southeast of Dhaka, Bangladesh in the Gazaria Upazila, along the Meghna River about 10 km south of Veast, and As concentrations in January 2006 were measured at 0.238 mg/L on average from deeper well groundwater (13-27 m depth, 30 m away from river) and 0.1 mg/L in riverbank porewater (0-7 m depth, 5 m away from river). The As concentrations Jung et al., (2015) observed are lower than at our study sites, but Jung et al., (2015) observed lower As concentrations in the riverbank porewater than the well groundwater. This same trend was observed in our study. Zheng et al., (2005) studied aqueous parameters of monitoring wells in small rural villages in Araihazar, Bangladesh. In January 2001, they observed As concentrations ranging from 0 to 0.582 mg/L, which are similar to the concentrations observed in this project. Overall As concentrations observed at our study sites are the same or higher than what other studies in southeast Asia have observed.

Aqueous Fe concentrations at both study sites ranged from 0 to 20 mg/L in the deeper monitoring wells and drive-point piezometers. Shaefer et al., (2016) observed Fe concentrations ranging from 0 to 40 mg/L across their study site. Jung et al., (2015) observed

`

Fe concentrations around 9 mg/L on average in deeper monitoring wells and 1-5 mg/L in riverbank porewater. Iron concentrations observed in our study were generally higher and some sharp increases in Fe concentrations were observed in the shallower drive-point piezometers. Zheng et al., (2005) observed 0-0.3 mmol/L Fe at their study sites and 0-0.4 mmol/L (Tables A5, A6) at our study sites. Overall the Fe concentrations observed at our study sites are similar to other studies performed in shallow aquifers along the Meghna River, in the region and in analogous settings in China; some studies observed Fe concentrations greater than that seen at our study site and some observed less.

Aqueous Mn concentrations at our study sites ranged from 0 to 4 mg/L or 0 to 0.08 mmol/L. Jung et al., (2015) observed an average Mn concentration of 1.5 mg/L in deeper well groundwater and 0.5-3.5 mg/L in riverbank porewater. The same trend is seen at our study sites; Mn concentrations range 0.5-2.4 mg/L in the deeper monitoring wells and some Mn concentrations spike in the drive-point piezometers. Zheng et al., (2005) observed Mn concentrations of 0.1-0.001 mmol/L which is similar to the Mn concentrations observed in our study.

Solid-phase As, Mn, and Fe concentrations in our study ranged from 31-48 mg/kg, 1,211-1,538 mg/kg, and 37,483-55,729 mg/kg respectively. Xie et al., (2014) performed an As study in the HZ of the Sanggan riverbanks in Shanxi Provence, China. They found As, Mn, and Fe solid-phase concentration ranging from 10-47 mg/kg, 400 -1,000 mg/kg, 17,000-39,000 mg/kg of As, Mn, and Fe respectively. The concentrations Xie et al., (2014) found were somewhat similar to that found at our study sites. Datta et al., (2009) did a study on the Meghna River in Bangladesh and used 1.2 N HCl and extracted 100-20,000 mg/kg of As in

`

subsurface sediment. The As, Mn, and Fe concentrations Datta et al., (2009) found were much higher than what was detected with XRF at our study sites. They likely found a natural reactive barrier (NRB) at their study site whereas boreholes for sediment analysis presented in this thesis were located too far from the riverbanks to detect an NRB. Shallow sediment cores were taken within the HZ at Veast in a companion study and these revealed ~700 mg/kg As (Berube et al., In Review).

6.7 Global Importance

This study produced key findings which compliment other studies performed across south and southeast Asia. Many regions within south and southeast Asia have similar hydrological characteristics including fast discharging rivers, low lying deltas, and seasonal tidal fluctuations. Surface water levels in the Yangtze River in China fluctuates annually 5-8 m (Shaefer, 2016). The two water mixing zones that are occurring at our study sites are likely occurring near the riverbanks of fast discharging rivers in southeast Asia.

Arsenic groundwater contamination is not only a problem in southeast Asia, it's a problem in other countries. Nagorski and Moore, (1999) collected water samples from the HZ of Silver Bow Creek in Montana and found dissolved As concentrations in pore-waters ranging from <65-2700 μg/L. Though the As concentrations in Silver Bow Creek were lower than dissolved As concentrations in the Meghna River and the As contamination in Silver Bow Creek is a result of mining, the HZ is a complex water mixing zone where biogeochemical reactions are occurring which could potentially play an important role in As and other metal/metalloid contamination.

`

7. CONCLUSION

The purpose of this thesis was to investigate the biogeochemical processes behind As and Fe cycling near the river banks. Most research focuses on the source of As in southeast Asia, further away from the major rivers. In contrast, this project focuses on the fate of As in the groundwater near the river banks of a major river.

The first objective was to explain the aqueous geochemical spatial trends observed in two different well transects along two different riverbank aquifers on opposing sides of a major river in Bangladesh. The hypothesis was that dilution of conservative elements are occurring at an equal rate and that precipitation and adsorption redox sensitive elements increases with proximity to the river. The aqueous geochemistry and excess elemental calculations confirmed that dilution in major cations charge and somewhat in alkalinity is occurring.

The second objective was to identify minerals present possibly contributing to As cycling near the river banks and an NRB. Since the segment of the aquifer is a reducing environment the hypothesis was that Fe reducing minerals would be present. The second hypothesis could not be completely confirmed. The XRD results suggested that pyrite could be present but that result is not certain. However, other minerals that could potentially play an important role in As cycling such as chlorite and biotite were identified. An NRB is likely not present where the boreholes were excavated. At Veast the NRB is likely much closer to the riverbanks as was suggested through direct coring and sequential extractions performed in Berube et al., (In Review) and by the rapid removal of As from solution within the 1-3 m deep zone sampled by the drive-point piezometers presented in this thesis.

`

The third and final objective was to determine if As and Fe oxidizing and reducing bacteria are present at Veast and where and the hypothesis tested was that the shallower drive-point piezometers closer to the river would contain more taxonomic diversity than the deeper monitoring wells farther from the river. It was determined that many As and Fe oxidizing and reducing bacteria do exist at the Veast study site but some are present only in certain wells. The groundwater within the well farthest from the river, T1, contained the most bacterial diversity likely due to the regular use of the irrigation pump located only 1 m away from it and screen across the shallow aquifer. The 1-3 m drive-point piezometers' locations and depths contained more taxonomy than the deeper monitoring wells which confirmed the third hypothesis. These wells also contained the greatest number of bacterial genera involved in Fe and As redox reactions, whereas well T1 contained few.

The aqueous geochemistry, microbiology, and geochemical modeling show evidence of an NRB and two different water mixing zones. The chemistry results show that the concentrations in As, Fe, and Mn vary along the groundwater flow path at both riverbank aquifers and show that they're being removed from solution and released at varying depths and distances from the river at both transects. Excess elemental calculations provided the strongest indication of the two mixing zones along the riverbanks of the Meghna River. The microbiology evidence at Veast suggests these two mixing zones impact the overall diversity and presence of genera involved in mediating As and Fe redox reactions within the riverbanks of the Meghna River.

The presence of two geochemically different mixing zones and the possible presence of an NRB are important geochemical factors behind As cycling. Explaining the

`

geochemistry behind the capture and release of As within the riverbanks can lead to a better understanding of the fate of As in groundwater discharging to rivers in Bangladesh. Other countries in southeast Asia including Vietnam, Cambodia, and China contain similar hydrological characteristics as Bangladesh so the presence of two mixing zones and an NRB could potentially exist at the riverbanks in these places as well. Any natural process which concentrates solid-phase As to such high levels observed in Datta et al., (2009) of 23,000 mg/kg deserves study because these levels are similar to sediments found downstream of unregulated mine waste (Nagorski and Moore, 1999).

`

REFERENCES

Acharyya, S.K. et al., "Arsenic toxicity of groundwater in parts of the Bengal basin in India and Bangladesh: the role of Quaternary stratigraphy and Holocene sea-level fluctuation" Environmental Geology 39 (10), 1127-1137, (2000).

Berube, Michelle et al., "The Fate of Arsenic in Groundwater Discharged to the Meghna River, Bangladesh" Environmental Chemistry (in review).

Borch, Thomas et al., "Biogeochemical Redox Processes and their Impact on Contaminant Dynamics" Environmental Science Technology 44, 15-23 (2010).

Clarke, K.R. "Non-parametric multivariate analysis of changes in community structure" Australian Journal of Ecology, 18 117-143 (1993).

Cummings, David E. et al., "Arsenic Mobilization by the Dissimilatory Fe(II)-Reducing Bacterium *Shewanella alga* BrY" Environmental Science Technology 33, 723-729 (1999).

Datta, S. et al., "Redox trapping of arsenic during groundwater discharge in sediments from the Meghna riverbank in Bangladesh" PNAS, vol. 106, 16930-16935, (2009).

Davis, J.C. Statistics and Data Analysis in Geology. John Wiley & Sons. (1986).

Deng, Y., G.N. White, and J.B. Dixon. 2014. Soil Mineralogy Laboratory Manual. 15th edition. Published by the authors, Department of Soil and Crop Sciences, Texas A&M University, College Station, Texas 77843-2474.

Desbarats, A.J. et al., "Groundwater flow dynamics and arsenic source characterization in an aquifer system of West Bengal, India" AGU Publications, Water Resources Research, 4974-5002, (2014).

Ehlert, Katrin et al., "Impact of Birnessite on Arsenic and Iron Speciation during Microbial Reduction of Arsenic-Bearing Ferrihydrite" Environmental Science & Technology 48, 11320-11329 (2014).

Fendorf, Scott et al., "Spatial and Temporal Variations of Groundwater Arsenic in South and Southast Asia" Science Magazine, Vol 328, (2010).

Feris, Kevin et al., "Differences in Hyporheic-Zone Microbial Community Structure along a Heavy-Metal Contamination Gradient" Applied and Environmental Microbiology 69, 5563-5573 (2003).

Feris, Kevin P. et al., "Seasonal Dynamics of Shallow-Hyporheic-Zone Microbial Community Structure along a Heavy-Metal Contamination Gradient" Applied Environmental Microbiology 70, 2323-2331 (2004).

Gan, Ping et al., "Sampling Methods to Determine the Spatial Gradients and Flux of Arsenic at a Groundwater Seepage Zone" Environmental Toxicology and Chemistry 25, 1487-1495 (2006).

Ghorbanzadeh, Nasrin et al., "Influence of clay minerals on sorption and bioreduction of arsenic under anoxic conditions" Environmental Geochemistry Health 37, 997-1005 (2015).

`

Goodbred, Steven L. et al., “Piecing together the Ganges-Brahmaputra-Meghna River delta: Use of sediment provenance to reconstruct the history and interaction of multiple fluvial systems during Holocene delta evolution” GSA Bulletin November/December 2014 126 (11/12) 1495-1510 (2014).

Gorny, Josselin et al., “Arsenic behavior in river sediments under redox gradient: A review” Science of the Total Environment 505, 423-434 (2015).

Harper, D.A.T. (ed.). 1999. Numerical Palaeobiology. John Wiley & Sons.

Huntington, Katharine. 2016. Article VII Density separations. Heavy Mineral Separation SOP, 5pp.

Jung, Hun Bok, Benjamin C. Bostick, and Yan Zheng “Field, Experimental, and Modeling Study of Arsenic Partitioning across a Redox Transition in a Bangladesh Aquifer” Environmental Science Technology 46 (3), 1388-1395 (2012).

Jung, Hun Bok et al., “Redox zonation and oscillation in the hyporheic zone of the Ganges-Brahmaputra-Meghna Delta: Implications for the fate of groundwater arsenic during discharge” Applied Geochemistry 63, 647-660 (2015).

Knappett, P.S.K. et al., “Vulnerability of low-arsenic aquifers to municipal pumping in Bangladesh” Journal of Hydrology 539, 674-686 (2016).

Knappett, Peter S. K. et al., “Unsealed tubewells lead to increased fecal contamination of drinking water” Journal of Water and Health 10.4, 565-578 (2012).

Kocar, Benjamin D., Shawn G. Benner, and Scott Fendorf “Deciphering and predicting spatial and temporal concentrations of arsenic within the Mekong Delta aquifer” Environmental Chemistry 11, 579-594 (2014).

Kocar, Benjamin D. and Scott Fendorf, “Thermodynamic Constraints on Reductive Reactions Influencing the Biogeochemistry of Arsenic in Soils and Sediments” Environmental Science Technology 43, 4871-4877 (2009).

Lin, Xueju et al., “Spatial and temporal dynamics of the microbial community in the Hanford unconfined aquifer” International Society for Microbial Ecology 6, 1665-1676 (2012).

MacKay, Allison A. et al., “Seasonal Arsenic Accumulation in Stream Sediments at a Groundwater Discharge Zone” Environmental Science & Technology 48, 920-929 (2014).

Mailloux, Brian J. et al., “Advection of surface-derived organic carbon fuels microbial reduction in Bangladesh groundwater” PNAS vol. 10, 14, 5331-5335 (2013).

Masuda, Harue, Yoshito Yamatani, and Mitsuru Okai “Transformation of arsenic compounds in modern intertidal sediments of Iriomote Island, Japan” Journal of Geochemical Exploration 87, 73-81 (2005).

Masuda, Harue et al., “Chlorite-source of arsenic groundwater pollution in the Holocene aquifer of Bangladesh” Geochemical Journal, Vol. 46, 381-391 (2012).

`

Muehe, E. Marie et al., “Arsenic(V) Incorporation in Vivianite during Microbial Reduction of Arsenic(V)-Bearing Biogenic Fe(III) (Oxyhydr)oxides” Environmental Science & Technology 50, 2281-2291 (2016).

Nagorski, Sonia A. and Johnnie N. Moore, “Arsenic mobilization in the hyporheic zone of a contaminated stream” Water Resources Research 35, 3441-3450 (1999).

Nickson, Ross et al., “Arsenic poisoning of Bangladesh groundwater” Nature (393) 338 (24 September 1998).

Nickson, R.T. et al., “Mechanism of arsenic release to groundwater, Bangladesh and West Bengal” Applied Geochemistry 15, 403-413 (2000).

Nordstrom, Kirk, “Worldwide Occurrences of Arsenic in Ground Water” Science Vol. 296, 2143-2144 (2002).

Postma, Dieke et al., “Mobilization of arsenic and iron from Red River floodplain sediments, Vietnam” Science Direct, 3367-3381 (2010).

Seddique, Ashraf Ali et al., “Arsenic release from biotite into a Holocene groundwater aquifer in Bangladesh” Applied Geochemistry 23, 2236-2248, (2008).

Shaefer, Michael V. et al., “Aquifer Arsenic Cycling Induced by Seasonal Hydrologic Changes within the Yangtze River Basin” Environmental Science & Technology 50, 3521-3529 (2016).

Shuai, Pin et al., “The Impact of the Degree of Aquifer Confinement and Anisotropy on Tidal Pulse Propagation” Ground Water (2017).

Stahl, Mason O. et al., “River bank geomorphology controls groundwater arsenic concentrations in aquifers adjacent to the Red River, Hanoi Vietnam” Water Resources Research 6321-6334 (2016).

Stollenwerk KG. 2003. “Geochemical processes controlling transport of arsenic” In Welch AH, Stollenwerk KG, eds, Arsenic in Groundwater: Geochemistry and Occurrence. Kluwer, Boston, MA, USA, pp 67-100.

Stuckey, Jason W. et al., “Reactivity and speciation of mineral-associated arsenic in seasonal and permanent wetlands of the Mekong Delta” Science Direct, 143-155, (2015).

Sutton, Nora B. et al., “Characterization of geochemical constituents and bacterial populations associated with As mobilization in deep and shallow tube wells in Bangladesh” Water Research 43, 1720-1730 (2009).

Swer, Sumarlin and O.P. Singh “Status of Water Quality in Coal Mining Areas of Meghalaya, India” Proceedings of the National Seminar on Environmental Engineering with special emphasis on Mining Environment, NSEEME, 19-20, March 2004

Tufano, Katharine J. and Scott Fendorf “Confounding Impacts of Iron Reduction on Arsenic Retention” Environmental Science & Technology Vol. 42, 4777-4783 (2008).

`

van Geen, A. et al., “Spatial variability of arsenic in 6000 tube wells in a 25 km^2 area of Bangladesh” Water Resources Research, 39 (5) 1140 (2003).

van Geen Alexander et al., “Retardation of arsenic transport through a Pleistocene aquifer” Nature 501, 204-207 (12 September 2013).

van Geen, Alexander et al., “Comparison of two blanket surveys of arsenic in tubewells conducted 12 years apart in a 25 km^2 area of Bangladesh” Science of the Total Environment (488-489) 484-492 (2014).

Weinman, Beth et al., “Contributions of floodplain stratigraphy and evolution to the spatial patterns of groundwater arsenic in Araihazar, Bangladesh” GSA Bulletin November/December 2008 120 (11/12) 1567-1580 (2008).

Welch, Alan H. et al., “Arsenic in Ground Water of the United States: Occurrence and Geochemistry” Ground Water Vol 38, No. 4, 589-604, (July-August 2000).

Wondzell, S.M. and F.J. Swanson “Seasonal and storm dynamics of the hyporheic zone of a 4^{th}-order mountain stream. I: Hydrologic processes” J.N. Am. Benthol Soc. 15 (1) 3-19 (1996).

Xie, Xianjun et al., “Pathways of arsenic from sediments to groundwater in the hyporheic zone: Evidence from an iron isotope study” Journal of Hydrology 511, 509-517, (2014).

Xiu, Wei et al., “Arsenic Removal and Transformation by *Pseudomonas* sp. Strain GE-1-Induced Ferrihydrite: Co-precipitation Versus Adsorption” Water Air Soil Pollution 226:167 (2015).

YSI Environmental. Measuring ORP on YSI 6-Series Sondes: Tips, Cautions and Limitations. 2005. Tech Note 0201 T608

Zheng, Y. et al., “Redox control of arsenic mobilization in Bangladesh groundwater” Applied Geochemistry 19, 201-214 (2004).

Zheng, Y. et al., “Geochemical and hydrogeological contrasts between shallow and deep aquifers in two villages of Araihazar, Bangladesh: Implications for deeper aquifers as drinking water sources” Applied Geochemistry 69, 5203-5218 (2005).

Zobrist, Juerg et al., “Mobilization of Arsenite by Dissimilatory Reduction of Adsorbed Arsenate” Environmental Science Technology 34, 4747-4753 (2000).

`

APPENDIX

Aqueous Geochemistry Results

The aqueous geochemistry results were measured in mg/L in the field and by the IC and ICP-MS. The tables in this section show the elemental and compound concentrations calculated in millimoles.

Table A1: Aqueous geochemistry results from the field at Veast in millimoles. N/A = not analyzed.

Well Name	Alkalinity (Mm)	Arsenic (Mm)	Iron (Mm)	Ammonia (Mm)	Sulfides (Mm)	Manganese (Mm)	Dissolved Oxygen (Mm)	Nitrate (Mm)	Phosphate (Mm)	Sulfate (Mm)
T1	5.164	0.007	0.477	0.026	0.005	0.029	0.008	0.105	N/A	N/A
T2	5.770	0.007	0.442	0.411	0.004	0.031	0.004	0.172	N/A	N/A
T3	4.787	0.007	0.416	0.437	0.003	0.043	0.006	0.154	N/A	N/A
T4	4.279	0.007	0.383	0.000	0.006	0.032	0.025	0.319	0.031	0.512
T5	4.131	0.004	0.310	0.082	0.003	0.034	0.008	0.419	0.033	0.466
T6	3.377	0.007	0.277	N/A	0.002	0.036	0.030	N/A	N/A	N/A
T6A	2.803	0.004	0.382	N/A	0.006	0.026	0.004	N/A	N/A	N/A
DP 2A	3.066	0.004	0.208	0.015	0.005	0.105	0.001	N/A	0.038	0.292
DP 3A	3.984	0.003	0.278	0.280	0.007	0.042	0.002	0.074	0.004	N/A
DP 2B	2.787	0.003	0.504	0.046	0.005	0.054	0.002	0.133	0.019	N/A
DP 3B	1.693	0.003	0.033	0.209	0.004	0.040	0.019	0.104	0.017	N/A
River	0.836	0.000	0.000	0.000	0.006	0.029	0.490	0.122	N/A	0.100

Table A2: Aqueous geochemistry results from the field at Vwest North in millimoles. N/A = not analyzed.

Well Name	Alkalinity (Mm)	Arsenic (Mm)	Iron (Mm)	Ammonia (Mm)	Sulfides (Mm)	Manganese (Mm)	Dissolved Oxygen (Mm)	Nitrate (Mm)	Phosphate (Mm)	Sulfate (Mm)
DP 1	3.328	0.000	0.217	0.033	0.004	0.023	0.104	0.090	N/A	N/A
1a	1.967	0.004	0.018	0.072	0.005	0.015	0.254	0.034	N/A	N/A
1b	4.180	0.004	0.080	0.105	0.005	0.000	0.047	0.044	N/A	N/A
2a	2.541	0.004	0.005	0.074	0.004	0.015	0.121	0.034	N/A	N/A
2b	3.803	0.004	0.029	0.087	0.002	0.016	0.189	0.037	N/A	N/A
3b	2.818	0.004	0.019	0.059	0.001	0.033	0.116	0.037	N/A	N/A

`

Table A3: Aqueous geochemistry results from the IC at Veast in millimoles. BDL = below detection limit.

Well Name	Fluoride (Mm)	Chloride (Mm)	Bromide (Mm)	Nitrate (Mm)	Nitrite (Mm)	Sulfate (Mm)	Phosphate (Mm)
T1	0.021	0.564	BDL	0.091	0.060	BDL	BDL
T2	0.017	0.126	BDL	BDL	0.156	BDL	BDL
T3	0.023	0.237	BDL	BDL	0.073	BDL	BDL
T4	0.017	0.303	BDL	BDL	0.058	BDL	BDL
T5	0.018	0.310	BDL	BDL	0.054	BDL	BDL
T6	0.020	0.206	BDL	0.002	0.061	BDL	BDL
T6A	0.014	0.463	BDL	0.002	0.116	BDL	BDL
DP 2A	0.014	0.967	BDL	BDL	0.106	BDL	BDL
DP 3A	0.010	0.264	BDL	0.006	0.042	BDL	BDL
DP 2B	0.015	0.519	BDL	BDL	0.085	BDL	BDL
DP 3B	0.008	0.152	BDL	0.004	0.028	BDL	BDL
River	0.010	0.114	BDL	0.022	0.005	0.085	BDL

Well Name	Sodium (Mm)	Ammonium (Mm)	Potassium (Mm)	Magnesium (Mm)	Calcium (Mm)
T1	0.620	1.095	0.159	0.924	1.684
T2	0.325	0.610	0.125	0.839	1.575
T3	0.356	0.585	0.133	0.876	1.671
T4	0.323	0.628	0.132	0.781	1.505
T5	0.309	0.604	0.133	0.750	1.563
T6	0.299	0.511	0.117	0.744	1.554
T6A	0.359	0.529	0.101	0.672	1.119
DP 2A	0.537	0.327	0.117	0.622	1.244
DP 3A	0.385	0.440	0.097	0.463	1.528
DP 2B	0.490	0.289	0.087	0.460	0.744
DP 3B	0.299	0.336	0.075	0.334	0.524
River	0.319	0.002	0.058	0.178	0.275

`

Table A4: Aqueous geochemistry results from the IC at Vwest North in millimoles. BDL = below detection limit.

Well Name	Fluoride (Mm)	Chloride (Mm)	Bromide (Mm)	Nitrate (Mm)	Nitrite (Mm)	Sulfate (Mm)	Phosphate (Mm)
DP1	0.012	0.225	BDL	BDL	0.045	0.152	BDL
1a	0.011	0.302	BDL	BDL	0.017	0.145	0.037
1b	0.014	0.204	BDL	BDL	0.043	0.002	0.018
2a	0.015	0.265	BDL	BDL	0.018	0.137	0.044
2b	0.013	0.075	BDL	BDL	0.141	0.002	0.028
3b	0.001	0.076	BDL	0.004	0.089	0.041	0.034
Well Name	**Sodium (Mm)**	**Ammonium (Mm)**	**Potassium (Mm)**	**Magnesium (Mm)**	**Calcium (Mm)**		
DP 1	0.409	0.052	0.078	0.270	0.480		
1a	0.341	0.085	0.093	0.399	1.029		
1b	0.446	0.116	0.113	0.633	1.696		
2a	0.328	0.085	0.090	0.401	1.028		
2b	0.401	0.101	0.109	0.631	1.711		
3b	0.375	0.075	0.097	0.502	1.226		

`

Table A5: Aqueous geochemistry results from the ICP-MS at Veast in millimoles. BDL = below detection limit.

Well Name	Fe56 (Mm)	Mn55 (Mm)	As75 (Mm)	Co59 (Mm)	Ni60 (Mm)	Cu63 (Mm)	Zn66 (Mm)
T1	0.333	0.028	0.005	0.000	0.000	0.000	0.001
T2	0.349	0.031	0.006	0.000	0.000	0.000	0.002
T3	0.286	0.044	0.006	0.000	0.000	0.000	0.005
T4	0.000	0.033	0.001	0.000	0.000	0.000	0.000
T5	0.193	0.030	0.008	0.000	0.000	0.000	0.002
T6	0.159	0.033	0.007	0.000	0.000	0.000	0.001
T6A	0.268	0.030	0.003	0.000	0.000	0.000	0.002
DP 2A	0.183	0.075	0.002	0.000	0.000	0.000	0.002
DP 3A	0.186	0.035	0.003	0.000	0.000	0.000	0.003
DP 2B	0.360	0.049	0.001	0.000	0.000	0.000	0.002
DP 3B	0.146	0.024	0.002	0.000	0.000	0.000	0.001
River	0.000	0.000	0.000	0.000	0.000	0.000	0.002

Well Name	Na23 (Mm)	K39 (Mm)	Mg26 (Mm)	Si30 (Mm)	Ca43 (Mm)	S32 (Mm)	P31 (Mm)
T1	0.517	0.101	0.742	0.366	1.436	0.002	0.023
T2	0.266	0.164	0.692	0.275	1.420	0.003	0.020
T3	0.304	0.120	0.741	0.288	1.537	0.005	0.006
T4	0.289	0.368	0.705	0.272	1.434	0.002	0.000
T5	0.254	0.000	0.625	0.266	1.400	0.004	0.003
T6	0.242	0.073	0.610	0.210	1.383	0.003	0.006
T6A	0.285	0.067	0.551	0.407	1.005	0.003	0.032
DP 2A	0.393	0.083	0.493	0.253	1.234	0.003	0.056
DP 3A	0.287	0.067	0.358	0.261	1.272	0.003	0.030
DP 2B	0.363	0.060	0.370	0.348	0.678	0.003	0.030
DP 3B	0.224	0.049	0.268	0.277	0.455	0.003	0.027
River	0.248	0.033	0.143	0.068	0.216	0.092	0.000

Well Name	Mo98 (Mm)	Cd111 (Mm)	Sb121 (Mm)	Ba137 (Mm)	Pb208 (Mm)	U238 (Mm)	Al27 (Mm)	Cr52 (Mm)
T1	0.000	0.000	0.000	0.000	0.000	0.000	0.000	0.000
T2	0.000	0.000	0.000	0.000	0.000	0.000	0.002	0.000
T3	0.000	0.000	0.000	0.000	0.000	0.000	0.000	0.000
T4	0.000	0.000	0.000	0.000	0.000	0.000	0.000	0.000
T5	0.000	0.000	0.000	0.000	0.000	0.000	0.001	0.000
T6	0.000	0.000	0.000	0.000	0.000	0.000	0.001	0.000
T6A	0.000	0.000	0.000	0.000	0.000	0.000	0.000	0.000
DP 2A	0.000	0.000	0.000	0.000	0.000	0.000	0.000	0.000
DP 3A	0.000	0.000	0.000	0.000	0.000	0.000	0.000	0.000
DP 2B	0.000	0.000	0.000	0.000	0.000	0.000	0.000	0.000
DP 3B	0.000	0.000	0.000	0.000	0.000	0.000	0.000	0.000
River	0.000	0.000	0.000	0.000	0.000	0.000	0.000	0.000

Table A6: Aqueous geochemistry results from the ICP-MS at Veast in millimoles. BDL = below detection limit.

Well Name	Fe56 (Mm)	Mn55 (Mm)	As75 (Mm)	Co59 (Mm)	Ni60 (Mm)	Cu63 (Mm)	Zn66 (Mm)
DP 1	0.164	0.021	0.000	0.000	0.000	0.000	0.001
1a	0.014	0.007	0.002	0.000	0.000	0.000	0.002
1b	0.066	0.010	0.003	0.000	0.000	0.000	0.002
2a	0.005	0.008	0.002	0.000	0.000	0.000	0.002
2b	0.028	0.012	0.003	0.000	0.000	0.000	0.001
3b	0.014	0.011	0.002	0.000	0.000	0.000	0.002

Well Name	Na23 (Mm)	K39 (Mm)	Mg26 (Mm)	Si30 (Mm)	Ca43 (Mm)	S32 (Mm)	P31 (Mm)
DP 1	0.323	0.049	0.216	0.263	0.411	0.153	0.052
1a	0.254	0.063	0.318	0.296	0.993	0.146	0.061
1b	0.335	0.081	0.501	0.275	1.438	0.005	0.062
2a	0.245	0.062	0.325	0.298	0.991	0.146	0.065
2b	0.306	0.076	0.491	0.284	1.433	0.004	0.065
3b	0.291	0.067	0.406	0.259	1.199	0.041	0.000

Well Name	Mo98 (Mm)	Cd111 (Mm)	Sb121 (Mm)	Ba137 (Mm)	Pb208 (Mm)	U208 (Mm)	Al27 (Mm)	Cr52 (Mm)
DP 1	0.000	0.000	0.000	0.000	0.000	0.000	0.000	0.000
1a	0.000	0.000	0.000	0.000	0.000	0.000	0.001	0.000
1b	0.000	0.000	0.000	0.000	0.000	0.000	0.000	0.000
2a	0.000	0.000	0.000	0.000	0.000	0.000	0.000	0.000
2b	0.000	0.000	0.000	0.000	0.000	0.000	0.000	0.000
3b	0.000	0.000	0.000	0.000	0.000	0.000	0.000	0.000

Aqueous geochemistry results for drive-point piezometers DP 3A and DP 3B were taken from the river 10.9 m away from the shoreline. Figure A1 shows a picture of this taking place.

`

Figure A1: Sampling drive-point piezometers DP 3A and DP 3B.

Borehole XRF Data

Tables A7-A10 show the As, Mn, and Fe concentrations collected by XRF for boreholes T7, 1b, 2b, and 3b respectively. The depth is in meters and the concentrations are in mg/kg.

`

Table A7: XRF concentrations for As, Mn, & Fe at borehole T7 at Veast

Depth (m)	As (mg/kg)	Mn (mg/kg)	Fe (mg/kg)
0.0	0.0	0.0	0.0
0.30	25.6	1778.4	25677.6
0.91	22.9	1296.9	39166.6
1.52	31.8	1490.3	36477.1
2.13	43.0	2139.7	60768.3
2.74	54.7	1546.2	59593.8
3.35	28.5	1311.9	38406.6
3.96	33.9	1532.1	29036.7
4.57	29.3	1426.6	37483.3
5.18	28.3	1437.0	34661.3
5.79	25.9	1171.8	37455.4
6.40	26.6	1331.1	35410.9
7.01	37.7	1503.4	37355.9
7.62	29.3	1311.5	40428.2
8.23	35.7	1192.7	41359.0
8.84	41.6	1130.2	41443.2
9.45	28.3	1194.4	38588.3
10.06	27.5	1086.4	37687.8
10.67	28.9	988.5	36238.6
11.28	31.6	1099.9	38489.5
11.89	41.5	1526.9	51552.2
12.50	34.0	879.1	30746.2
13.11	29.9	1210.5	33203.9
13.72	31.1	1169.3	35976.0
14.33	31.1	1169.3	35976.0
14.94	29.0	1091.3	39236.0
15.54	38.6	933.4	32818.4
16.15	31.8	1138.8	37788.4

`

Table A8: XRF concentrations for As, Mn, & Fe at borehole 1b at Vwest North

Depth (m)	As (mg/kg)	Mn (mg/kg)	Fe (mg/kg)
0.0	0.0	0.0	0.0
0.30	111.9	1517.0	68011.3
0.91	103.6	1978.2	65743.6
1.52	56.7	1240.5	54181.6
2.13	36.3	1082.6	45832.2
2.74	42.4	1305.4	42616.1
3.35	32.2	1588.7	37320.5
3.96	49.2	1494.8	45267.3
4.57	32.1	1466.1	59967.2
5.18	31.8	1333.6	48640.2
5.79	41.8	1434.4	52460.7
6.40	31.1	1285.5	47307.1
7.01	38.9	1531.1	51782.4
7.62	33.4	1481.2	46385.6
8.23	28.9	1232.9	45665.2
8.84	35.9	1512.4	55289.0
9.45	41.8	1583.9	62907.8
10.06	67.1	1721.9	59630.9
10.67	35.9	1218.5	46650.3
11.28	58.6	1241.0	54349.6
11.89	72.1	1746.2	62089.3
12.50	33.7	1269.6	46022.4
13.11	36.1	1145.4	46223.9
13.72	34.5	1360.6	54146.2
14.33	56.0	1493.6	59381.8
14.94	37.6	1261.6	43861.6
15.54	30.0	1187.2	45313.1
16.15	45.6	1346.9	53014.1
16.76	41.9	1243.9	49550.7
17.37	36.7	1104.8	43148.9
17.98	50.1	1594.6	62599.9
18.59	36.9	1108.1	45183.5
19.20	33.0	1074.7	42504.9
19.81	57.2	1598.2	58674.7
20.42	33.6	1377.0	43638.6
21.03	112.0	823.1	63208.3

`

Table A9: XRF concentrations for As, Mn, & Fe at borehole 2b at Vwest North

Depth (m)	As (mg/kg)	Mn (mg/kg)	Fe (mg/kg)
0.0	0.0	0.0	0.0
1.52	56.7	1588.1	59718.1
2.74	28.5	1135.4	33549.2
3.35	66.6	1517.3	63703.9
5.18	30.4	1181.7	47118.0
6.40	40.8	1462.3	53256.5
8.23	55.7	1538.0	66418.5
9.45	76.1	1834.3	79940.5
10.67	39.2	1365.8	50793.6
11.89	47.9	1554.9	46444.8
12.50	88.7	1750.1	60961.7
13.72	35.0	977.9	43747.1
14.94	36.7	1194.9	50936.3
16.15	54.8	1585.9	70699.5
17.37	41.0	1572.4	55728.8
18.59	53.5	1862.2	72043.7

`

Table A10: XRF concentrations for As, Mn, & Fe at borehole 3b at Vwest North

Depth (m)	As (mg/kg)	Mn (mg/kg)	Fe (mg/kg)
0.0	0.0	0.0	0.0
0.30	30.0	38585	1503.3
1.52	28.7	37809	1580.1
2.13	66.0	64906	1838.8
3.35	34.1	49726	1486.3
4.57	33.9	45023	1427.9
5.18	28.8	40535	1284.9
7.01	43.1	52141	1445.9
8.23	54.1	62205	1603.7
9.45	43.9	47307	977.7
10.67	34.0	45697	1108.7
11.28	86.4	62414	1751.2
11.89	33.0	41750	1244.7
12.50	46.7	66826	1712.1
14.33	35.4	63872	1283.2
15.54	28.8	42621	1025.1
16.76	43.8	50233	1251.5
17.98	45.2	67319	1576.7
18.59	46.3	59517	1516.5
20.42	37.5	46593	1491.6

`

Table A11 shows the lithology observed while excavating the boreholes at Veast and Vwest North (left) and a grain size distribution/key (right).

Table A11: XRF lithology & key for boreholes T7, 1b, 2b, & 3b

Depth (m)	T7A	VWN 1b	VWN 2b	VWN 3b
0.3	vvf-vf s	cl (mtld)	slt cl	vvf s (br)
0.9	vvf-vf s	cl (mtld)	cl	vvf s (br)
1.5	vvf-vf s	f s	cl	vvf s (br)
2.1	cl	vf-f s	vf-f s	cl
2.7	slt cl	vf s	vf-f s	vf s
3.4	vf s	vf s	cl	vf s & org
4	vf s	slt & vf s	slt cl	vf s
4.6	vf s	vf s	vf s	vvf-vf s
5.2	vf s	vf s	vf s	vvf s
5.8	vf s	vf s	vvf s	vvf s & org
6.4	vf s	vf s	vvf s	vf s
7	vvf s	vvf s	vvf s	vvf-vf s
7.6	vf s	vvf s	slt-vvf s	vvf-vf s
8.2	vf-f s	vvf s	slt-vvf s	vvf s & org
8.8	vf-f s	vvf s	slt-vvf s	vvf s & org
9.4	f s	vvf s	vvf s	vf s
10.1	f s	slt cl	vvf-vf s	vvf-vf s
10.7	f s	vf-f s	vvf-vf s	vvf-vf s
11.3	f s	f s	vf s	cl
11.9	f s	slt cl	vf s & org	vvf s
12.5	mf s	vf-f s	slt cl	vvf s
13.1	m s	vf s	vvf s	vvf-vf s
13.7	m s	slt	vf s & org	vvf s
14.3	mf s	slt	vvf-vf s	vvf s
14.9	mf s	slt	vvf-vf s	vvf-vf s
15.5	mf s	slt	vvf-vf s	vvf-vf s
16.2	mf s	vvf s	vf s	vvf-vf s
16.8	mf s	vvf s	vvf s	vvf-vf s
17.4	mf s	vf s	vvf s	vvf-vf s
18	mf s	vvf s	vvf s	vvf-vf s & org
18.6	m	slt-vvf s		vvf s
19.2		vvf s		vvf s
19.8		vvf-vf s		vvf-vf s
20.4		vvf-vf s		vvf-vf s & org
21		vvf & mf s		vvf-vf s
21.7		slt cl & org		

Grain Size distribution & Key	
cl	clay
slt cl	silty clay
slt	slt
slt-vvf s	
vvf s	very very fine sand
vvf-vf s	
vf s	very fine sand
vf-f s	
f s	fine sand
f-m s	
m s	medium sand
mtld	mottled (with iron oxide nodules)
f	fine
vf	very fine sand
vvf	very very fine sand (almost silt)
org	organic particles (leaf and wood litter)
s	sand
cl	clay
m	medium fine sand (> fine)

`